The impact of climate change on the glaciers of the Canadian Rocky Mountain eastern slopes and implications for water resource-related adaptation in the Canadian prairies

"Phase I"❄ - Headwaters of the North Saskatchewan River Basin

Climate Change Action Fund - Prairie Adaptation Research Collaborative

PARC Project P55

M.N. Demuth[1] and A. Pietroniro[2]

[1]Geological Survey of Canada
Earth Sciences Sector
Natural Resources Canada
601 Booth Street
Ottawa, ON K1A 0E8

[2]National Water Research Institute
Environmental Conservations Service
Environment Canada
11 Innovation Boulevard
Saskatoon, SK S7N 3H5

Mike.Demuth@NRCan.GC.CA

❄ This report also submitted as GSC Open File # 4322 (abridged version as Poster and PDF file on Compact Disc).

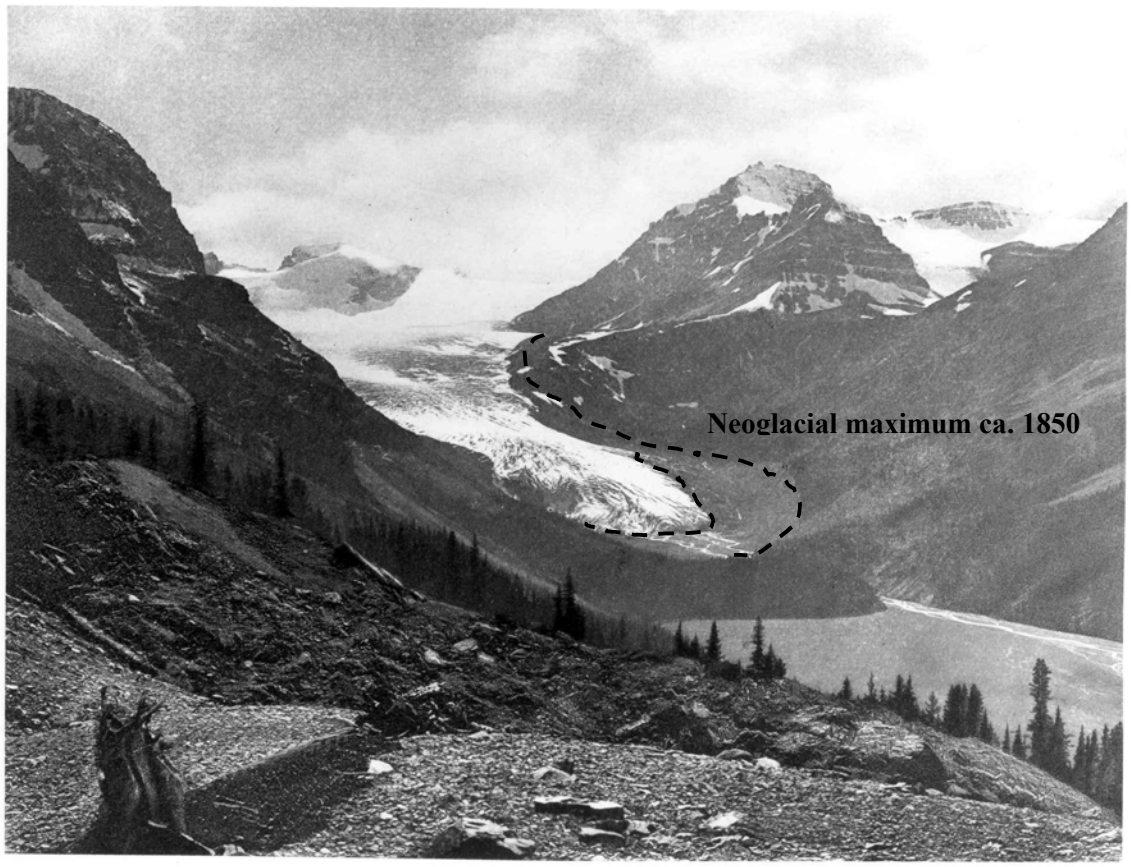

Peyto Glacier 1896 - Walter Wilcox (With Permission Whyte Museum of the Canadian Rockies)

"Peyto Glacier
retreat 1896-present.avi"

PARC
Prairie Adaptation Research Collaborative

C-CIARN
Canadian Climate Impacts and Adaptation Research Network

Forward

'From Grapes to Carrots'

In the summer of 1972, my mentor and colleague, Prof. Gunnar Østrem, was leading a UNESCO-sponsored mission to Argentina to instruct engineers and hydrologists on the principles and methods of glacier mass balance measurements and the study of glacier hydrology. During one of their many field excursions to the front ranges of the Andes above Mendosa, they came upon a small village whose people made their livelihood from the production of grapes. The villagers drew water from a stream that had its source in the alpine, where one distinct valley glacier had been present. They found they could extract 1.0 L s^{-1} from this stream to sustainably irrigate each 1000 m^2 of their crop. After some time had passed, they found they could only extract 0.8 L s^{-1}. After an examination of land-use changes and meteorological records, Professor Østrem concluded that the valley glacier had contracted to such a degree that its ability to augment seasonal streamflow had diminished significantly. As a result, Professor Østrem went on to explain, "…*the people of this small village then decided to grow carrots instead !*"

_____

Michael N. Demuth, P.Eng., P.Geo.
Glaciologist – Snow and Ice Specialist
2003 – February – 29

Summary – Key Findings and Recommendations of P55

The major conclusion of CCAF - PARC Study P55 is that the reliability of water flow from the glaciated headwater basins of the upper North Saskatchewan River Basin has declined since the mid-1900s, and that hydrologic and ecological regimes dependant on the timing and magnitude of glacier-derived meltwater may already be experiencing the medium-long-term impacts of climate change discussed by the IPCC. The reduction in the reliability of glacier-derived flows is in association with significant and accelerating glacier cover contraction fueled by glacier cover dynamic readjustment since the Neoglacial maximum and enhanced radiative forcing effects on glacier mass wastage over the last century. Exacerbating but complicating the partitioning of these responses, are the extra-tropical influences of the El Niño Southern Oscillation (ENSO) on atmospheric circulation and the advection of moisture into the Cordillera, imparting dramatic inter-decadal effects on total winter snow pack amounts and the nourishment of glaciers throughout the entire southern Cordillera. Moreover, temporal and spatial variability of ENSO-driven snow pack anomalies is coherent throughout the western Prairies. It will be increasingly important to document the sensitivity of glaciers and snow cover to these modes of atmospheric variability since, their associated responses will be superimposed on greenhouse gas-induced climate changes, and because certain modes of atmospheric variability may be more frequent under a warmer climate.

While the Neo-glacial 'bonus water' (personal communication R. Halliday) is rapidly depleting (derived largely from outlet valley glaciers), it has been suggested that an ephemeral period of enhanced flow from glacier sources may be re-established when large areas of upland ice (e.g., Clemenceau, Columbia, Northern Wapta icefields) are subject to persistent melting conditions resulting from a protracted shift to higher elevations of the regional equilibrium line. Unknowns related to shifts in the precipitation regime, however, complicate forecasting the timing, duration and magnitude of such a reprieve period. Some assistance in this regard can be offered by ongoing studies that are documenting the variation in the mass balance gradient of glacier cover in regions such as the eastern slopes of Alberta. This information and continued monitoring of moisture and heat flux gradients along mountain slopes where perennial ice cover is

still present will assist climate and ice cover response modeling efforts at the regional scale.

Specific findings include:

⇒ Transition-to-Base-Flow (TBF) yields from the glacierised catchments of the upper North Saskatchewan River Basin have decreased since the mid 1900s. The reduction in TBF yields is observed despite generally warmer summer conditions that would suggest an increase in the vertical water fluxes released by perennial ice cover, particularly in the two decades following the 1970s. Moreover, the reduction in TBF yields is observed despite modest but significant increases in precipitation (for the TBF period) documented for the montane region since 1950.

⇒ From 1950-present, results suggest that minimum and mean flows from glacierised catchments are decreasing for the annual and TBF periods, and that this response is commensurate with reductions in the area-wise extent of glacier cover after accounting for variations in regional precipitation amounts and air temperature.

⇒ The variability of streamflow during the TBF period from the glacierised basins of the upper North Saskatchewan River Basin has increased since the mid-1900s in association with decreasing glacier cover. This increase in flow variability may also be linked to a modest increase detected in the maximum flow record for the glacierised basins. An increase in observed maximum flows may be in association with long-term reductions in the glacier firn pack, predicating amplification in the diurnal fluctuations of discharge and reducing the lag times associated with meltwater production from high alpine sources.

⇒ Glacier cover reductions since the Neoglacial maximum for the region (ca.1840) have been marked. While data availability may contribute to an aliasing of the perspective derived for the period 1840 - 1950, there is evidence of an accelerated contraction in the later half of the 20th century.

⇒ While partitioning the observed glacier cover reduction between that resulting from internal glacier-climate variability and that caused by external forcing is far from complete, analysis suggests that glacier cover in North Saskatchewan River Basin headwaters (eastern slopes of the Canadian Rockies) is rapidly approaching (ca. 50 a) the state that may have existed during the early Holocene warm interval (i.e., the

warm limit of Holocene variability), and certainly a state that available morpho-stratigraphic and botanical evidence suggests has not existed for several millennia.

⇒ The association of the aforementioned observations with shifts in synoptic climate is established through available data describing the variation of sea surface temperature, atmospheric circulation, seasonal snow and perennial ice. A mid-1970s shift to lower winter balance is synchronous with an increase in the frequency of non-snow producing synoptic weather types and a decrease in the frequency of snow producing weather types as influenced by a modulation of the Pacific-Decadal-Oscillation, the El Niño Southern Oscillation and their influence on the Pacific-North-American atmospheric circulation pattern. The strong spatial and temporal coherence of anomalous patterns in the availability of seasonal snow in the eastern slopes and western prairies, and the mass balance of alpine glaciers in relation to ocean-atmosphere phenomena is encouraging. Such knowledge should assist in the development of better forecasting tools for use in water resource management under scenarios of climate variability.

Recommended Research:

Looking to the past

Glacier mass balance records can provide an integrated portrayal of seasonal climate variations and an analogue for the contribution of glacial runoff to streamflow. While climate variations in the Rocky Mountains and their influence on the snow and ice resources located there have likely influenced the seasonality and magnitude of river flows to the western Canadian Prairies for some time, annual glacier mass balance records for the leeward slopes of the montane Cordillera are not available prior to 1966. There is a need, however, to hind-cast mass balance records to extend our understanding of glacio-hydro-meteorological interactions prior to the period of study considered by this investigation. Due to recent advances in digital stereo photogrammetry and the availability of high-resolution laser altimeter data for several reference mass balance glaciers (e.g., Demuth *et al*., 2001; Hopkinson *et al.*, 2001) it has been possible to recreate accurate digital terrain models describing glacier elevation and elevation change from archived aerial photography (personal communication M. Sitar). Such efforts will

provide constraint and verification for multiple regression mass balance modeling efforts making use of historical meteorological data.

When one considers multi-century time scales and the context such records could provide, it is fortuitous that instrumental records (e.g., air temperature) for the central Canadian Rockies extend back to the late 1880s. Coupled with the strong Pacific Decadal Oscillation relationship to winter balance variability (PDO record extends back to 1890), it should be possible to reconstruct the seasonal and net mass balance time series back to the time when Walter Wilcox first photographed Peyto Glacier in 1896. Indeed, in combination with the extensive geo-botanical data available for the study region, initial efforts to hind-cast Peyto Glacier mass balances over the scale of several millennia are underway (personal communication B. Luckman). In addition, Demuth and Holdsworth (1997) and Holdsworth *et al*. (2002), have determined that it would be feasible to obtain a 300-400 year ice core record from the upper reaches of the Peyto Glacier. Such a record would place the current perspective on the variation of snow cover and glacier nourishment over the last half of the 20th century, in a very useful context, particularly as they concern alpine water resource variability.

Looking to the future

This study has established a framework with which to conduct glacio-hydro-meteorological modelling studies to predict runoff and river flows under future climate scenarios. It is suggested that the application of this framework could be extended to the South Saskatchewan River Basin. Coupled with 'Water Use Analysis Models' (personal communication M. Sydor) and the impetus imparted by other efforts where water resources are thematically important (e.g., PERD – CCIES POL), it is feasible that we will thereby be in a position to reach the ultimate objective of helping to understand the water resource adaptation needs of both the North and the South Saskatchewan River basins - in particular, the vulnerability imposed by changing land cover states, projected patterns of temperature and precipitation, and the requirements of historical, sectoral and trans-boundary water allocation, on the adaptive capacity of downstream surface water systems.

1966

W.E.S Henoch

2001

M.N. Demuth

Along the eastern slopes of the Canadian Rocky Mountains, glacier cover has been decreasing rapidly in recent years, and total cover is now approaching the least extent experienced in the last several millenia. As the glacial cover has decreased, so have the downstream flow volumes. While this finding appears to contradict the IPCC projection that warmer temperatures will cause glacial contributions to downstream flow regimes to increase in the short-term, historical streamflow and meteorological data indicate that this increased flow phase has already past, and that the basins have entered a potentially long-term trend of declining flows. The reliability of river flow augmentation during dry periods is in measurable decline compared to the middle of the last century. A continuation of this trend will exacerbate water shortages that are already apparent across many areas of Alberta and Saskatchewan owing to drought.

Acknowledgments

This work was only possible because of the support and facilitation afforded by the generosity and skill of the following individuals: Ms Jane Yetter and Mr Norm Crookshank (National Research Council-Canadian Hydraulic Centre), Prof. Taha Ouarda (INRS-Eau), Ms Krysha Dukacz (National Water Research Institute), Ms Jessika Töyra (NWRI), Mr Kelly Best (NWRI), Mr Jean-Guy Zakrevsky (Water Survey of Canada), Mr John Taggart, Mr Sal Figliuzzi and Mr Ron Bothe (Alberta Environment - Water Sciences Branch), and Mr Roger Drurey (Trans Alta Utilities).

The interest and support of the Canadian Parks Service cannot go unrecognized, and they and their staff are thanked for continued access to field sites, infrastructure permitting and environmental outreach efforts within Banff National Park and Yoho National Park. The residents of the Prairie Provinces are thanked for providing discussion and for their interest in the work.

The authors also thank Prof. D. Scott Munro, Prof. R. Dan Moore, Dr Chris Hopkinson, Dr Corinne Schuster, Mr Alistair Wallace, Dr Terry Prowse, Mr Malcolm Conelly, Dr Steve Grasby and Dr Don Lemmen for valuable discussions and access to their collective experience. Dr Fred Wrona, Dr Kevin Cash and Mr Robert Halliday were instrumental in supporting the relevance and evolution of this work and they are thanked.

The interest, support and patience of CCAF-PARC and, in particular, Prof. David Sauchyn, Dr Malcom Wilson, Dr Elaine Wheaton and Mr Ross Herrington are much appreciated.

Table of Contents

List of Illustrations

List of Tables

1. Introduction

Over the last number of years, there has been a growing awareness of the need to protect and properly manage Canadian water resources, specifically under the supply/demand conditions that are suggested will exist under a warming climate (IPCC, 2001). A recent national assessment (Maxwell *et al.*, 1997) highlighted that a complete understanding of the changes in water resources in Canada resulting from changing climate is far from complete. It is understood that the impacts across Canada will be quite varied and the implications more profound in some areas than in others (Clair *et al.*, 1988; Linton, 1997). Steep climatic gradients in mountain watersheds make their hydrological and ecological regimes particularly sensitive to a changing climate (Denniston, 1995; Young, 1985). Western Canada's mountain watersheds, many of which are glacierised, provide freshwater for domestic and industrial use. Moreover, the ecology of glacier streams are strongly affected by longitudinal temperature gradients and hydraulic conditions that vary with headwater extension (glacier advance) and contraction (glacier retreat) (Milner and Petts, 1994; Petts *et al*., 2002). Proponents of the CCAF, PARC and PERD initiatives related to climate change, the Canada Country Study (www.ec.gc.ca/climate/ccs/) and climate change perspectives provided by other national and international programs (e.g., IPCC, 2001), have prescribed that further work is necessary to characterise the vulnerability of streamflow in the mountains, and regions adjacent to them, to future changes in the amount of glacier cover.

In a mountain watershed, the influence of even small areas of perennial ice on the seasonal variation of runoff is marked (Young, 1985; see also Hopkinson and Young, 1998). The duration of snowmelt runoff is extended since, in general, glacial catchments extend to higher elevations than those that are solely nival; the major nival/glacial contrast resulting from the limited life of the snow reservoir. As the seasonal snowline ascends to higher elevations, increasing areas of glacier ice and firn, having a lower albedo than snow, are exposed, increasing rates of meltwater production. Moreover, melt is augmented by the action of supra-glacial, en-glacial, or sub-glacial water flow, regardless of its origin as precipitation (rain) or surface melt from latent heat exchange. Often, a late spring snowfall will radically delay the timing of seasonal flow contributions, while contiguous, non-glacial areas, subject to the same snowfall but very different heat flux regimes, will respond more rapidly.

Temperate mountain glaciers manifest a delayed and extended period of maximum seasonal discharge, and a regulatory effect over streamflow such that annual and monthly variations are reduced (Fountain and Tangborn, 1985). Glaciers act as storage reservoirs that can contribute to streamflow during periods that would otherwise be in a state of low flow. They also act as a source of disturbance during intense weather when, for example, rain-on-ice persists for several days, causing extreme flow events and dramatic geomorphic shifts. The sudden release of englacial and/or subglacial water can also result in extreme flow events (Johnson and Power, 1985). A typical annual hydrograph exhibits base flow augmentation by snowmelt runoff during a period of rising temperature; followed by peak flows resulting from rainfall superimposed upon glacier melt (Figure 1). At the daily-scale, glacial streams, near the glacier margins, exhibit a late afternoon diurnal flow peak (e.g., Schuster and Young, 2002).

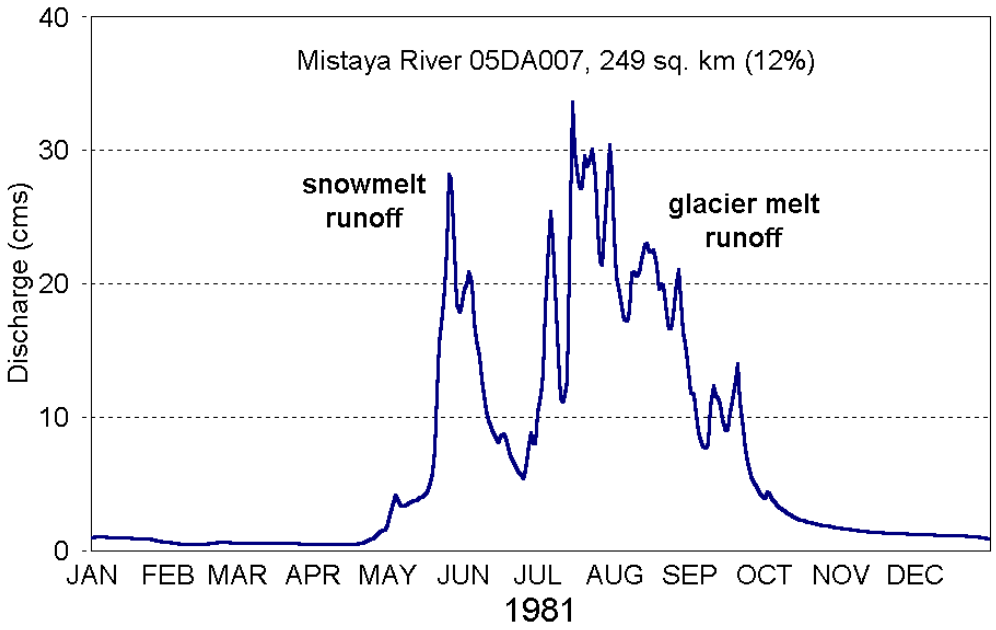

Figure 1 - A characteristic hydrograph for a headwater stream in the Canadian Rocky Mountains. Total contributing area and percent glacier cover are shown.

The water-resources in the western Canadian prairies are under increasing pressure from: i) the need to provide adaptation strategies based on a reduced reliance on fossil fuel energy sources

under the Kyoto Protocol; ii) interests outside Alberta and Canada regarding bulk water transfers and flow fragmentation (e.g., Manitoba-North Dakota; iii) evolving concerns amongst the Prairie provinces regarding inter-provincial water allocation. Glacial meltwater from the eastern slopes of the Rocky Mountains is recognised as an important factor in adapting to these pressures; the principle question being, "*For how long can such sources reliably regulate streamflow under known and projected variations in climate*?". Moreover, current activities within Canada (Environment Canada) regarding the rationalisation of the hydrometric network have been responsive to the importance of glaciers in terms of identifying hydrological regimes which are of high scientific merit (e.g., Reference Hydrometric Basin Network, personal communication M. Kowalchuck).

Several researchers have examined the upper North Saskatchewan River Basin over varying periods from the point of view that glacier mass wastage will augment basin yields when precipitation is absent (e.g., Henoch, 1971; Young, 1991). Given the importance of late-season glacier meltwater contributions to habitat maintenance, pre-winter reservoir adjustments and other demands, a reconnaissance investigation (precursor to the present study) was conducted to examine the nature of the *Transition to Base Flow* (TBF) sub-period of the annual hydro-period for two contrasting (glacier cover) basins in the headwaters of the North Saskatchewan River Basin (Siffleur and North Ram catchments; Demuth, 1996). The TBF is defined as a period where glacier meltwater is nominally the most significant contributor to headwater streamflow, notwithstanding high antecedent snow pack conditions or significant precipitation. For the purposes of this study and the temperate glacio-climatic regime existing in the Rocky Mountain eastern slopes, the TBF is defined as the three months of August, September and October. The reconnaissance study revealed that TBF yields and flow variability in the headwater catchments subject to similar meteorological conditions, varied according to the amount of glacier cover in each. This confirmed the findings of Fountain and Tangborn (1985) and set the stage for a more detailed examination of the *temporal evolution* of basin yields and flow variability for a broader network of contributing basins – the goal of this study.

In association with this, we make use of data describing the marked seasonality of the energy and moisture fluxes associated with glaciers (e.g., glacier mass balance), and a memory function represented by changes in the areal extent of glaciation (e.g., advance/retreat of the glacier

margins), to develop both short-term and historical climate perspectives. Based on a recent assessment by Demuth and Keller (2002) of the influence of recent and past-century climate variability on the mass balance of a GCOS/GTN-G[1] reference mass balance glacier situated in the upper North Saskatchewan River Basin, we will first describe the nature and significance of its recent and past-century fluctuation. This perspective is supplemented by the present work through a regional assessment of a glacier cover changes since the Neoglacial maximum for the region (ca. 1850). This will be followed by analysis and discussion of the hydrologic impacts of such fluctuations and their glacio-climatological attribution. Finally, we present and discuss current and future efforts to affect a time-line for the evolution of future climate-glacier-streamflow states. This later activity will use an improved representation of glacier cover within a distributed hydrological model (WatFlood), IPCC climate scenarios and General Circulation Model outputs that have been evaluated using baseline climatology for the North Saskatchewan River Basin.

2. Method of Approach

2.1 Analysis of Glacier Fluctuations

For the purpose of this study, perspectives on recent and past-century glacier fluctuations in the NSRB headwaters are, in part, provided by the results of systematic glacier mass balance-climatic attribution assessments after Demuth and Keller (2002). These site-specific results are placed in a post-Neoglacial/past-century context using the results of repeated mapping surveys (Glenday, 1991; Wallace, 1994) and the comprehensive morphostratigraphic delineations and botanical evidence presented by Luckman (2002). The present work also updates and examines glacier inventory records derived from existing topographic maps and remote sensing products (e.g., vertical and oblique aerial photography, artificial satellite thematic imagery) and the results of glacier area-perimeter-volume scaling to provide a regional context. Detailed methodological considerations and references are provided in the relevant sections of this report.

---

[1] WMO's Global Climate Observing System-Global Terrestrial Network-Glacier. The Canadian contribution to GTN-G is the National Reference Glacier-Climate Observing Network. It is comprised of reference mass balance glaciers in the Canadian Cordillera and Arctic Islands and contributes to regional and global glacier-climate assessments for GCOS and UNESCO-IHP through the World Glacier Monitoring Service and the CNC-IHP. NRGCON is administered and operated by the Geological Survey of Canada-Terrain Sciences Division and the Canada Centre for Remote Sensing – Applications Division (NRCan), with the support of Environment Canada-NWRI and CRYSYS partners.

2.2 Analysis of Hydrological Impacts and Glacier-Climate Attribution

Armed with the perspectives generated by previous studies in the region (e.g., Henoch, 1971; Young, 1991; Demuth, 1996) we examine the influence of changing glacier cover by conducting parametric statistical trend analysis of streamflow and basin yield for several reference headwater catchments. Young (1991) illustrated the effect of glacier runoff on basin yield during periods of precipitation deficit, but went onto suggest that basin yield will decline and inter-annual variability in flows will increase with continued glacier shrinkage. By analysing a longer sequence of historical streamflow data in relation to secular glacier-climate variability (1950-1998), we examine to what degree this suggestion is actually evolving and illustrate for each of the research catchments, how the reliability of flow augmentation from glacier melt is changing.

The superposition of melt sources and the multiplicity of factors influencing their timing and magnitude, contribute to the low signal to noise ratio often exhibited in lower-catchment hydrometric records. Moreover, hydro-meteorological time series often contain gaps and do not meet conditions for normality (requisite for *parametric* statistical analysis). We also, therefore, apply a range of non-parametric uni- and multi-variate statistical analysis useful for identifying the magnitude and timing of shifts in hydrological time series, their significance and their attribution (e.g., Lettenmaier, 1976). This analysis then also considers a broader network of contributing catchments bounded by Rocky Mountain House, Alberta. Detailed methodological considerations and references are provided in the relevant sections of this report.

3. Study Region

This study examines several glacial catchments of the North Saskatchewan River Basin (NSRB) headwaters. Located along the Continental Divide between Alberta and British Columbia, NSRB contains one of several extensive areas of glacier cover that exist within the eastern slopes of the montane Cordillera; the Canadian portion of which extends from the Border Ranges near Waterton National Park (Oldman River) to the Resthaven Icefield region (Smokey River headwaters). As summarised by Young (1991) for a typical catchment in the upper North Saskatchewan River Basin, "…there is a general progression from lakes at low elevations through forest and bare rock surfaces to glaciers at high elevations…". The underlying geological structure (a series of sedimentary beds dipping westward to produce east-facing scarp

features separated by wide benches of relatively uniform elevation) contributes to a basin hypsography characterised by extensive areas interspersed by those that are less extensive. Above approximately 2100 m a.s.l., these wide benches foster the accumulation of snow and the formation of glaciers. See Heusser (1956) for additional physiographic information.

Along a typical west-east transect through the eastern slopes of the montane Cordillera, one first encounters numerous outlet valley glaciers, whose source of nourishment are the high altitude icefields distributed along the continental divide (e.g., *Saskatchewan Glacier* flows from the *Columbia Icefield*) (Figure 2 and Figure 3). A complex of discrete, dynamically active, valley glaciers or 'glacier evacuators'[2] are also found. Typical, glacier coverage amounts to approximately 12% or more. Further east, a zone, having few large interconnected icefields, exhibits numerous smaller valley glaciers, cirque glaciers and 'glacier reservoirs'[2] (glacier coverage ≈ 6%). From this zone eastward, glacier coverage drops off dramatically to typically less than 1%. Generally speaking, the west-east transect illustrates the influence of altitude and a leeward-slope precipitation gradient.

Three reference catchments will be discussed in greater detail later in the report. The Mistaya River catchment has a glacier coverage of about 12%; typical of the NSRB above Abraham Lake as a whole (Figure 2). To the east lies the Siffleur River, whose contributing area is roughly twice that of the Mistaya basin, and exhibits glacier coverage of approximately 6%. Directly adjacent and to the northeast lies the North Ram River catchment, whose flow eventually contributes to the Ram River and the North Saskatchewan River below Abraham Lake. It has less than 0.5% glacier coverage and, for the purposes of this study, is examined to a point bounded by a gauging station within the foothill-alpine transition (Figure 2). Abraham Lake lies below the North Saskatchewan main stem and the Mistaya, Siffleur and Cline River catchments and was created in 1977 by the construction of the Bighorn Dam and Hydro-electric Station (118 MW) (Figure 2). It is the largest facility within the eastern slopes and contributes to the 400kV corridor between Calgary and Edmonton (EMR 1987).

---

[2]The term 'Glacier Evacuator' refers to a dynamically active glacier whose response to changes in mass are realized by variations in the areal extent of the glacier through flow and the fluctuation of the glacier margin position. 'Glacier Reservoir' refers to a glacier whose response to mass changes are only realised through changes in its thickness; its nature and situation precluding deformation and ice flow.

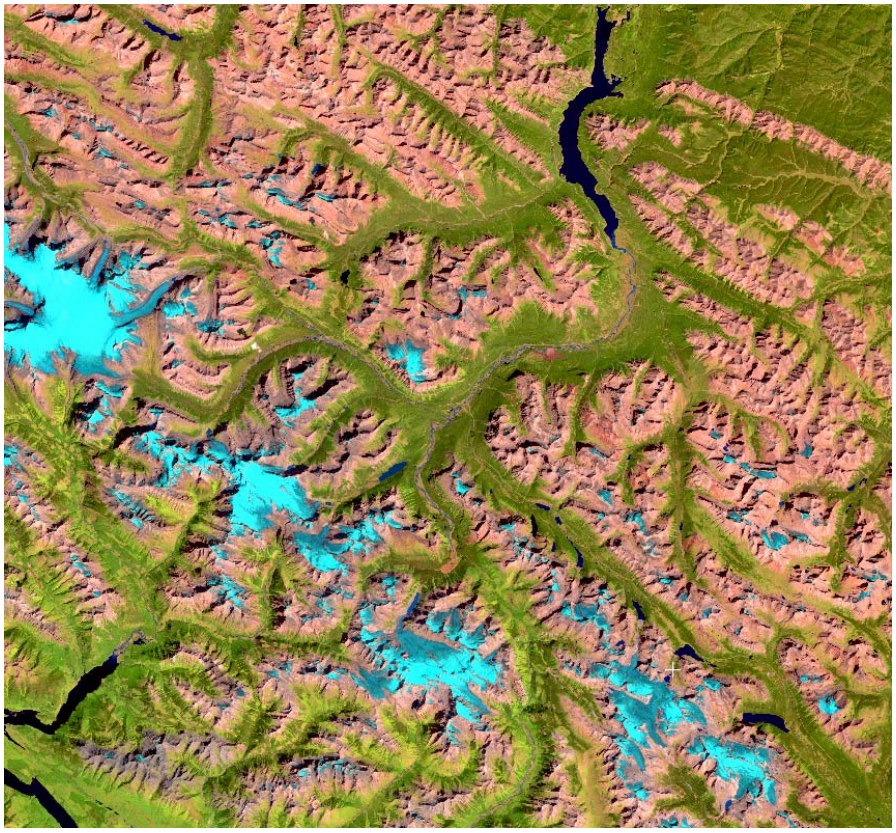

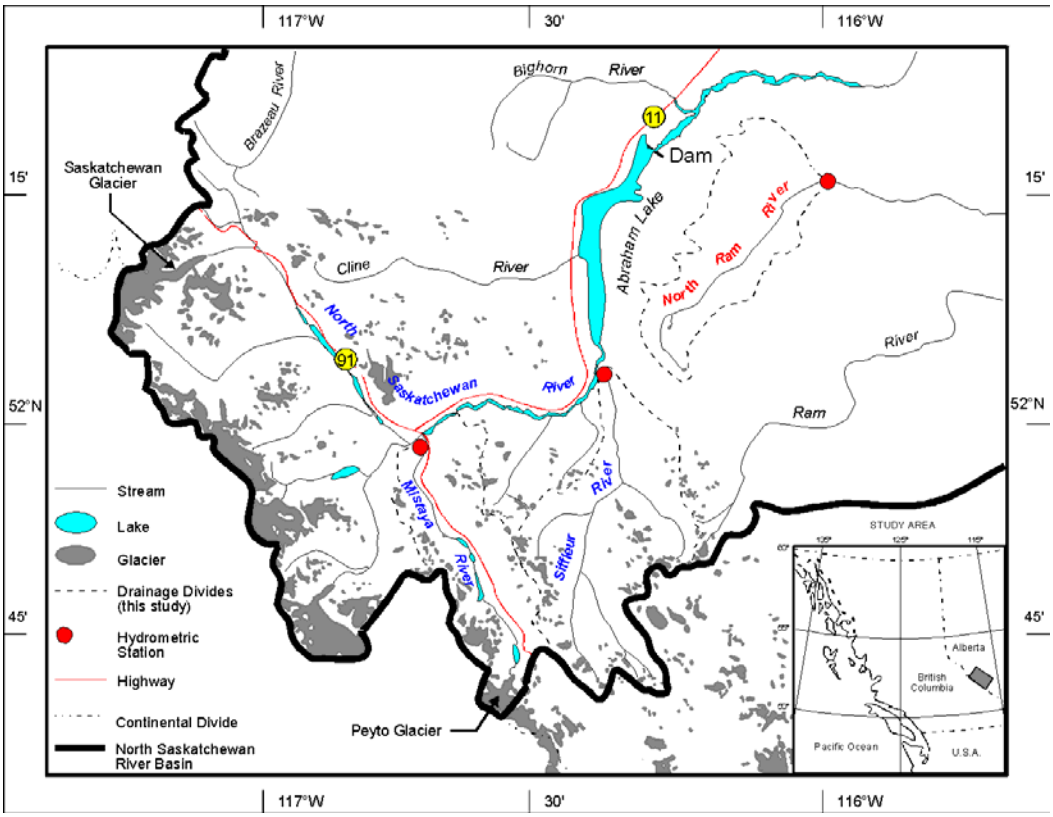

Figure 2 - The headwater contributing basins of the North Saskatchewan River, Alberta, including Peyto Glacier. The reference case-study catchments and their respective hydrometric stations are delineated. Glacier coverage is derived from the Glacier Atlas of Canada - plates 7-3 and 7.4 (Ommanney, 1989).

Figure 3 - Glacier Atlas of Canada plate 7-4 North Saskatchewan River Basin (http://atlas.gc.ca; click on Map Archives and Glacier Atlas of Canada; see also Ommanney 1989).

4. Analysis and Discussion: Glacier Fluctuations in the Headwaters of the North Saskatchewan River Basin

4.1 Recent and Past-Century Glacier Mass Imbalance and Wastage

For the purposes of illustrating the headwater glacier-climate regime of the North Saskatchewan River Basin, we have synthesised data from the well studied Peyto Glacier situated at the headwaters of the Mistaya River catchment (Figure 2). Peyto Glacier is a reference glacier-climate observing site of the World Glacier Monitoring Service and the GTN-G of WMOs Global Climate Observing System. Peyto Glacier has been monitored annually by the since 1966 (Young, 1981; Demuth and Keller, 2002).

Demuth and Keller (2002) provide analysis of the recent pattern of seasonal and net mass balance (1966-1995) for Peyto Glacier, and evidence of the nature and timing of broader synoptic-scale and atmospheric circulation influences, that shed light on questions contemplated by Young (1981):

'*... whether the negative balances of so many glaciers this century in the Rocky Mountains and elsewhere may not be largely the results of the occasional exceptional year than gradual change through time*' and '*… to what extent the events recorded on Peyto are typical of the events on surrounding glaciers*.' Some of their results are discussed below.

4.1.1 Seasonal and Net Specific Mass Balance

The seasonal (B_w, B_s) and net (B_n) mass balances for Peyto Glacier are illustrated in Figure 4. The long-term seasonal and net mass balances are $B_w^{66\text{-}95} = +1195$, *se* 66 mm w.e. a^{-1}; $B_s^{66\text{-}95} = -1690$, *se* 77 mm w.e. a^{-1} and $B_n^{66\text{-}95} = -495$, *se* 104 mm w.e. a^{-1}. While the individual time series exhibit high inter-annual variability, the extreme variations in the net balance observed in the early part of the record are to be contrasted with the consistent trend of negative net balance beginning in the mid-1970's. The winter balance also appears to have decreased substantially over the same period.

4.1.2 Equilibrium Line Altitude and Accumulation Area Ratio

The Equilibrium Line Altitude (*ELA*) defines the glacier elevation where there is zero net mass balance; above it there is mass gain, below it, mass loss. Its determination is a mathematical by-product of the average net mass balance (b_n)-elevation (h) relationship (h @ $b_n(h)$=0). For temperate glaciers, the ELA is closely associated [not universally; see Meier (1962), Demuth and Pietroniro (1999, 2000)] with the maximum altitude attained by the transient snowline. The long-term *ELA* for Peyto Glacier is $ELA^{66\text{-}95} = 2695$, *se* 16 m a.s.l. while the long-term *ELA* trend is $dELA/dt^{95} = +2.5$, *se* 1.9 m a^{-1}. The documented rise in the equilibrium rise of some 75 m corresponds roughly to a warming of 1 *K* over the period of observation .

A related parameter, the Accumulation Area Ratio (*AAR*), is defined as the amount of area above the *ELA* divided by the total glacier area. The value of *AAR* for a glacier in balance (B_n=0) is dependent on the shape of $b_n(h)$ and the distribution of glacier area (a) about its median altitude, $a(h)$. In general, if $b_n(h)$ is linear and $a(h)$ is symmetrical about the median elevation of the

glacier then an *AAR* of 0.5 corresponds to B_n=0. $b_n(h)$ is usually somewhat non-linear [i.e., dB_n/dh is generally greater at lower altitudes than higher altitudes (Meier and Post, 1962)] and so B_n=0 would correspond to an AAR > 0.5. In general, Rocky Mountain glaciers experiencing net mass loss exhibit AAR's ranging from 0.3-0.5, but periodically much less than 0.3. The $B_n(ARR)$ regression (Figure 4) yields an *AAR* of 0.53 for B_n=0. The long-term *AAR* for Peyto Glacier is $AAR^{66\text{-}95}$ = 0.4, *se* 0.026 and corresponds to the glacier experiencing a long-term negative net balance.

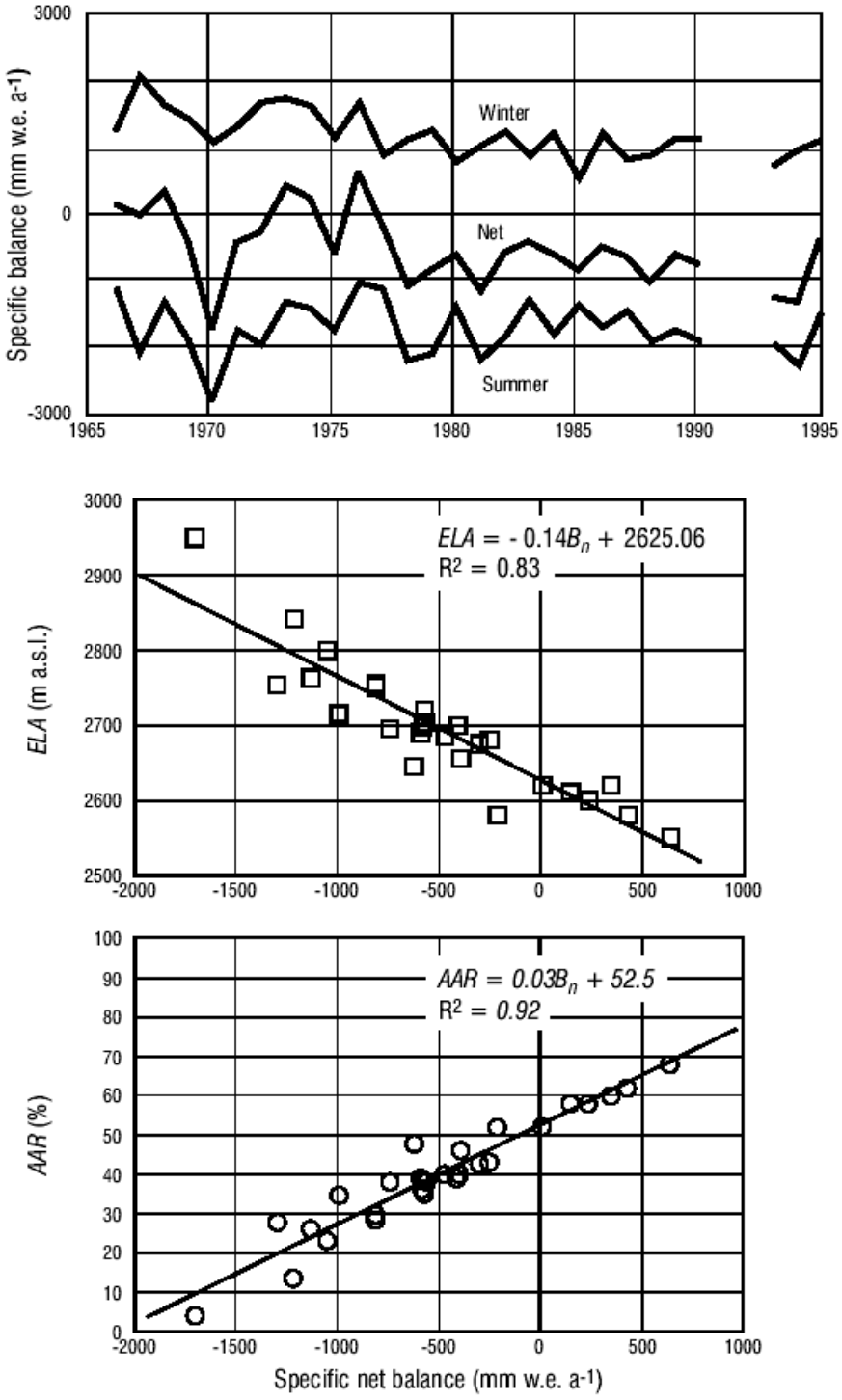

Figure 4 - Specific winter, summer, net mass balances and the net balance - ELA, AAR relationships for Peyto Glacier (1966-1995) (after Demuth and Keller, 2002).

4.1.3 Temporal Variations of Net and Seasonal Mass Balance

From an initial examination of the time series data (Figure 4), it is evident that the variation of B_n, for the record up to the mid 1970s, is relatively random (mean $B_n \approx$ -140 *se* 195 mm w.e. a^{-1}) with the occurrence of occasional exceptional years (e.g., Young, 1981). At this point no evidence of a plausible 'trend' in B_n is evident. By contrast, the record since the mid-1970s is characterized by continuous series of negative net balances ($B_n \approx$ -725 *se* 78 mm w.e. a^{-1}). Separating B_n into its winter (B_w) and summer (B_s) balance components (Figure 4) provides fundamental information on the relative role of the nourishment (accumulation) and ablation phases. The seasonal time series data appear to exhibit a marked mid-1970's shift in B_w towards lower winter balance, and a random fluctuation of B_s. The timing and magnitude of B_w and B_s variations are now examined in more detail.

Figure 5 illustrates the departure of the net and seasonal mass balance from their respective long-term means. A strong shift in B_w is evident in the mid 1970s with its impact on B_n exacerbated by above average B_s in the late 1970s - early 1980s, and again more recently. Notwithstanding the dependence between the seasonal and the net balance data (i.e., $B_n=B_w+B_s$), the relative role of the winter and summer balances is illustrated by the correlation of their 5-year running means to that for the net balance: 0.81 and 0.63 respectively.

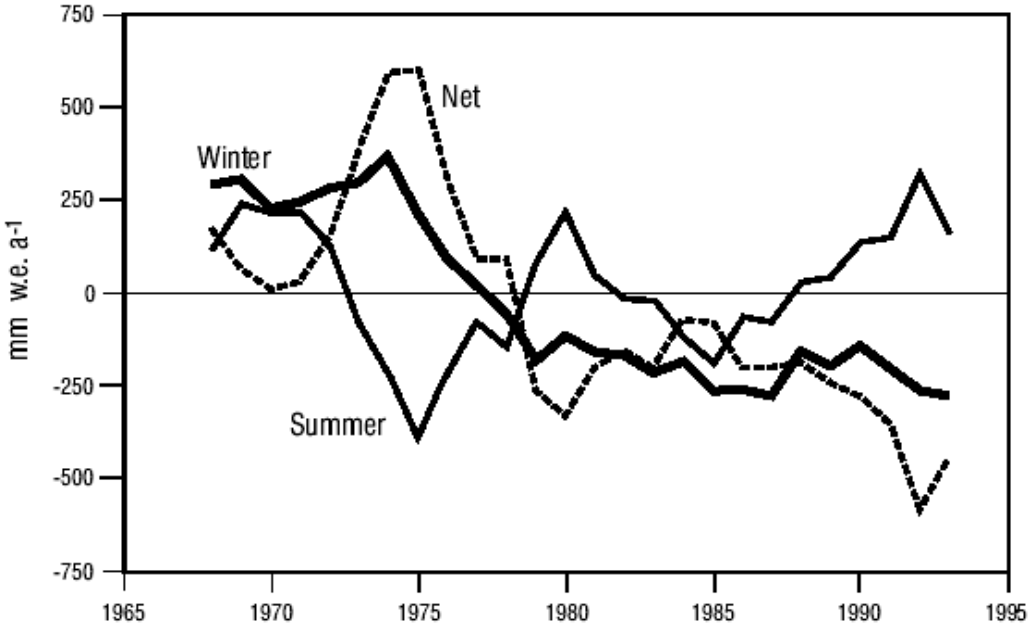

Figure 5 - Five year moving averages (centred) of Peyto Glacier seasonal and net mass balances expressed as departures from their respective1966-1995 means (after Demuth, 1996).

To further demonstrate the relative roles of winter and summer balance, refine the timing of balance shifts and verify the persistence of any trends in the time series, the method of *residual mass curves* is used (e.g., Buishand, 1982). The *cumulative* percentage departure of the mass balance after *i* years of record, $B^i \uparrow\downarrow$, is determined according to the equation:

$$B^i \uparrow\downarrow = 100\sum_{i=1}^{N_y}[\frac{B_i}{\langle B \rangle} - 1]$$

where N_y is the number of years of record, B_i is the value for year i, and $<B>$ is the mean balance for the period of record. When $B^i \uparrow\downarrow$ is plotted against time (Figure 6) a negative slope between two datums indicates that the magnitude corresponding to the latter datum is less than the mean; a positive slope signifies the opposite.

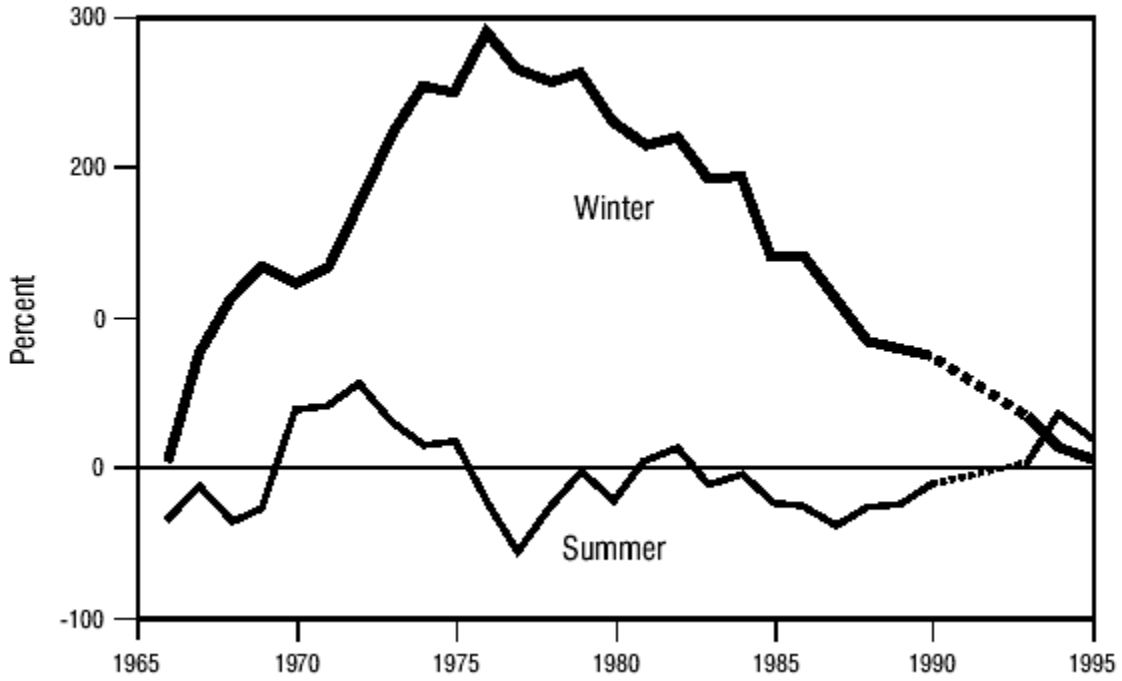

Figure 6 - Cumulative percentage departure for Peyto Glacier winter and summer balance using the residual mass curve approach (Demuth and Keller, 2002).

For B_w , Figure 6 verifies a mid 1970's break point (specifically, the 1976 balance year) to lower Winter balance: $<B_w>^{66\text{-}76} =$ 1505 *se* 89 mm w.e. a^{-1} while $<B_w>^{77\text{-}95} =$ 992 *se* 50 mm w.e. a^{-1}. A **t**-test for a shift in $<B_w>$ at 1976 (i.e., two time series either side of the apparent break point) resulted in the rejection of H[$<B_w>^{66\text{-}76} = <B_w>^{77\text{-}95}$] at the 95% significance level. **t**-tests on

other sub-series within the record length indicated no significant differences in the sub-series means at the 95% confidence level. Beginning in the late 1980's, there appears to be an attenuation of the lower-than-average winter balance trend. While perhaps somewhat speculative, especially given the missing data for 1991 and 1992, this later observation is supported by other studies of winter snow pack variability for the region (e.g., Keller, 1997; Brown and Braaten, 1997).

It is evident from Figure 5 and Figure 6 that the role of B_s is also important as it concerns the year-to-year change of the net balance; either reinforcing the impact of lower than average Winter balance or 'compensating' for it. Interestingly, marked increases in B_w, reinforced by similarly significant decreases in B_s during the early to mid 1970s, resulted in positive B_n for several years. When the time series after the mid 1970s shift is considered, however, it is clear that the variation in Winter balance has played a dominant role in the evolution of the net balance for Peyto Glacier and its recent drastic cumulative mass losses. Despite the 1991-1992 record gap, data for 1993-1995 (Figure 4) and from more recent assessments (since 1995; Demuth and Pietroniro, 1999; Demuth, 1999), confirms persistence in the trend of lower than average B_w. Summer conditions, however, played an important role in generating near-record[3] net mass losses (1970, 1993, 1994) and, by contrast, the most modest net losses (1995, 1996) observed since 1977.

4.1.4 Recent Mass Wastage in Relation to Past-Century Variations and Global Climate Change

For context purposes, reference to the historical time scale is warranted. Several studies have examined the past-century variation of the volume of Peyto Glacier (Table 1). Notably, Holdsworth *et al*. (2002) provide, for the first time, a reliable reconnaissance-order volume for the glacier. Such knowledge casts volume change and mass balance data in a particularly useful water-resources context. For example, using the total volume estimate provided by Holdsworth *et al*. and the mass balance data reported by Demuth and Keller (2002), the glacier lost approximately 25% of its 1966 volume by 1995. With respect to the past century, Wallace (1995) estimated a loss of 1 088.6 x 10^6 m^3 of ice between 1896 and 1966. This translates into approximately 60% of the 1896 volume. Collectively, this evidence yields that Peyto Glacier has

[3] Record net mass losses for Peyto Glacier were reporting for 1998, due primarily to drastic mass wastage in summer (Demuth, 1999).

lost roughly 70% of its volume since the first direct observation of its extent by W. Wilcox one-century ago. The associated surface area changes described in Østrem (2002, Figure 2) are certainly dramatic (see also page vii in this report). However, the past-century *thinning* below ≈ 2550 m a.s.l., where the glacier begins to transition into the step/icefall and the confines of the elevated valley containing the glacier snout, is perhaps more demonstrative of the past-century mass loss (Figure 7).

*Table 1 - Summary of volume (**V**) and volume change (**ΔV**) studies conducted for Peyto Glacier.*

Time Period	Quantity	Methods	Reference
1896-1917 1917-1966	***ΔV*** ***ΔV***	Geographical Information Systems (GIS), historical mapping and oblique photography.	Wallace (1995)
1966-1989	***ΔV***	Terrestrial trigonometric surveys and GIS.	Glenday (1991)
1966-1984	***V*** , ***ΔV***	Terrestrial trigonometric surveys and RaDAR Echo Sounding	Holdsworth *et al*. (2002)

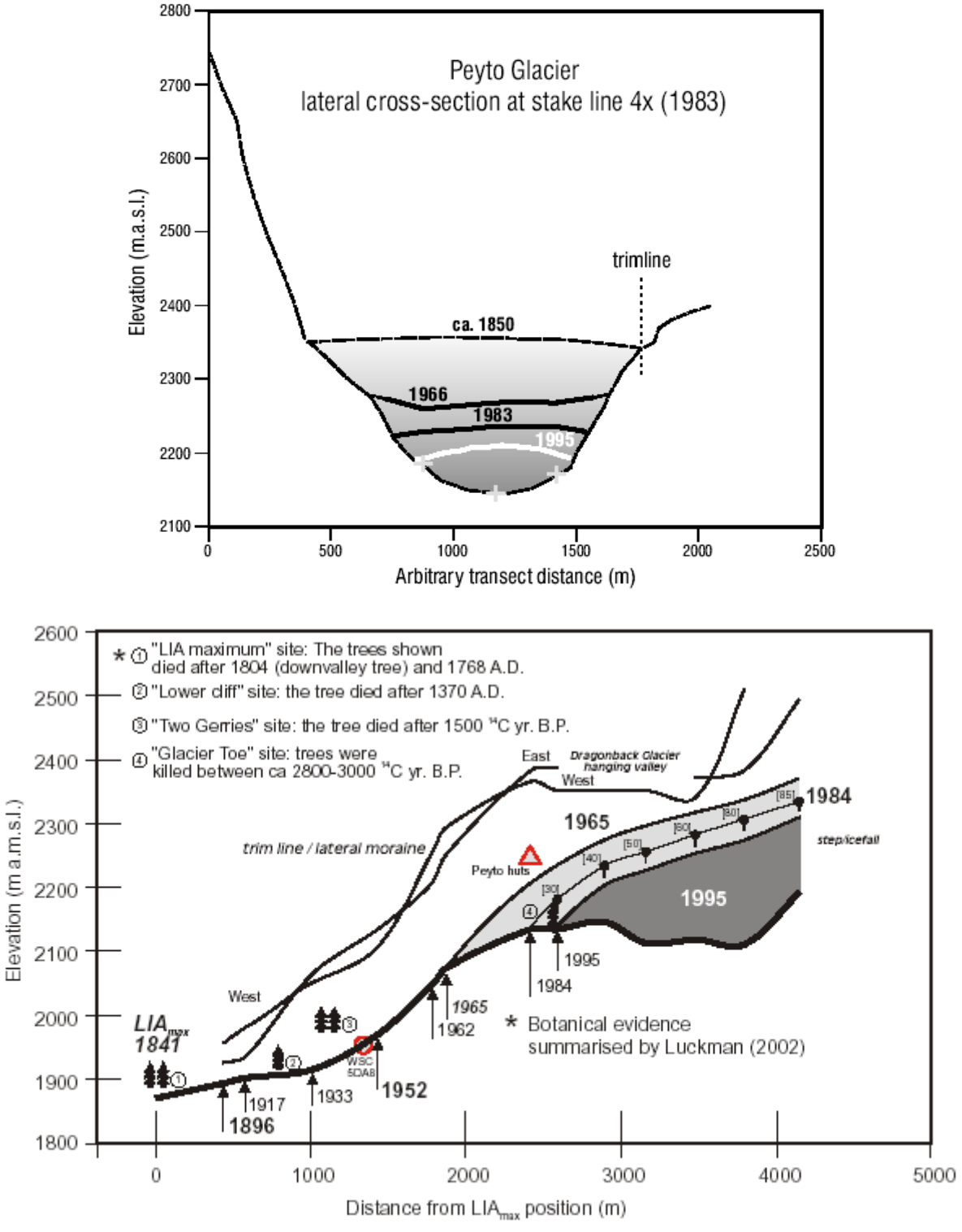

Figure 7 - Typical ice surface and bedrock cross-section profiles for Peyto Glacier below 2550 m a.s.l. referenced to the Little Ice Age maximum lateral moraines and trimlines, and front positions. The location of "stake line 4x" in the lateral cross-section corresponds to "[40]" in the length-wise cross section (after Demuth, 1996 and Demuth *et al*., 2002).

Haeberli (1990) notes that the mass loss of small mountain glaciers globally was most apparent during the first half of the century 20th Century, followed, in mid-century, by a period of more modest losses and even occasional sustained mass gains in the 1970s and early 1980s. This general pattern is consistent with observations for the Cordillera (Meier and Tangborn, 1965; Young, 1981; Luckman *et al*., 1993; IAHS(ICSI)/UNEP/UNESCO, 1996). In association with the aforementioned pattern, the data shown in Figure 8 provide a perspective on the relative rate of change of the energy associated with glacier melting for Peyto Glacier [i.e., over a period of approximately 1 century, a ΔB_n of 1 dm w.e. $a^{-1} \approx \equiv 1$ W/m^2 (Haeberli and Hoelzle, 1995; Oerlemans 1994)].

More recently, particularly since the mid-1970s, the rate of mass loss for Peyto Glacier shows signs of re-attaining early-century values, notably at a rate broadly consistent with estimated man-induced radiative forcing (2-3 W/m^2: IPCC, 1992; UNEP, 1994). Moreover, data in IAHS(ICSI)/UNEP/UNESCO (1996) point to such an increase being synchronous for many regions of the globe (primarily moderate latitude maritime and continental regions). Interestingly, the drastic early-century variations took place during relatively weak anthropogenic forcing.

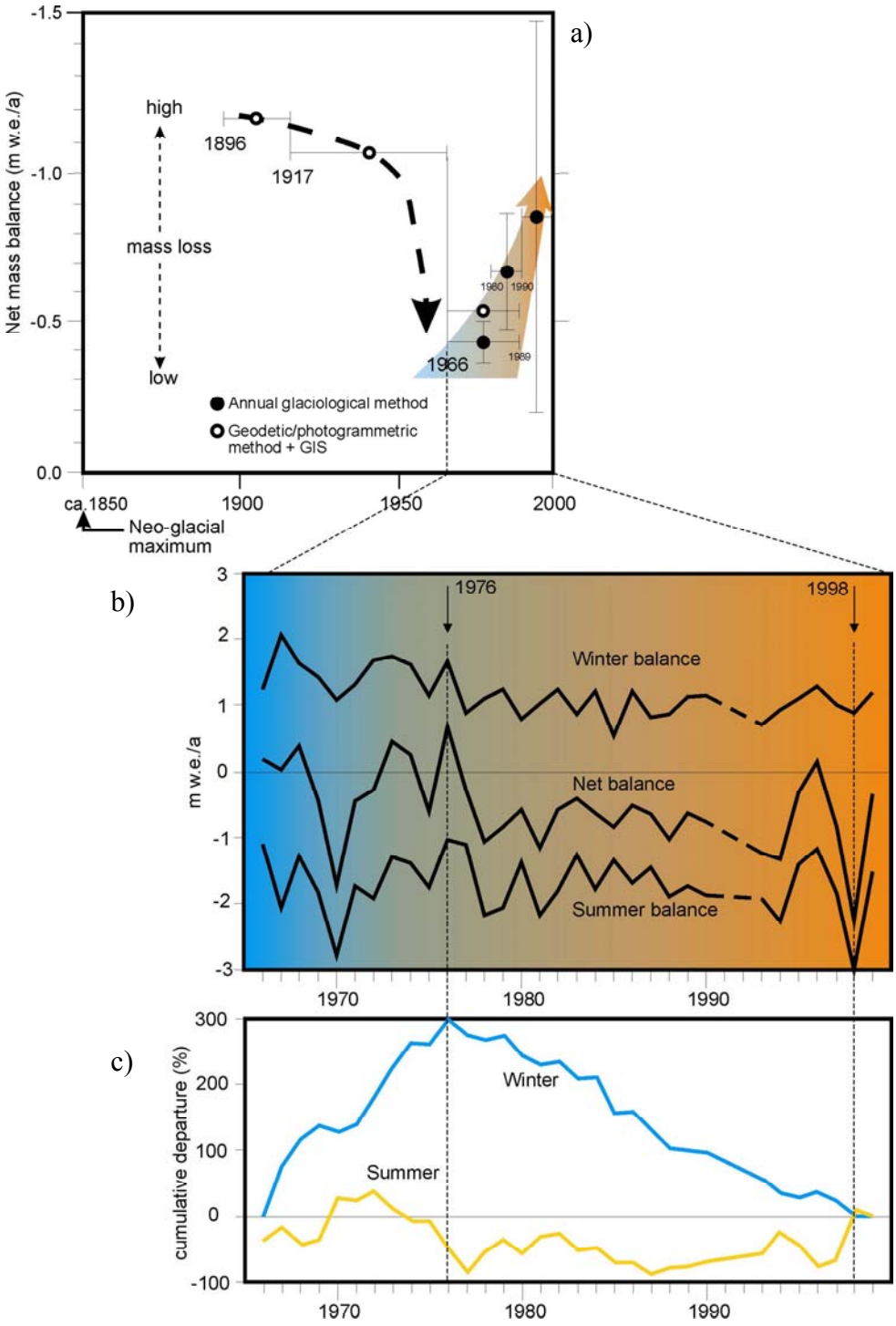

Figure 8 - a) past-century and recent decadal variations in the energy flux associated with glacier melting as indicated by glacier mass balance (<u>negative</u> B_n plotted <u>up</u>). Geodetically-determined estimates adapted from Wallace (1995; from 1896-1917-1966), Glenday (1991; from 1966-1989) and Demuth and Keller (2002). Vertical fiducia, where applicable, represent ± one standard deviation; b) mass balance data includes that determined for the glacier since 1995 and c) the associated residual mass curve analysis.

Relevant to concerns of possible greenhouse warming, the average net balance change (ΔB_n) can be related to the mean annual air temperature change (ΔT) using the Oerlemans and Fortuin (1992) model:

$$\Delta B_{(1K)} = -0.512 - 0.662 \log_{10}(P)$$

and

$$\Delta T \approx 1K \frac{\Delta B_n}{\Delta B_{(1K)}}$$

where $\Delta B_{(1K)}$ is the mass balance response to a 1K change in the mean annual air temperature and P is the mean annual precipitation averaged over the glacier.

Assuming that P remains constant (approximately 1.6 m w.e. a^{-1}; see Demuth and Keller, 2002, page 87) and that Peyto Glacier was in steady state (i.e., zero mass balance) in the mid 1960s, a ΔB_n = - 0.5 m w.e. a^{-1} for Peyto Glacier corresponds to a $\Delta T \approx$ + 1.3 K. Several cautions are warranted: i) precipitation is not constant; ii) the modelled temperature change does not account for the influence of glacier dynamics and so ΔB_n will also reflect, in part, a change in the elevation of the glacier surface. Sapiano *et al*. (1998) and Rabus and Echelmeyer (1998) expressed such prudence while determining such *temperature derivatives* for the net balance change of several other glaciers in the Cordillera. While the above assumptions may limit the absolute usefulness of such derivatives, it is interesting to note that the estimated temperature increase since the 1960s is consistent with the mean annual regional temperature anomaly documented for the central Canadian Rockies (e.g., Luckman *et al*. 1998).

4.2 Spatial and Temporal Coherence of Recent Glacier Fluctuations Regionally

Commensurate with the results shown earlier (the dominant role of winter balance in manifesting a post-1976 monotonic pattern of negative net mass balance), a portion of the analysis and discussion is devoted to examining variations in the winter climatology for the region. We begin from the point-of-view of establishing the spatial coherence of mass balance variations. Notwithstanding work by Yarnel (1984a), links to synoptic climatology are established through several studies, which allow an instructive examination of the frequency of winter

precipitation/non-precipitation atmospheric circulation patterns over the Canadian Cordillera (e.g., Brown and Braaten, 1997; Keller, 1997; Moore and McKendry, 1996; Bitz and Battisti, 1999; Moore and Demuth, 2001). This will illustrate to what extent the events documented for Peyto Glacier are typical of those for other glaciers in western Canada and the North-West United States.

Numerous ocean-atmosphere studies point to a coherent variation in the Pacific-North-American (PNA) atmospheric circulation pattern (a system of ridges and troughs influencing the zonal flow of moisture-laden air across the Cordillera) and the El Niño Southern Oscillation (ENSO) [e.g., Cayan and Peterson, 1989; Trenberth, 1990; Ebbesmeyer *et al.*, 1991; Gutzler and Rosen, 1992 and Trenberth and Hurrell, 1994]. These studies have firmly demonstrated the influence of variations in PNA atmospheric circulation on snowfall, streamflow and temperature in the western half of North America. Notably, the collective evidence reported herein and in the available literature supports the suggestion by Aguado *et al*. (1990) and Cayan (1996) that inter-annual variability of accumulation, as influenced by large-scale atmospheric circulation during the continuous snow cover period, is coherent over scales of at least several hundred kilometers. Decadal variability of accumulation appears to be coherent over much larger distances.

A comprehensive spatial and temporal analysis (principal component analysis; see Brown, 1996) of Winter snow depth and snow cover duration for Canada, by Brown and Braaten (1997), points to a significant mid-1970s shift to lower values for a region extending from the western Canadian prairie, well into the inner and coastal montane of British Columbia (peronsal communication R. Brown; Brown and Goodison, 1996). While the station distribution is strongly biased to lower elevations it is likely that the response to synoptic-scale variations in atmospheric circulation would be similar for the higher elevations (e.g., Keller, 1997). Notably, Figure 9 illustrates the close relationship between the variation of Peyto Glacier Winter balance and that of integrated snow depth for stations in the western prairie and eastern slopes.

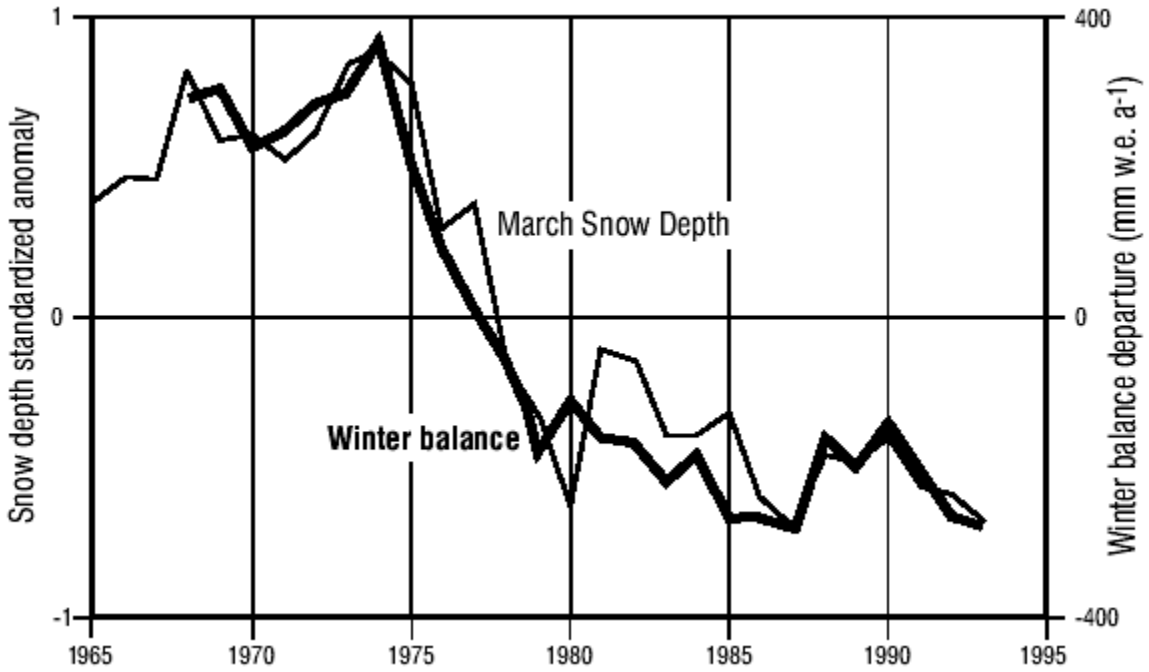

Figure 9 - Five-year moving average (centred) of March snow depth fluctuation for the Canadian eastern slopes/western prairies (1955-1995 series adapted from Brown and Braaton, 1997) and winter balance departure from the 1966-1995 mean for Peyto Glacier (after Demuth and Keller 2002).

In an examination of winter snow pack anomalies for British Columbia, Moore and McKendry (1996) report corresponding shifts of dominant atmospheric circulation types and net winter accumulations (as at April 1). 1976 was identified as the cut-off between a period of relatively heavy winter precipitation and one that was characterized by lighter winter accumulations. Moreover, a significant north-south spatial variation was identified in which winter accumulations were generally heavier in the south and lighter in the north from 1966-1976. A reversal of this spatial pattern was occurred during the period 1977-1992. Moore and McKendry went on to illustrate the association of these anomalous spatial and temporal snow pack variations with decadal shifts in atmospheric circulation over the North Pacific. A post-1976 reduction in the frequency of broad zonal flow patterns and a synchronous increase in the frequency of southwesterly upper-level flows was detected.

Keller (1997) investigated variations of winter maximum snow pack for the northeastern cordillera and boreal montane, and found a concomitant pattern in the frequency of synoptic-scale 'snow' and 'non-snow' atmospheric circulation patterns. Applying a precipitation

efficiency index for several snow course/meteorological stations and a Kirchhofer classification (e.g., Yarnel, 1984b) of gridded surface and 500 mbar atmospheric pressure fields over western Canada, Keller (1997) identified numerous key winter (defined as November 1 - March 31) atmospheric circulation types. Frequency analysis led to the conclusion that after 1976, a significant shift towards increasing frequency of non-snow producing atmospheric circulation patterns had occurred. Correspondingly, a synchronous decrease in the frequency of snow producing weather patterns was detected (Table 2). Keller (1997) detected a reversal of this pattern after 1988.

Table 2 - Frequency of 50 kPa level synoptic type categories (1947-1992) in percentage of days in winter: November 1 – March 31 (after Demuth and Keller, 2002).

Synoptic Type @ 50 kPa level	**Timing increase↗ decrease↘**	**Mean 1947-1976 (%)**	**Mean 1965*-1976 (%)**	**Mean 1977-1988 (%)**	**Mean 1989-1992 (%)**	**α**
Non-snow	1976↗ 1988↘	44.8	46.0	57.1	40.7	95%
Snow	1976↘ 1988↗	55.3	54.1	43.1	59.4	95%

* Initiation of mass balance record (winter balance during 1965-1966)

Typical non-snow atmospheric circulation patterns influencing the central Rocky Mountains include the presence of a dominant high pressure system over the Canadian Rocky Mountains and/or a low pressure center lying well to the northeast of the continental divide, inducing the circulation of cold, dry Arctic air over the eastern slopes. Typical snow producing atmospheric circulation patterns involve a broad zonal flow of moist maritime air from the Pacific Ocean or the circulation of moisture-laden air from the Pacific Ocean about a dominant low pressure centre lying just offshore of the Canadian/United States west coast.

The change in the frequency of the synoptic patterns during the mid-1970s parallels a documented shift in the position of the Aleutian Low and its influence over the tracking of snow-bearing weather systems. This effect can be especially strong during the E1 Niño phase of the Southern Oscillation (Trenberth, 1990; Tanimoto *et al*., 1993; Miller *et al*., 1993; Wang, 1995). From 1977 to 1988, the Aleutian low-pressure system was deeper and shifted eastward, producing anomalously warm southwesterly flow over the northeastern Pacific. This configuration corresponded to an intensification of the PNA pattern, which has been shown to

produce generally lighter snow packs over British Columbia and Alberta (Moore and McKendry, 1996; Keller 1997). Trenberth and Hurrell (1994) noted the anomalous North Pacific circulation ended in 1988 with the onset of a strong La Niña event.

The Pacific Decadal Oscillation (PDO; e.g., Mantua *et al*., 1997), has been associated with North Pacific climate variability and the advection of moisture over the Cordillera (Bitz and Battisti, 1999; Moore and Demuth, 2001). Defined by sea surface temperature anomalies for the Pacific Ocean Basin poleward of 20° N, the PDO appears to modulate climate over similar spatial scales as ENSO, but over markedly different temporal scales. It has been described as a "long-lived El Niño-like" pattern with a persistence of some 20-30 years as compared to typical ENSO persistence of 1 ± 0.5 years (Bitz and Battisti, 1999).

The relationship between PNA circulation anomalies (for the period November 1 - March 31), the PDO (November 1 - March 31) and the winter balance of Peyto Glacier is remarkably clear (Figure 10), with the 1976 breakpoint identifying a shift from a PDO cool phase to the present warm phase. Examining data describing precipitation and temperature anomalies for the Central Canadian Rockies (e.g., Luckman *et al.*, 1998) and North Pacific sea surface temperature and windstress (e.g., Bitz and Battisti, 1999), the PDO warm phase appears to manifest meridonal flow of dryer air into the Cordillera in winter and generally warmer summers. The cold phase appears to correspond with the strong advection moisture over the Cordillera in winter, and summers that are generally cooler. Notably, other glacier mass balance time series for the Cordillera also point to a mid-seventies shift in net balance, again, predominantly associated with the variations in winter balance manifested by PDO/PNA sea surface temperature/atmospheric circulation anomalies (e.g., south Coast Mountains of British Columbia and the northern Cascade Mountains of Washington (McCabe and Fountain, 1995; Moore and Demuth, 2001).

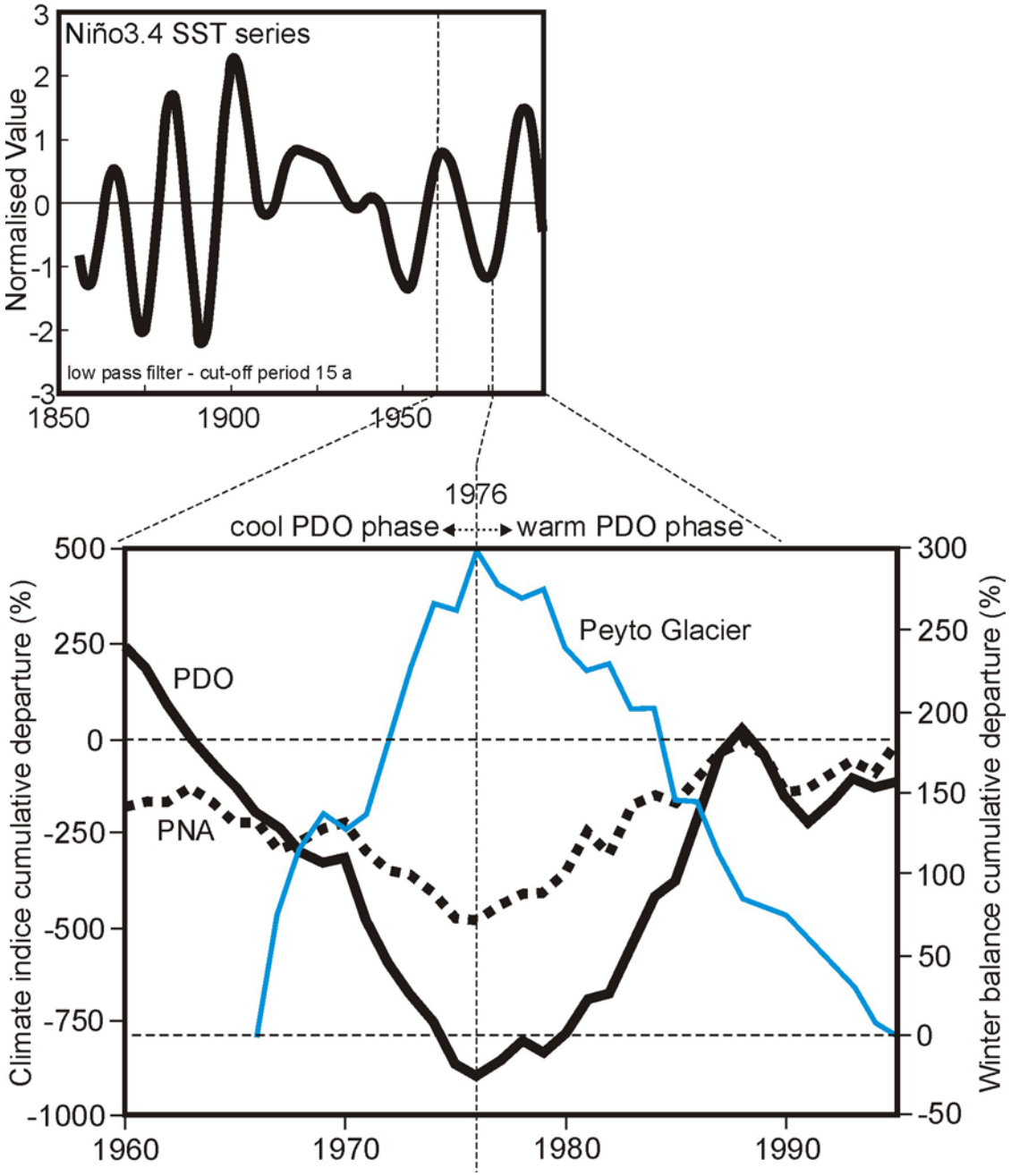

Figure 10 - November-March PNA and PDO climate indice and winter balance regime shifts expressed as cumulative departures. The Niño3.4 SST series is after Kaplan et al. 1998.

The causes of such large spatial and sudden temporal shifts in the sea surface temperature (PDO) and atmospheric circulation (PNA) are not yet completely understood. However, if the causal factors are related to atmosphere-ocean processes adjusting to new equilibria over scales of a decade or more, then their impacts could be predicted for time scales useful for water resource and aquatic ecosystem management. Moreover, the instrumental record (e.g., air temperature)

for the Central Canadian Rockies extends back to the late 1880s (e.g., Luckman *et al*., 1998). Coupled with the strong PDO relationship to winter balance variability (PDO record extends back to 1890), it should be possible to reconstruct the seasonal and net mass balance time series back to the time when Walter Wilcox first photographed Peyto Glacier in 1896.

To summarise:

-The advection of moisture over the Cordillera is determined, in part, by North Pacific climate variability and the influence of the Pacific Decadal Oscillation (PDO). The PDO is defined by sea surface temperature anomalies for the Pacific Ocean Basin pole-ward of 20º N. The PDO appears to modulate climate over similar spatial scales as the El-Niño Southern Oscillation (ENSO), but over markedly different temporal scales. It has been described as a "long-lived El Niño-like" pattern with a persistence of some 20-30 years as compared to typical ENSO persistence of 1 +/- .5 a.

-The relationship between the PDO and its capacity to manifest anomalous Pacific North American (PNA) circulation and related Peyto Glacier winter mass balance and regional snow accumulation variability is remarkably clear, with the 1976 breakpoint identifying a shift from a PDO cool phase to the following warm phase.

-Examining data describing precipitation and air temperature anomalies for the Central Canadian Rockies and North Pacific sea surface temperature, the PDO warm phase appears to manifest meridonal flow of dryer air into the Cordillera in winter and generally warmer summers. The cold phase appears to correspond with the strong advection moisture over the Cordillera in winter, and summers that are generally cooler.

-The change in the frequency of snow vs non-snow bearing synoptic patterns during the mid-1970's parallels a documented shift in the position of the Aleutian Low and its influence over the tracking of snow-bearing weather systems. This effect can be especially strong during the E1-Niño phase of the Southern Oscillation . From 1977 to 1988, the Aleutian low-pressure system was deeper and shifted eastward, producing anomalously warm south-westerly flow over the northeastern Pacific. This configuration corresponded to an intensification of the PNA pattern,

which tends to produce generally lighter snow packs in the southern Cordillera and the western Prairies.

The previous analysis and discussion attended mass and volumetric considerations, and to some degree, site specific (Peyto Glacier) margin variations, in relation to energy and moisture fluxes, and regional climatology. Next, we illustrate the variation of the glacier margins regionally.

4.3 Regional Glacier Fluctuations in the Upper North Saskatchewan River Basin

To provide a quantitative regional perspective of the variation of glacier cover we delineated glacier extents using earth observation data for two of the reference headwater catchments (Mistaya and Siffleur, Figure 2). For these two small catchments, it was deemed problematic to digitise the available paper maps or use vectors from the digital NTS database, since it has been our experience that areas of known perennial snow and ice are often missing from these sources. Glacier extents for the mid-19th (Neoglacial maximum or "Little Ice Age" maximum; ca. 1850) and 20th centuries were therefore delineated from aerial photography acquired in the early 1950s for the Canadian Glacier Inventory (CGI) project (e.g., Ommanney *et al*., 1973; Ommanney, 1980). For each catchment, an ortho-photo mosaic was created. The photography was ortho-rectified (within PCI Orthoengine) using Ground Control Points (GCPs), and a DEM for the region (BCTrim, 1986). GCPs were collected from 1:50 000 NTS map sheets. LandSat 5 TM imagery was acquired for 1991 and ortho-rectified using GCPs, satellite ephemeris data and the same DEM (Figure 11).

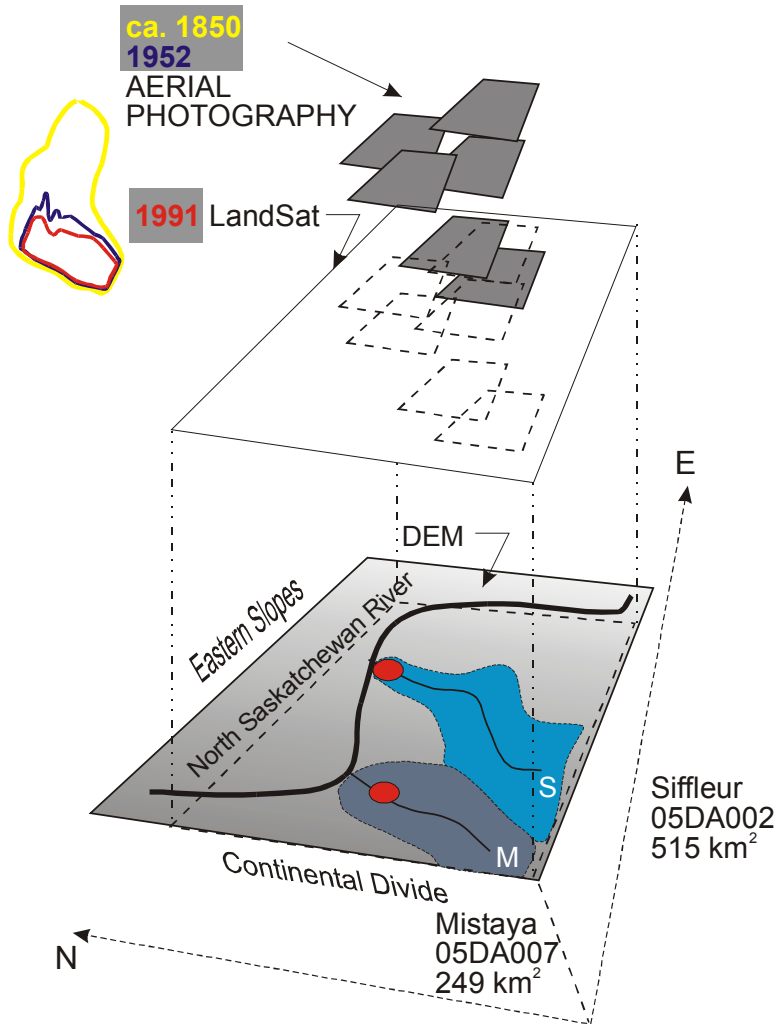

Figure 11 - Schematic illustrating the method of extracting geo-referenced thematic data from Canadian Glacier Inventory photography and earth observation data (LandSat 5 TM).

From these rectified and geo-referenced sources, glacier cover extend was demarcated using a combination of automatic and manual methods within a GIS framework (PCI). Some guidance to the mid-20th century extent delineation was provided by the CGI record, while that for the Neoglacial maximum stage was derived, where possible, from the configuration of lateral and end-moraine complexes and trim lines.

Figure 12 illustrates the reduction of glacier cover in the reference research catchments since the Neoglacial maximum. Relating the glacier perimeter to the glacier area, in part, illustrates the sensitivity of glacier size to regional climate forcing. For the Mistaya catchment for example, we illustrate the rate of change over the three time slices, of the largest and smallest glaciers in

the sample (see the coloured fiducia in Figure 12). It is postulated, in related work being conducted by the authors, that as glaciers reach some threshold according to their perimeter-area characteristic, surface albedo-energy balance feedback begins to dominate the local climate-mass balance-margin variation response. An analogue to this is the role of *patchiness* during snow cover melting and the advection of energy from the lower albedo regions surrounding the snow patches (e.g., Neumann, 1999). This variation has been described using fractal statistics (e.g., Schook, 1993), which may, in part, contribute towards projecting future glacier cover extents.

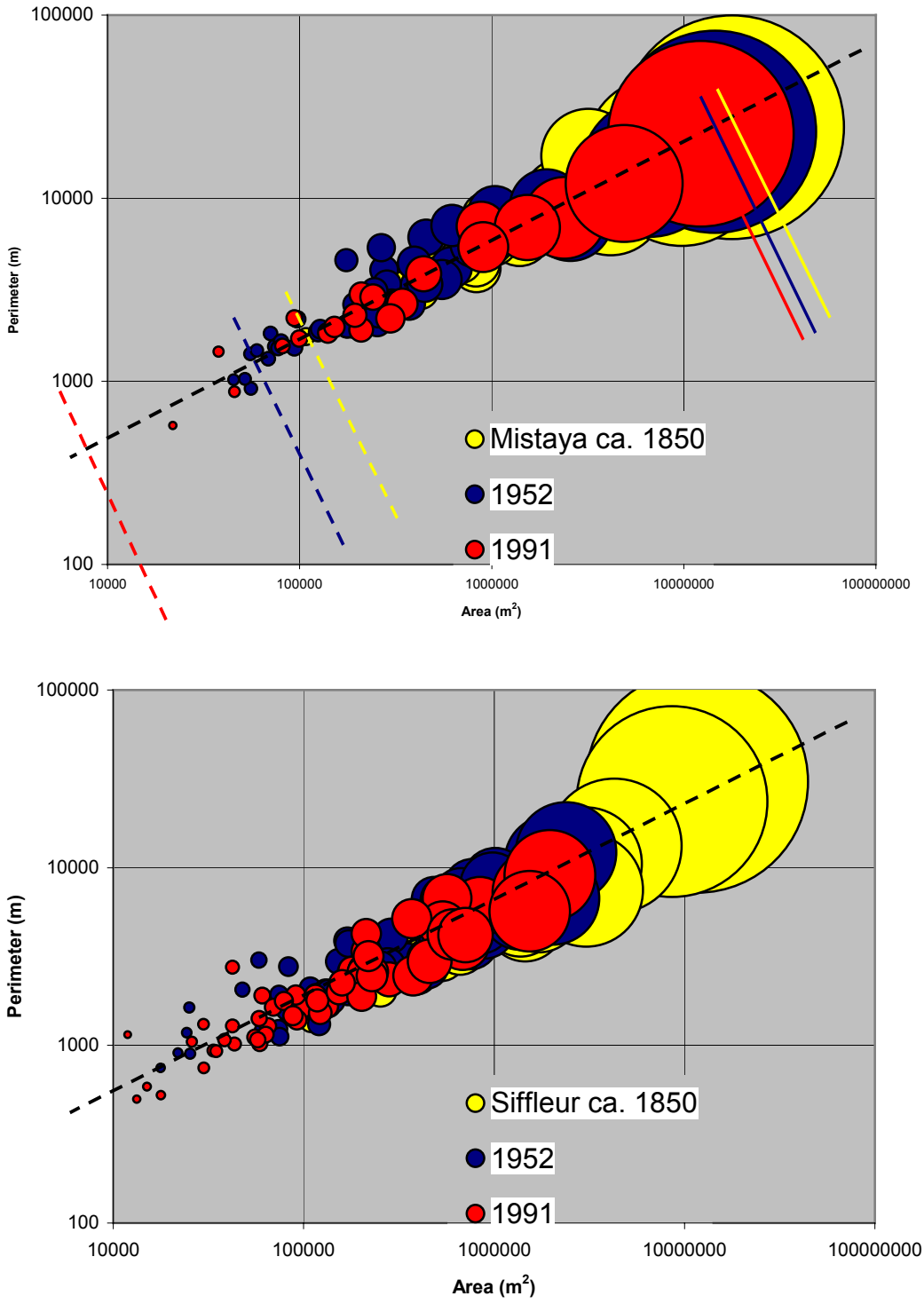

Figure 12 - Glacier cover in the Mistaya and Siffleur catchments for the Neoglacial maximum stage (ca. 1850), 1952 and 1991. Glacier area is also represented by the diameter of the data point (circle) for each location. Coloured fiducia illustrate the rate of change of the largest and smallest glaciers over the time period considered in the sample.

In addition to the time slices noted above, more recent data (1998) is derived from the land cover classification of LandSat imagery acquired for the hydrological modelling work detailed later in the report (Table 5). Table 3 and Figure 13 summarise the change in the extent of glacier cover for each of the four time slices.

Table 3 - Past-century percentage glacier cover for the reference study catchments

Catchment % glacier cover	ca. 1850	1952	1991	1998
Mistaya River bounded by 05DA007	24.6	14.8	10.3	7.2
Siffleur River bounded by 05DA002	11.7	5.2	3.3	2.15

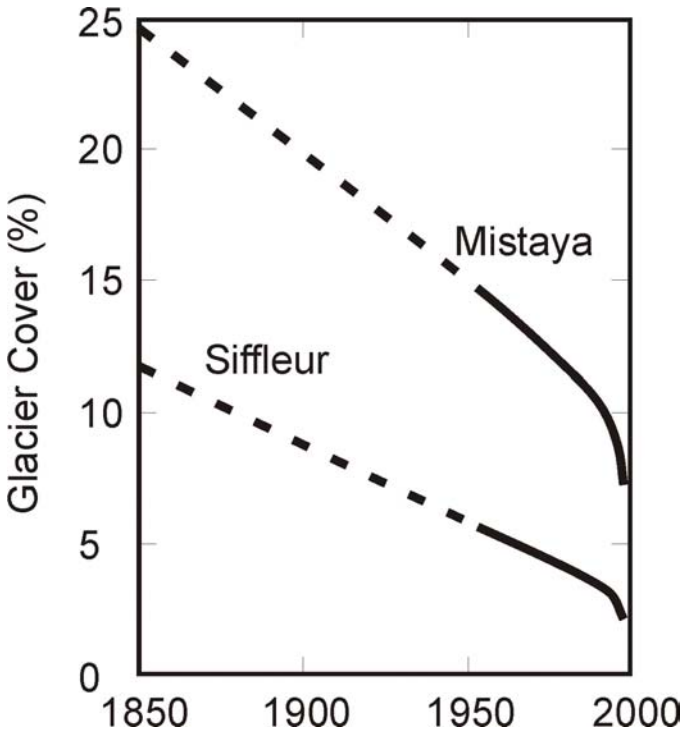

Figure 13 - Past-century percentage glacier cover for the reference study catchments.

Data in Table 3 and Figure 13 suggest a recent regional acceleration in the rate of glacier contraction, though, as previously described, data sources used for extracting glacier cover extent varied. Planimetric checks using more recent photography coincident with the LandSat imagery, however, reveal that the methods and thematic data extracted from these sources are relatively homogenous over the end points considered by the analysis. The planimetric checks were

performed over the full range of glacier sizes represented in the data set. The aforementioned acceleration is likely due to the response of the numerous smaller ice masses in the region. The changes in the secular size-distribution changes for the region are under investigation.

In Figure 13 we dashed the trend lines from the Neoglacial maximum extent to the mid 20th-century extent since this one-century interval may alias intervening margin variations. Valuable perspective for this interval is provided for, however, from the margin observations and geo-botanical data represented in Figure 7 (Peyto Glacier). For example, wood samples collected near the terminus of Peyto Glacier ("Glacier Toe" site; killed ca. 2800-3000 ^{14}C years B.P.) may have originated from a small stand of forest surrounding a lake that may have occupied the obvious over deepened valley (Figure 7; between 3600-3900 m along the length-wise cross-section) currently occupied by ice (personal communication G. Holdsworth). If we assume Peyto Glacier can represent an anologue for the variation of glaciers in the upper Saskatchewan River Basin, we conclude that the extent of glacier cover is rapidly approaching the warm limit of Holocene variability (see also Luckman *et al*. 1993; Luckman, 2002) and that the documented past-century and recent losses in glacier mass and extent are unprecedented in the last several millennia.

We now turn our attention to quantifying the impacts of the changes since the mid-1900s on the hydrological regime of the upper North Saskatchewan River Basin.

5. Analysis and Discussion: Hydrological Regime Shifts and Glacier-Climate Attribution

5.1 Parametric Statistical Analysis of Streamflow Trends

We investigated the influence of changing glacier cover and corresponding meltwater contributions by conducting simple statistical trend analysis of basin yield, precipitation and streamflow for the Mistaya and Siffleur catchments. As previously introduced, we examined the Transition to Base Flow season, thereby concentrating the statistical power from the variance ascribed to glacier melt contributions. Reference mass balance data, snow course data and anecdotal evidence allowed us to identify years when high antecedent snow cover conditions may dilute the contribution of glacier meltwater to the variance in the streamflow records.

Initially, both the Mistaya and Siffleur river streamflow records were examined. However, because of the relatively short period of record for the Siffleur (initiated in 1977), we concentrated our parametric analysis efforts using the Mistaya record (initiated in 1950). Figure 14 illustrates the yield from the Mistaya catchment for the period of study. The trend line shown includes all data and depicts declining yields for the Transition to Base Flow period despite evidence that precipitation in the montane is increasing for the same period (Aug 1 – Oct 31). The coefficient of variation (standard deviation/mean) for the streamflow (Figure 14) is increasing over the available record suggesting that the ability of the glacier cover to regulate streamflow may have been in decline since the mid-1900s.

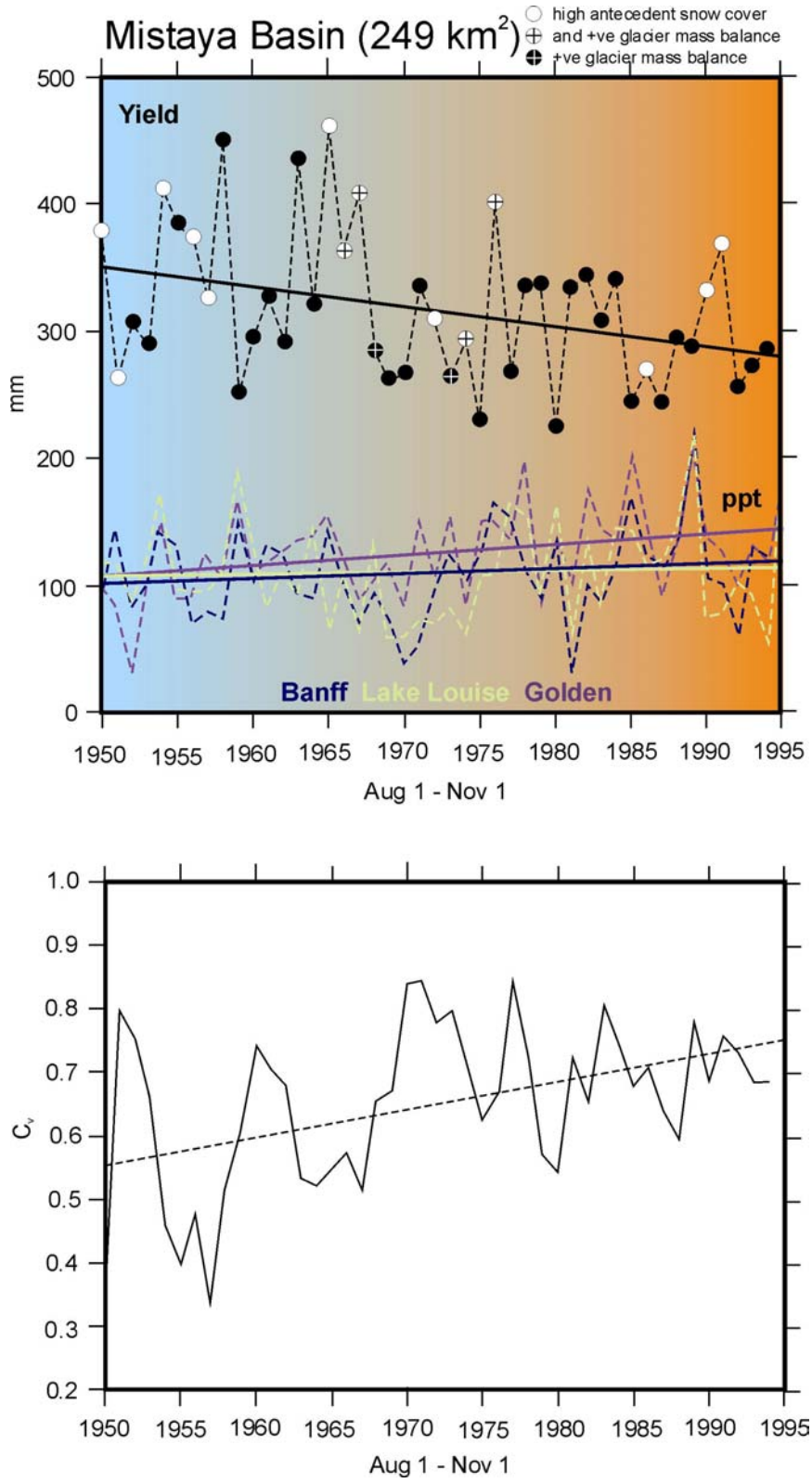

Figure 14 - Yield, precipitation and streamflow coefficient of variation (C_v) for the Mistaya River catchment at gauge 05DA007 over the TBF period.

We also examined the stream flow regime using the minimum, mean and maximum daily discharge data available from the Water Survey of Canada (Environment Canada, 2000). The TBF change for the Mistaya basin (1950-1998) is quantified using a simple linear regression analysis. The regression results are depicted in

Figure 15. We find there is a significant decreasing trend in the mean (r^2=0.33) and minimum (r^2=0.43) TBF time series, and a weaker increasing trend in the maximum (r^2= 0.02) TBF time series (Figure 15).

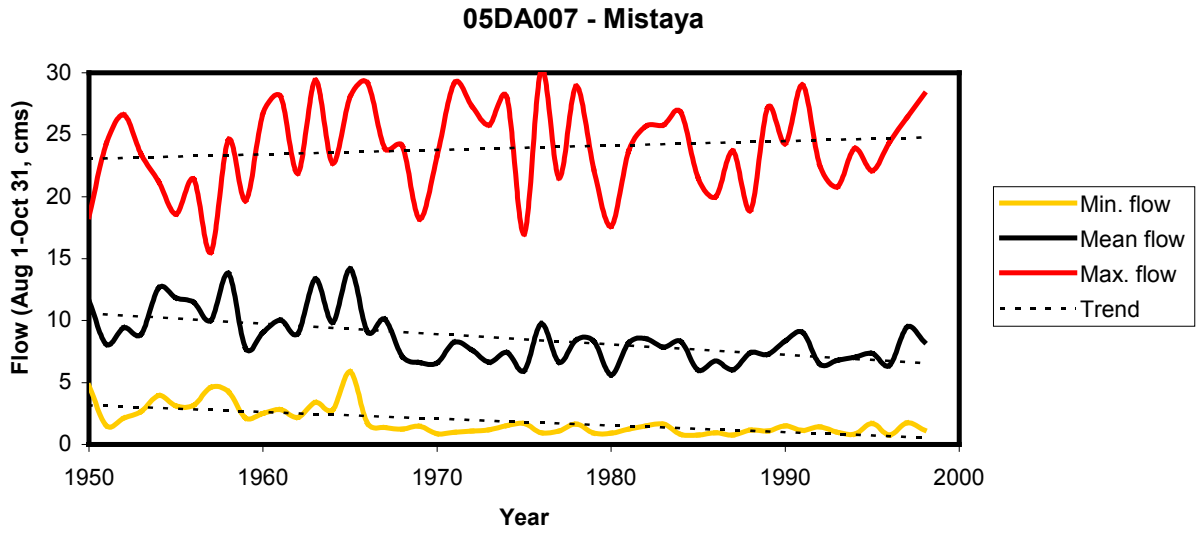

Figure 15 - Regression analysis for TBF flow period showing trends in minimum, mean and maximum flows for the Mistaya Basin.

The total change in minimum, mean and maximum streamflow for the 49 year period of analysis is - 2.67, - 4.12 and + 1.78 $m^3 \cdot s^{-1}$ respectively. Using 1950-1960 as a reference period, this change is normalised using:

$$\Delta\overline{\overline{Q_{N_y}}} = \frac{m\, N_y}{\langle Q \rangle_{ref}}$$

where m is the slope of the regression model, N_y is the number of years of observation, and $\langle Q \rangle_{ref}$ is the average flow for the reference period. The normalised change for minimum, mean and maximum flows is presented as a percentage in Table 4.

Table 4 - Regression analysis for minimum, mean and maximum TBF time series, Mistaya River gauge 05DA007.

	Minimum	**Mean**	**Maximum**
Average streamflow 1950-60 ($m^3 \cdot s^{-1}$)	3.23	10.56	21.37
Average streamflow 1950-98 ($m^3 \cdot s^{-1}$)	1.87	8.59	23.92
Change 1950-1998 ($m^3 \cdot s^{-1}$)	-2.67	-4.12	+1.78
Normalised **%** change from 1950-1960 ref.	**-82.7**	**-39.0**	**+8.3**

Our initial inference is that significant reductions in the mean and minimum flow regimes and increasing flow variability are the result of extensive glacier contraction to the degree that glacier melt contributions during dry periods, notwithstanding high antecedent snow cover conditions, have been in decline over the period of observation. Notwithstanding that precipitation records more representative of the reference study catchment are unavailable, support of the aforementioned attribution is provided by indications from more distant, but never-the-less montane, locations, which show a modest increase in precipitation for the TBF season.

Interesting is the modest increase in the maximum flow regime. For a glacierised region subject to conditions that encourage long-term net mass wastage and glacier contraction, the firn pack of the high alpine will also become progressively more depleted (Braun and Escher-Vetter, 1996; Demuth and Moore, 2001). The reduction in firn pack may predicate an amplification in the diurnal fluctuations of discharge and reduce the lag times associated with the transport of liquid precipitation and surface meltwater over and through the glacier (e.g., Collins, 1989; Schuster and Young, 2002). Moreover, previously discussed evidence indicates glacier nourishment has diminished substantially over the last several decades, imparting a long-term increase in the rate of annual glacier ice exposure and related reductions in surface albedo (annual snow-line ascension; unpublished data, MND).

5.2 Non-parametric Statistical Analysis of Hydro-meteorological Variables

The superposition of melt sources and the multiplicity of factors influencing their timing and magnitude, contribute to the low signal to noise ratio often exhibited in lower-catchment hydrometric records. Moreover, hydro-meteorological time series often contain gaps and do not meet conditions for normality (requisite for *parametric* statistical analysis). As an extension of the parametric streamflow trend analysis presented above, we apply a range of non-parametric

uni- and multi-variate statistical analysis useful for identifying the magnitude and timing of shifts in hydrological time series, their significance and their attribution. In particular, we examine minimum, mean and maximum streamflow time series for both TBF and annual periods. This analysis also considers a broader network of contributing catchments than the reference study catchments described earlier (i.e., study area is bounded by Rocky Mountain House, Alberta). The study also conducted non-parametric analyses of numerous meteorological and glacier mass balance variables in association with the attribution of streamflow variability (see Technical Appendix A[4]; separate from the master report document). A selection of these more comprehensive results will be discussed.

For this component of the investigation, a trend analysis using the Kendall Test is used. The Kendall Test is a non-parametric test that looks at the sum of positive or negative trends for the time series being examined (for example, river discharge). The equation is given as:

$$S = \sum_{k=1}^{n-1} \sum_{j=k+1}^{n} sign\left(X_j - X_k\right)$$

In conjunction with the trend analysis, the same variables were tested for shifts in the mean. The procedure was based on the application of two statistical tests. The first is a Bayesian analysis of the time series information. This test can be best described as one that assesses the maximum likelihood of two distributions being different. The statistical model examines the time series X(1)…X(n) where n is the sample size, and defines a date of change τ, where the time series is divided into two sub series, T1 before τ and T2 after τ:

T1: $X(1), X(2), X(3), ..., X(\tau) \sim N(\mu_1, \sigma)$

T2: $X(\tau+1), X(\tau+2), ..., X(n) \sim N(\mu_2, \sigma)$

A likelihood estimate for τ results in an estimate of the most probable year of change. If $\tau = n$ then no change is detected. The amplitude of the shift is estimated by the difference in the

[4] Technical Appendix A, PARC P55 – Demuth and Pietroniro, Non-parametric Statistical Analysis of Hydro-meteorological and Glacier Mass Balance Data: Headwaters of the North Saskatchewan River Basin.

means ($\mu_2 - \mu_1$). Second, a Wilcoxen Test for shift in the mean is applied on the same time series using the Bayesian estimate for the year of most probable shift. The Wilcoxen test is a non-parametric statistic that tests the difference in means for T1 and T2. This is a basic non-parametric test that is equivalent to the well-known parametric t-test. In this case the two samples (before and after τ) are ranked. Under the null hypothesis of no differences in means, the ranks are expected to be the same. The test statistic is simply given as:

$$W = \sum_{i=1}^{n1} Ri$$

The river discharge time series data used in the analysis are for the headwater stream flow gauging stations in the North Saskatchewan River Basin. The data were derived from existing Water Survey of Canada records (Environment Canada, 2000). This study examined the minimum, maximum and mean streamflows estimated for the annual and *transition to base-flow* (TBF) periods. The streamflow stations for which time-series data were derived are listed in Table 5. Their locations within the watersheds are noted in Figure 16.

Table 5 - Streamflow stations used in statistical analysis.

STATION NAME	ID	Area km^2	Latitude	Longitude	Period of Record	Glacier Cover % *
North Ram River at Forestry Road	05DC011	343	52° 16' 55"	-115° 59' 30"	1975-1998	0.00
North Saskatchewan River at Saskatchewan Crossing	05DA006	1290	51° 58' 00"	-116° 43' 30"	1951-1970	15.64
North Saskatchewan River at Whirlpool Point	05DA009	1920	52° 00' 06"	-116° 28' 10"	1970-1998	2.09
Siffleur River Near the Mouth	05DA002	521	52° 02' 39"	-116° 23' 02"	1975-1996	2.15
Mistaya River Near Saskatchewan Crossing	05DA007	249	51° 53' 04"	-116° 41' 17"	1950-1998	7.21

* based on supervised classification of 1998 LandSat 5 TM imagery (Annex B3 Generating Land Cover Data).

Daily minimum, mean and maximum air temperature and daily total precipitation (rainfall + snowfall) records from six meteorological stations were also analyzed. The total precipitation was also analyzed on a monthly and seasonal basis (i.e. from June to July and from August to

November). Table 6 indicates the location and elevation of the meteorological stations in relation to the study basins. Since the trend/shift analysis was performed on annual and seasonal time series, the annual and seasonal averages were calculated for the minimum, mean and maximum temperatures from the daily records.

Table 6 - Meteorological stations used in statistical analysis.

Station ID	Station Name	Latitude	Longitude	Elevation (m)
3050520	Banff	51° 18'	-115° 57'	1384
3053760	Lake Louise	51° 43'	-116° 22'	1524
3015520	Rocky Mountain House	52° 38'	-114° 92'	1015
3053520	Jasper	52° 88'	-118° 07'	1062
1172870	Field	51° 38'	-116° 48'	1239
1173210	Golden	51° 30'	-116° 98'	785

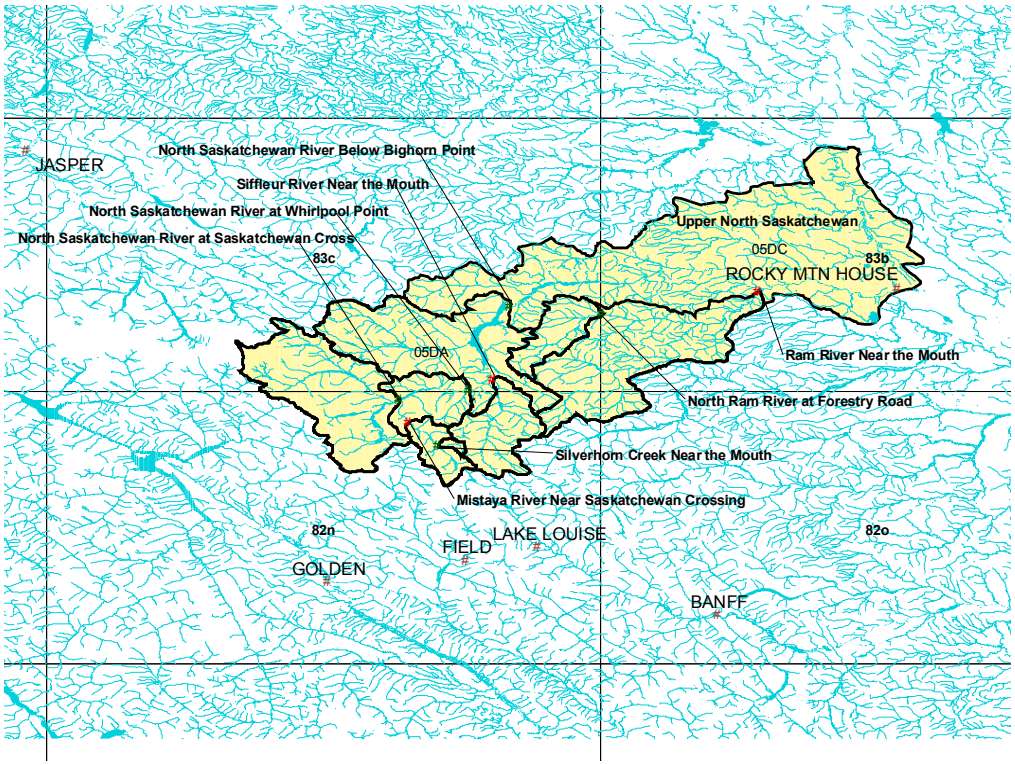

Figure 16 - Location of streamflow and meteorological stations used in the statistical analysis.

Missing data was noted for the temperatures and the precipitation time series information. Consequently, in addition to the years with no data at all, some years were left out when the percentage of missing data (calculated on the annual and seasonal basis) was judged to be too high.

Table 7 gives a complete list of the years of data retained for each station and for each variable, except for the stations Rocky Mountain House (3015520) and Field (1172870) which present complete records over the periods 1945-1977 and 1923-1936 respectively. By examination of the table, it can be seen that there are never more than two consecutive missing years in the different series, except for the total precipitation from the stations Jasper (3053520) and Golden (1173210), where gaps of 3 to 5 years are observed at the very beginning of the series.

It is reasonable to suppose that the performance of the different non-parametric statistical tests used in this work (including the Bayesian procedure) should not be affected by the fact that these series are incomplete. Moreover, treatment of missing data is already embedded in the bivariate (Bayesian) procedure (personal communication T. Ouarda).

Table 7 - Meteorological stations and data availability by year.

Variable	Years of data used in the trend/shift analysis		
	June 1-July 31	**August 1-October 31**	**Annual**
Banff (3050520)			
Minimum temperature Mean temperature Maximum temperature	1894-1935; 1938-1947; 1949-1994	1901-1935; 1938-1994	1894-1935; 1938-1947; 1949-1994
Total precipitation	1890-1891;1893-1935; 1938-1947; 1949-1994	1890-1891; 1893-1935; 1938-1994	1890-1891; 1894-1935; 1938-1947; 1949-1994
Lake Louise (3053760)			
Minimum temperature	1919-1938; 1941-1994; 1996-1998	1919-1938; 1940-1974; 1976-1998	1919-1938; 1941-1951; 1953-1964; 1966-1974; 1976-1994; 1997-1998
Mean temperature		1951; 1953-1974; 1976-1998	
Maximum temperature		1919-1938; 1940-1974; 1976-1998	1919-1938; 1941-1974; 1976-1994; 1997-1998
Total precipitation	1915; 1917; 1919-1994; 1996-1997; 1999	1915; 1917; 1919-1938; 1940-1995	1919-1938; 1940-1994
Jasper (3053520)			
Minimum temperature Mean temperature Maximum temperature	1932-1933; 1935-1936; 1938-1995	1936; 1938-1995	1936; 1938-1939; 1941-1995
Total precipitation	1927; 1932-1933; 1935-1936; 1938-1995	1931-1932; 1936; 1938-1995	1932; 1936; 1938-1939; 1941-1995
Golden (1173210)			
Minimum temperature	1902-1915; 1917-1918; 1920-1928; 1930-1998	1902-1905; 1907-1914; 1916-1927; 1930-1998	1907-1914; 1916; 1918; 1920-1927; 1930-1959; 1961-1979; 1982-1998
Mean temperature		1902-1905; 1907-1914; 1916-1927; 1930-1944; 1946-1998	1907-1914; 1916; 1918; 1920-1927; 1930-1944; 1946-1959; 1961-1979; 1982-1998
Maximum temperature		1902-1905; 1907-1914; 1916-1928; 1930-1944; 1946-1998	1907-1914; 1916; 1918; 1920-1927; 1930-1944; 1946-1959; 1961-1979; 1982-1998
Total precipitation	1902-1903; 1908-1928; 1930-1998	1902-1903; 1908-1914; 1916-1928; 1930-1998	1903; 1909-1914; 1916; 1918-1928; 1930-1979; 1982-1998

5.2.1 Streamflow Trend Analysis

As described earlier, a number of non-parametric tests were applied to the streamflow time series. These include a Bayesian analysis for detection of most probable date of a shift in trend, Wilcoxen test to determine the significance of a shift in the mean (based on the most probable date determined with the Bayesian analysis) and the Kendall test for trend. Figure 17 illustrates the results of the Kendall/Wilcoxen/Bayesian tests for minimum streamflow for the annual and TBF periods. All basins that exhibited a significant trend are highlighted in red (decrease) and blue (increase). Similar maps depicting changes in the mean and maximum streamflow are presented in Figure 18 and Figure 19 respectively.

The results clearly indicate that minimum and mean streamflow for both the annual and TBF periods are on the decline in the glaciated headwater basins. These estimates are significant at the 5% confidence level. It is important to note that there is a decreasing trend in the annual mean and maximum for the North Saskatchewan River at Saskatchewan Crossing, which was not observed for the TBF period. This may be due to the limited period of record for that station, since gauging station locations along the main stem of the North Saskatchewan River were changed (i.e., Saskatchewan Crossing to Whirlpool Point in 1970; see Table 5).

In general, basins with significant but rapidly changing glacier cover during the period of observation, exhibit a strong decreasing trend as well as a significant shift in the mean for annual and TBF time series.

It is interesting to note that there is no significant trend in minimum, mean and maximum streamflow for the annual and TBF periods for the headwater study basin with no glacier cover (North Ram River) nor the Siffleur River, which has approximately half of the %-glacier cover of the Mistaya basin. Due to the limited observing period for these two catchments, such a conclusion may be premature.

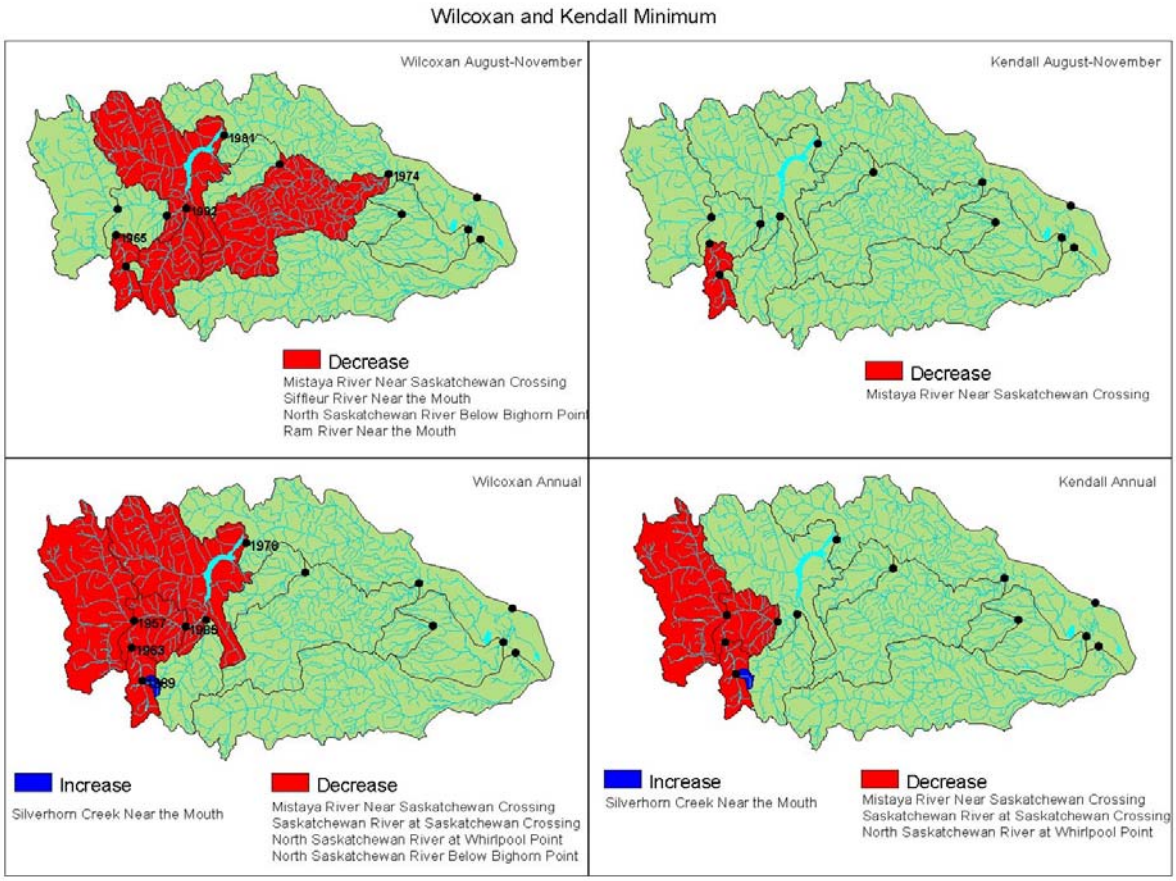

Figure 17 - Results of the Wilcoxan and Kendall trend analysis for minimum streamflow. Note, the dates indicated in the Wilcoxen analysis are those identified by the Bayesian analysis as the most probable dates for a shift in the time series.

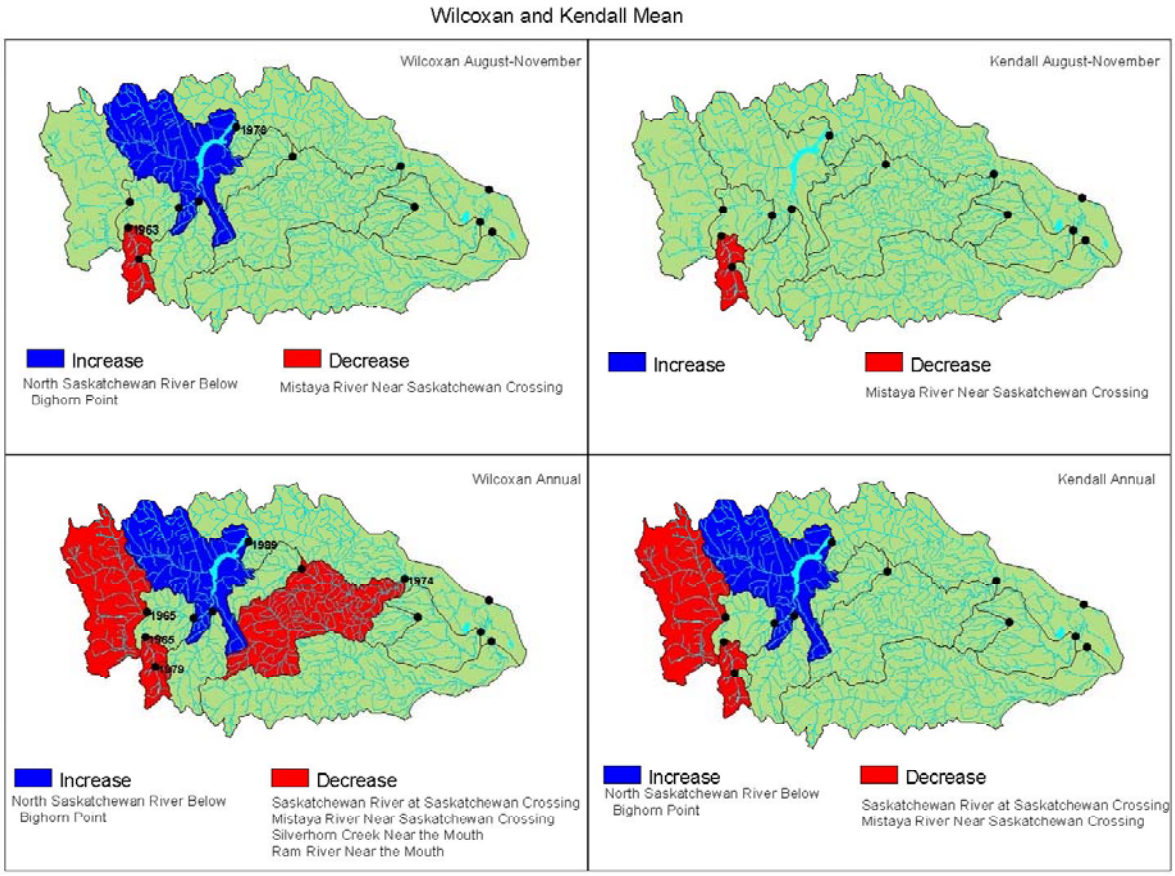

Figure 18 - Results of the Wilcoxan and Kendall trend analysis for the mean streamflow. Note, the dates indicated in the Wilcoxen analysis are those identified by the Bayesian analysis as the most probable dates for a shift in the time series.

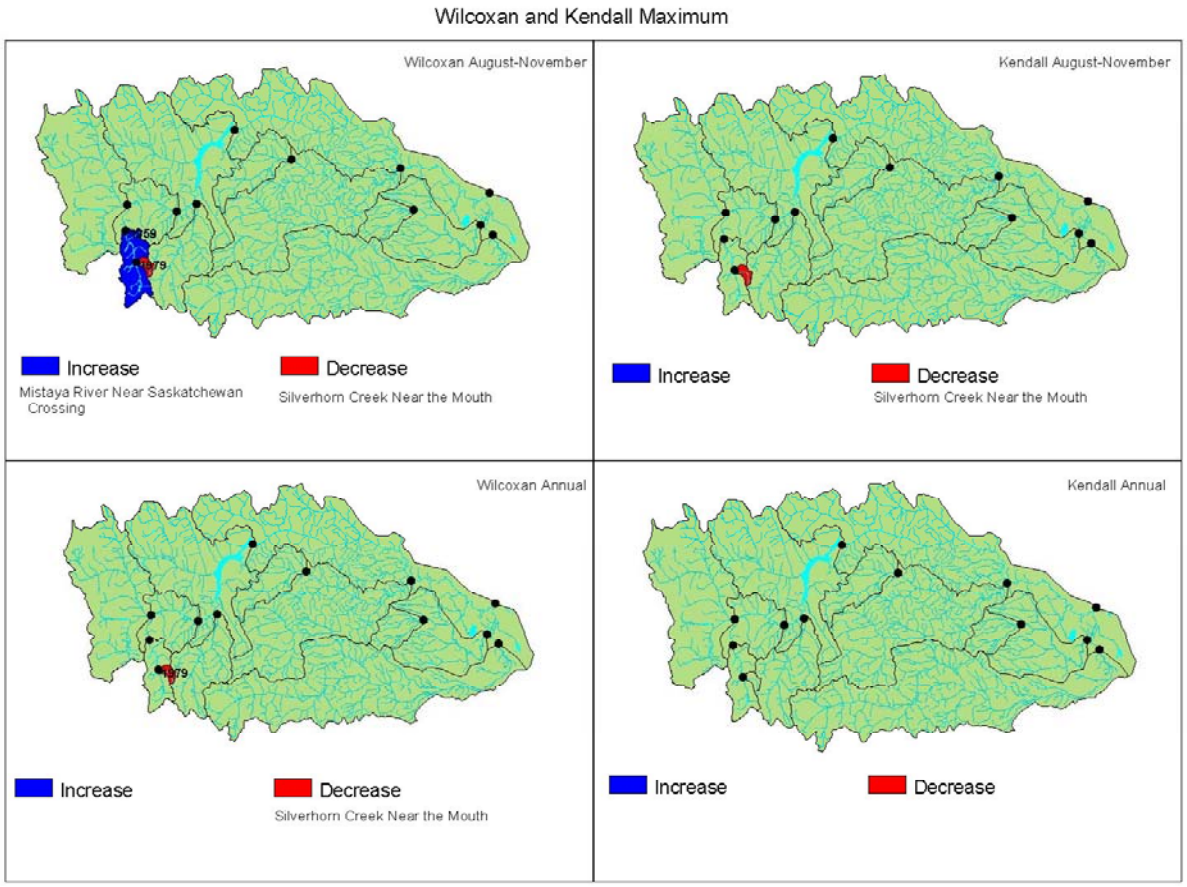

Figure 19 - Results of the Wilcoxan and Kendall trend analysis for maximum streamflow. Note, the dates indicated in the Wilcoxen analysis are those identified by the Bayesian analysis as the most probable dates for a shift in the time series.

5.2.2 Correlation Analysis of Meteorological Variables

A correlation analysis was performed on multiple variables to assess any linear correlation between those variables. The mass-balance record at Peyto glacier was also incorporated into the analysis. Summer (June-July and TBF runoff were estimated for each of the catchment areas along with corresponding meteorological variables of precipitation and temperature. Stations analysed are noted in Table 5 and Table 6.

The Pearson correlation coefficient measures the extent to which two continuous variables are linearly related. The p-value indicates if the correlation coefficient is significantly different from 0 with the alpha level typically set at 0.05. For reference, P values are given in Technical Appendix A (separate from this report).

The variables tested were:

Bw : Winter mass-balance (Peyto Glacier)
Bs : Summer mass-balance (Peyto Glacier)
Bn : Net mass-balance (Peyto Glacier)
Qs : Summer flows
Qf : Fall flows
Ts : Summer mean temperatures
Tf : Fall mean temperatures
Ps : Summer total precipitation
Pf : Fall total precipitation
(Summer season: June 1-July 31; Fall season: August 1-October 31)

Correlations for mean (Table 8), minimum (Table 9) and maximum (Table 10) flows for the Mistaya River streamflow station and the Banff meteorological station are listed. The correlation analysis provides some insight into attribution of streamflow. For the purposes of discussion here, the TBF flow period is highlighted. Clearly reasonable correlation values are obtained for the mean, minimum and max TBF flow period (Qf in the tables). Not surprisingly winter mass-balance and net mass-balance are reasonably well correlated to TBF flows for the Mistaya basin. Interestingly, both summer and fall precipitation show very little correlation ($r < 0.15$) with the TBF flow, yet fall temperature is slightly correlated ($r = 0.3685$). This confirms the importance of glacier melt during the TBF period, but also highlights the very non-linear response of the Mistaya basin, for example, to precipitation and temperature forcing. This also highlights the

importance of sophisticated hydrological modeling for attribution and understanding of streamflow changes. Correlation tables for all meteorological and streamflow stations are given in Technical Appendix A (separate from this report).

Table 8 - Correlation for Banff Meteorological Station, Flows from the Mistaya Basin and Peyto Mass Balance – Mean Flows

	Bw	**Bs**	**Bn**	**Qs**	**Qf**	**Ts**	**Tf**	**Ps**	**Pf**
Bw	1.0000	0.0473	0.6524	0.5398	0.5295	-0.0766	0.3784	-0.1694	-0.2182
Bs	0.0473	1.0000	0.7057	-0.3385	-0.0608	-0.3729	-0.0982	-0.1092	0.3695
Bn	0.6524	0.7057	1.0000	0.0475	0.3419	-0.5340	0.2708	-0.0471	0.0383
Qs	0.5398	-0.3385	0.0475	1.0000	0.4493	0.3738	0.1401	0.0663	0.2096
Qf	0.5295	-0.0608	0.3419	0.4493	1.0000	0.1001	0.3685	0.1450	0.1410
Ts	-0.0766	-0.3729	-0.5340	0.3738	0.1001	1.0000	-0.1594	-0.2057	0.0780
Tf	0.3784	-0.0982	0.2708	0.1401	0.3685	-0.1594	1.0000	0.2667	-0.3286
Ps	-0.1694	-0.1092	-0.0471	0.0663	0.1450	-0.2057	0.2667	1.0000	-0.0818
Pf	-0.2182	0.3695	0.0383	0.2096	0.1410	0.0780	-0.3286	-0.0818	1.0000

Table 9 - Correlation for Banff Meteorological Station, Flows from the Mistaya Basin and Peyto Mass Balance – Minimum Flows

	Bw	**Bs**	**Bn**	**Qs**	**Qf**	**Ts**	**Tf**	**Ps**	**Pf**
Bw	1.0000	0.0473	0.6524	0.2192	0.2803	-0.0766	0.3784	-0.1694	-0.2182
Bs	0.0473	1.0000	0.7057	-0.0480	0.1149	-0.3729	-0.0982	-0.1092	0.3695
Bn	0.6524	0.7057	1.0000	0.0379	0.2813	-0.5340	0.2708	-0.0471	0.0383
Qs	0.2192	-0.0480	0.0379	1.0000	0.4238	0.1972	0.2527	0.2788	-0.0241
Qf	0.2803	0.1149	0.2813	0.4238	1.0000	0.1631	0.2535	0.1198	0.2818
Ts	-0.0766	-0.3729	-0.5340	0.1972	0.1631	1.0000	-0.1594	-0.2057	0.0780
Tf	0.3784	-0.0982	0.2708	0.2527	0.2535	-0.1594	1.0000	0.2667	-0.3286
Ps	-0.1694	-0.1092	-0.0471	0.2788	0.1198	-0.2057	0.2667	1.0000	-0.0818
Pf	-0.2182	0.3695	0.0383	-0.0241	0.2818	0.0780	-0.3286	-0.0818	1.0000

Table 10 - Correlation for Banff Meteorological Station, Flows from the Mistaya Basin and Peyto Mass Balance – Maximum Flows

	Bw	**Bs**	**Bn**	**Qs**	**Qf**	**Ts**	**Tf**	**Ps**	**Pf**
Pf	1.0000	0.0473	0.6524	0.3201	0.4049	-0.0766	0.3784	-0.1694	-0.2182
Bs	0.0473	1.0000	0.7057	0.1128	0.1526	-0.3729	-0.0982	-0.1092	0.3695
Bn	0.6524	0.7057	1.0000	0.3148	0.3715	-0.5340	0.2708	-0.0471	0.0383
Qs	0.3201	0.1128	0.3148	1.0000	0.0236	-0.1193	0.1308	0.0334	0.2769
Qf	0.4049	0.1526	0.3715	0.0236	1.0000	0.0646	0.1509	-0.0286	-0.0966
Ts	-0.0766	-0.3729	-0.5340	-0.1193	0.0646	1.0000	-0.1594	-0.2057	0.0780
Tf	0.3784	-0.0982	0.2708	0.1308	0.1509	-0.1594	1.0000	0.2667	-0.3286
Ps	-0.1694	-0.1092	-0.0471	0.0334	-0.0286	-0.2057	0.2667	1.0000	-0.0818
Pf	-0.2182	0.3695	0.0383	0.2769	-0.0966	0.0780	-0.3286	-0.0818	1.0000

Other observations relevant at this juncture and born out of the non-parametric analysis of meteorological variables, include a significant increase in the minimum air temperatures exhibited by the montane meteorological stations (see Technical Appendix A – Kendall test for stationarity, p32-33; Wilcox test for shift in the mean p36-37). While the significance level varies, these trends and shifts appear to be widespread through the montane Cordillera for both the summer (June-July) and annual periods. Moreover, the local meteorological record available at Peyto Glacier (ca. 12 years) also appears to show indications of rising minimum air temperatures (personal communication D.S. Munro). While such a tendency may attenuate diurnal energy fluctuations, the net effect may lead to a more rapid ripening of the snow cover over seasonal scales and contribute to the evolution of the increasing trend exhibited in the maximum flow regime discussed earlier. Other impacts may include accelerated transient snowline rise and increased down wasting of glaciers.

The extensive glacier-hydro-meteorological attribution data set made available by this study has not yet been fully assessed (see Technical Appendix A) and is the subject of continued study and synthesis by the authors.

6. Next Steps - Strategy to Assess Past and Future Glacio-hydro-meteorological Interactions

Part of this investigation has involved developing and constructing a framework with which to conduct glacio-hydro-meteorological modelling studies to predict runoff and river flows under future climate scenarios. Figure 20 and Figure 21 illustrate the concept and the components of such a strategy; Annex B and Annex C detail efforts conducted to date towards its development.

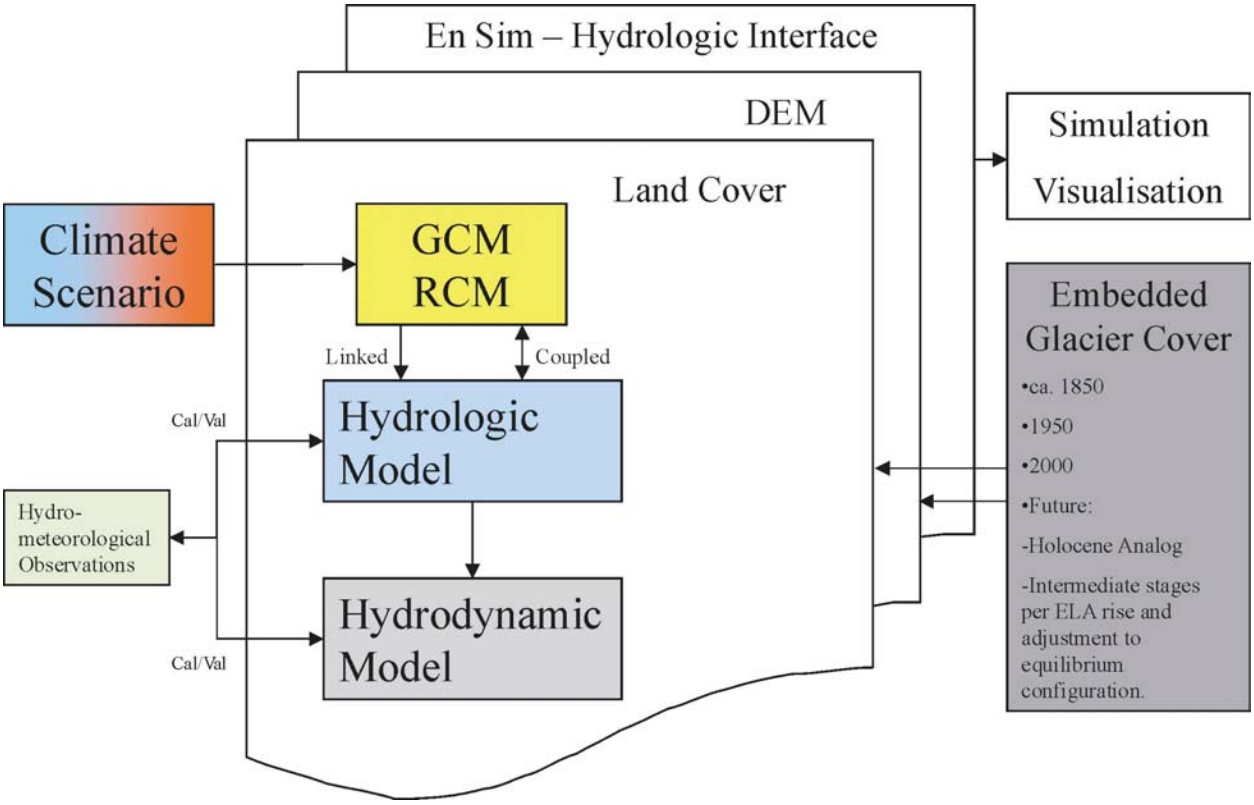

Figure 20 – An integrated glacio-hydro-meteorological modeling framework for studying the impact of future climate and linked glacier cover states on runoff and streamflow.

An important component of this work has and continues to involve the assessment of GCM performance against 1961-1990 baseline climatology derived from using gridded normals of temperature and precipitation (see Annex C).

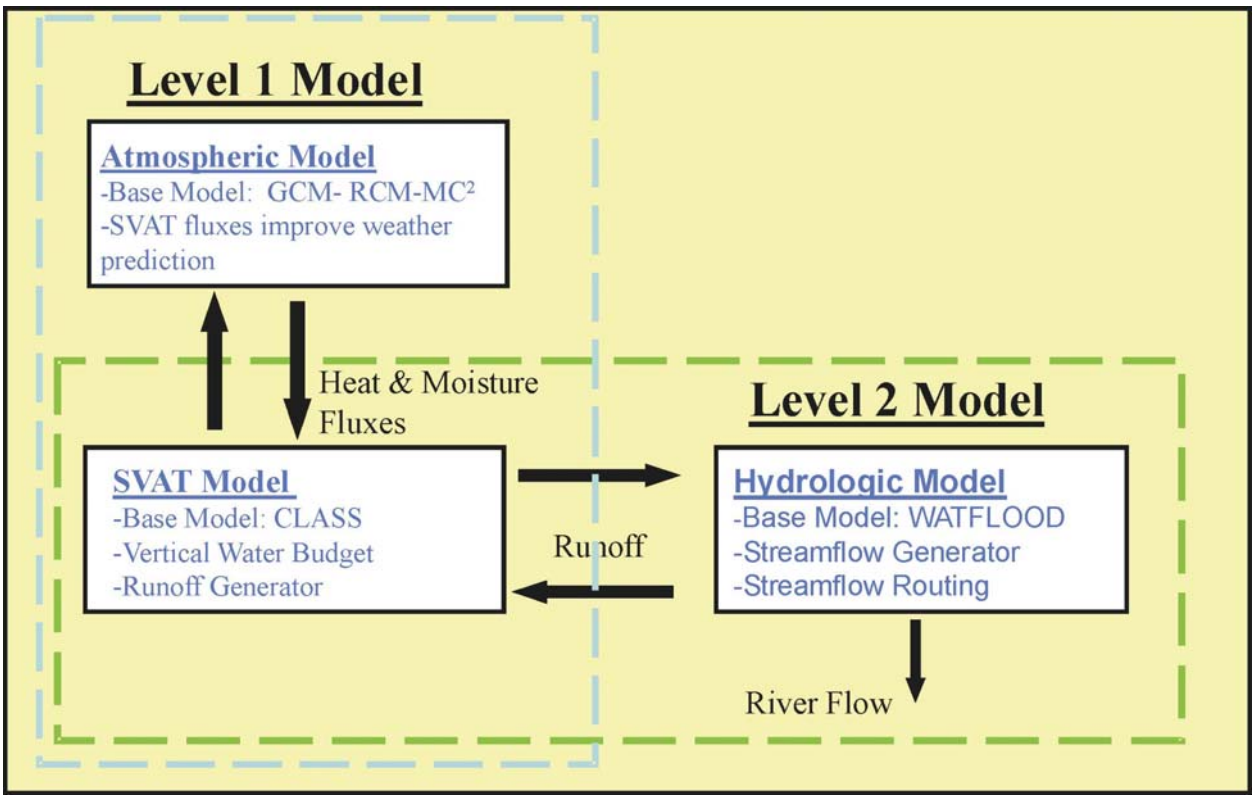

Figure 21 - A general climate change-river flow impacts modelling strategy coupling atmospheric, SVAT (Soil-Vegetation-Atmospheric Transport) and hydrologic models to create a "Level 3" capable modelling framework.

Other tasks currently underway include:

- A better representation of glacier cover within the Canada Land Surface Scheme (Figure 22) and the WATFLOOD GRU scheme. WATFLOOD presently treats perennial ice as a continuous snow cover. This is the subject of a PhD thesis project being conducted at the University of Waterloo and co-supervised by the AP.

- Regional Equilibrium Line Altitude evaluation for ca.1850, 1950, 2000 and future time slices based on prescribed climatological change of the equilibrium line and adjustment to an equilibrium configuration based on topographic variables and glacier geometry.

- A reconnaissance-order assessment of the volume of the ice resources remaining in the upper North Saskatchewan River Basin derived from the application of continuity (mass conservation) and ice flow (momentum conservation) scaling principles (area-volume scaling; e.g., Bahr et al., 1997).

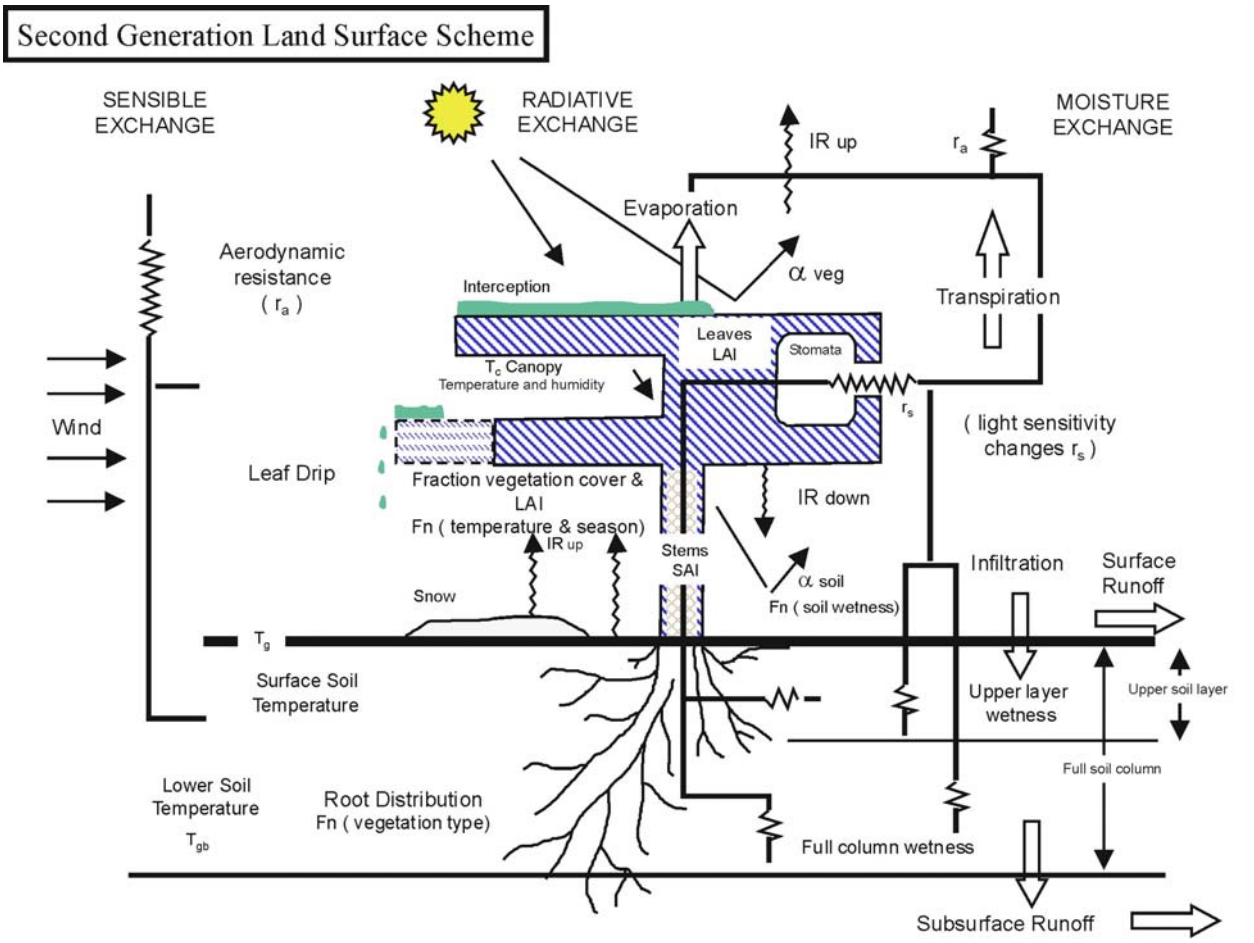

Figure 22 - Second Generation Canada Land Surface Scheme.

7. Conclusions

The reliability of water flow from the glaciated headwater basins of the upper North Saskatchewan River Basin has declined since the mid-1900s. Hydrologic and ecological regimes dependant on the timing and magnitude of glacier-derived meltwater may already be experiencing the medium-long-term impacts of climate change discussed by the IPCC. The reduction in the reliability of glacier-derived flows is in association with significant and accelerating glacier cover contraction fueled by glacier cover dynamic readjustment since the Neoglacial maximum and enhanced radiative forcing effects on glacier mass wastage over the last century. Exacerbating these responses are the extra-tropical influences of the El Niño Southern Oscillation (ENSO) on atmospheric circulation and the advection of moisture into the

Cordillera, imparting dramatic inter-decadal effects on total winter snow pack amounts and the nourishment of glaciers throughout the entire southern Cordillera. Moreover, temporal and spatial variability of ENSO-driven snow pack anomalies is coherent throughout the western Prairies. It will be increasingly important to document the sensitivity of glaciers and snow cover to these modes of atmospheric variability since, their associated responses will be superimposed on greenhouse gas-induced climate changes, and because certain modes of atmospheric variability may be more frequent under a warmer climate.

The study has established a framework with which to conduct glacio-hydro-meteorological modelling studies to predict runoff and river flows under future climate scenarios. It is suggested that the application of this framework could be extended to the South Saskatchewan River Basin. Coupled with 'Water Use Analysis Models' (personal communication M. Sydor) and the impetus imparted by other efforts (e.g., PERD – CCIES POL), it is feasible that we will thereby be in a position to reach the ultimate objective of helping to understand the water resource adaptation needs of both the North and the South Saskatchewan River basins - in particular, the vulnerability imposed by changing land cover states, projected patterns of temperature and precipitation, and the requirements of historical, sectoral and trans-boundary water allocation, on the adaptive capacity of downstream surface water systems.

8. Literature Cited

Aguado, E., D.R. Cayan, L. Riddle, M. Roos. 1990. Climatic fluctuations and the timing of West Coast streamflow. *J. Climate* **5**:1468-1483

Bahr, D.B., M.F. Meier, and S.D. Peckham. 1997. The physical basis of glacier volume-area scaling. *J. Geophys. Res.* **102**(20), 355-362.

Bitz, C.M. and D.S. Battisti. 1999. Inter annual to decadal variability in climate and the glacier mass balance in Washington, Western Canada, and Alaska. *J. Climate* **12**:3181-3196.

Braun, L.N. and H. Escher-Vetter. 1996. Glacial discharge as affected by climate change. Internationales Symposion – Interpraevent 1996 – Garmisch-Partenkirchen. Tagungspublikation **1**:65-74.

Brown, R.D. 1996. Evaluation of methods for climatological reconstruction of snow depth and snow cover duration at Canadian meteorological stations. *Proceedings of the 53rd Eastern Snow Conference*. May, 1996, Williamsburg, Virginia, USA, 55-65.

Brown, R.D. and R.O. Braaten. 1997. Spatial and temporal variability of Canadian monthly snow depths, 1946-1995. *Proc. 54th Eastern Snow Conference*. May 1997, Banff, Canada. 248-259.

Brown, R.D. and B.E. Goodison. 1996. Interannual variability in reconstructed Canadian snow cover, 1915-1992. *J. Climate* **9**:1299-1318.

Buishand, T.A. 1982. Some methods for testing the homogeneity of rainfall records. *J. Hydrology* **58**:11-27.

Cayan, D.R. 1996. Interannual climate variability and snowpack in the western United States. *J. Climate* **9**: 928-948.

Cayan, D.R. and D.H. Peterson. 1989. The influence of north pacific atmospheric circulation on streamflow in the west. In – *Aspects of Climate Variability in the Pacific and the Western Americas*, D.H. Peterson (ed.). Geophysical Monograph **55**, American Geophysical Union, 375- 397.

Collins, D.N. 1989. Hydrometeorological conditions, mass balance and runoff from alpine glaciers. In - Glacier Fluctuations and Climatic Change, Oerlemans, J., (ed.), 235-60. Kulwer Academic Publishers, Dordrecht; Boston. 417p.

Denniston, D. 1995. High priorities : Conserving mountain ecosystem and cultures. Worldwatch Paper 123, Worldwatch Institute, Washington, D.C., 80 pp.

Demuth, M.N. 1996. Effects of short-term and historical glacier variations on cold stream hydro-ecology: A synthesis and case study. Ecological Monitoring and Assessment

Network 2nd National Science Meeting. January 1996, Halifax, Canada. *National Hydrology Research Institute Contribution Series* CS-96003, 15p.

Demuth 1999. Extensive information for Peyto Glacier. In - *Glacier Mass Balance Bulletin* **6**: 29-33 (Haeberli, Hoelzle and Frauenfelder, eds.), IAHS(ICSI)/UNEP/UNESCO, 93p.

Demuth, M.N. and G. Holdsworth. 1997. Peyto Glacier, Alberta: An interpretation of the modern mass balance record and the potential reconstruction of a net accumulation time series into the 18th Century. *Proc. Canadian Geophysical Union*-Hydrology Section annual meeting (joint with the Eastern Snow Conference and Western Snow Conference), Banff, May 4-9, 1997. 167.

Demuth, M.N. and A. Pietroniro. 1999. Inferring glacier mass balance using RADARSat: Results from Peyto Glacier, Canada. *Geografiska Annaler* **81A**(4): 521-540.

Demuth, M.N. and A. Pietroniro. 2000. Glacier monitoring using RADARSAT - Results from Peyto Glacier, Canada. In - Applications of Remote Sensing in Hydrology, Proceedings of the Fourth International Workshop, Santa-Fe, USA. 285-302.

Demuth, M.N. and R. Keller 2002. An assessment of the mass balance of Peyto Glacier (1966-1995) and its relation to recent and past-century climatic variability. In - Peyto Glacier: One Century of Science, M.N. Demuth, D.S. Munro and G.J. Young (eds.). *National Hydrology Research Institute Science Report* **8**:83-132.

Demuth, M.N., C. Hopkinson, M. Sitar, A. Pietroniro, and L. Chasmer. 2001. Airborne scanning LASER terrain mapping of Peyto Glacier, Wapta and Waputik Icefields, Canada: First results and future prospects. *Geological Survey of Canada Open File.*

Demuth, M.N., D.S. Munro and G.J. Young (Editors) 2002. Peyto Glacier: One Century of Science. *National Hydrology Research Institute Science Report* **8**, 276pp.

Demuth, M.N., A. Pietroniro, T.B.M.J. Ouarda and J. Yetter. 2002. The impact of climate change on the glaciers of the Canadian Rocky Mountain eastern slopes and implications for water resource adaptation in the Canadian prairies. *Geological Survey of Canada Open File 4322*.

Environment Canada. 2000. HyDat for Windows, Canadian Hydrological Data, Environment Canada HyDat CD.

Ebbesmeyer, C.C., D.R. Cayan, D.R. McLain, F.H. Nichols, D.H. Peterson and K.T. Redmond. 1991. 1976 step in the Pacific climate: forty environmental changes between 1968-1975 and 1977-1984. *Proc. 7th Annual Pacific Climate Workshop*, Pacific Grove, USA, 115-126.

Fountain, A.G. and W.V. Tangborn. 1985. The effect of glaciers on streamflow variations. *Water Resources Res.* **21**(4):579-586.

Glenday, P. 1991. Determination of morphologic and volumetric change, Peyto Glacier, Alberta, 1966-1989. Unpublished Masters Thesis, Wilfrid Laurier University, Canada, 130pp.

Gutzler, D.S. and R.D. Rosen. 1992. Interannual variability of winter time snow cover across the Northern Hemisphere. *J. Climate* **5**:1441-1447.

Haeberli, W. 1990. Glacier and permafrost signals of 20th-century warming. *Ann. Glaciol.* **14**:99-101.

Haeberli, W. 1994. Accelerated glacier and permafrost changes in the Alps. In - *Mountain Environments in Changing Climates*, Beniston, M. (ed.). Routledge, London and New York.

Haeberli, W. and M. Hoelzle. 1995. Application of inventory data for estimating characteristics of and regional climate change effects on mountain glaciers - a pilot study with the European Alps. *Ann. Glaciol.* **21**:206-212.

Henoch, W.E.S. 1971. Estimate of glaciers secular (1948-1966) volumetric change and its contribution to the discharge in the upper North Saskatchewan River Basin. *J. Hydrology* **12**(145-160).

Heusser, C.J. 1956. Postglacial environments in the Canadian Rocky Mountains. *Ecological Monographs* **26**(3):263-302.

Holdsworth, G., M.N. Demuth and T.M.H. Beck 2002. Radar measurements of ice thickness on Peyto Glacier, Alberta - Geophysical and Climatic Implications. In - Peyto Glacier: One Century of Science, M.N. Demuth, D.S. Munro and G.J. Young (eds.). *National Hydrology Research Institute Science Report* **8**:59-79.

Hopkinson, C. and G.J. Young. 1998. The effect of glacier wastage on the flow of the Bow River at Banff, Alberta, 1951-1993. *Hydrol. Process.* **12**:1745-1762.

Hopkinson, C., M.N. Demuth, M. Sitar, and L. Chasmer. 2001. Applications of LiDAR mapping in a glacierised mountainous terrain. *Proc. IGARSS,* Sydney, Australia. July 9 – 14.

IAHS(ICSI)/UNEP/UNESCO. 1996. *Glacier Mass Balance Bulletin No.4 (1994-1995)*, (Haeberli, W., S. Zuter and M. Hoelzle, (eds.). World Glacier Monitoring Service, IAHS(ICSI)/UNEP/ UNESCO. 89p.

IPCC. 1992. Climate Change 1992 - the supplementary report to the IPCC scientific assessment. WMO and UNEP, Cambridge University Press.

IPCC, 2001. Climate change 2001: impacts, adaptation, and vulnerability. J.J. McCarthy, O.F. Canziani, N.A. Leary, D.J.Dokken, K.S.White (eds.).

Johnson, P.G., and J.M. Power. 1985. Flood and landslide events, Peyto Glacier terminus, Alberta, Canada, 11-14 July 1983. *J. Glaciol.* **31**:86-91.

Kaplan, A., M. Cane, Y. Kushnir, A. Clement, M. Blumenthal and B. Rajagopalan. Analyses of global sea surface temperature 1856-1991 *J. Geophys. Res.* **103**:18,567-18,589, (1998).

Keller, R. 1997. Variability in spring snow pack and winter atmospheric circulation pattern frequency in the Peace River Basin. Unpublished Masters Thesis, University of Saskatchewan, Canada, 146p.

Lettenmaier, D.P. 1976. Detection of trends in water quality data from records with dependent observations. *Water Resources Res.* **12**(5):1037-1046.

Luckman, B.H. 2002. The Neoglacial history of Peyto Glacier. In - Peyto Glacier: One Century of Science, M.N. Demuth, D.S. Munro and G.J. Young (eds.). *National Hydrology Research Institute Science Report* **8**:25-57.

Luckman, B.H., G. Holdsworth and G.D. Osborn. 1993. Neoglacial glacier fluctuation in the Canadian Rockies. *Quaternary Res.* **39**:144-153.

Luckman, B.H., D.P. McCarthy, E. Watson, R.S. St. George, T.A. Kavanagh, B.J. Robinson and M.E. Colenutt. 1998. Field Investigations in the Canadian Rockies in 1997. Report to Parks Canada and the British Columbia Parks Service. 66p.

McCabe *Jr*., G.J. and A.G. Fountain. 1995. Relation between atmospheric circulation and changes in South Cascade Glacier, Washington. *Arctic and Alpine Res.* **27**, 226-233.

Meier, M.F. 1962. Proposed definitions for glacier mass budget terms. *J. Glaciol.* **4**(33):252-261.

Meier, M.F. and A.S. Post. 1962. Recent variations in mass net budgets of glaciers in western North America. Obergurgl Symposium on the Variations of the Regime of Existing Glaciers, *International Association of Scientific Hydrology Publication* **58**:63-77.

Meier, M.F. and W.V. Tangborn. 1965. Net budget and flow of South Cascade Glacier, Washington. *J. Glaciol.* **5**(41):547-566.

Miller, A.J., D.R. Cayan, T.P. Barnett, N.E. Graham and J.M. Oberhuber. 1993. Interdecadal variability of the Pacific Ocean: Model responses to observed heat flux and wind stress anomalies. *Climate Dynamics* **9**: 287-302.

Milner, A.M. and G.E. Petts. 1994. Glacial rivers: Physical habitat and ecology. *Freshwater Biology*, **32**(295-307).

Moore, R.D. and M.N. Demuth 2001. Mass balance and streamflow variability at Place Glacier, Canada, in relation to recent climate fluctuations. *Hydrol. Process.* **15**(3473-3486).

Moore, R.D. and I.G. McKendry. 1996. Spring snowpack anomaly patterns and winter climatic variability, British Columbia, Canada. *Water Resources Res.* **32**:623-632.

Neumann, N.N. 1999. Local advection of sensible heat in the Arctic snowmelt landscape. Unpulished Masters Thesis, University of Saskatchewan, 123pp.

Oerlemans, J. 1994. Quantifying global warming from the retreat of glaciers. *Science* **264**:243-245.

Oerlemans, J. and J.P.F. Fortuin. 1992. Sensitivity of glaciers and small ice caps to greenhouse warming. *Science* **258**(5079):115-117.

Ommanney, C.S.L. 1980. The inventory of Canadian glaciers: procedures, techniques, progress and applications. *International Association of Hydrological* Sciences Publication **126**:35-44.

Ommanney, C.S.L. 1989. Glacier Atlas of Canada, National Hydrology Research Institute, Saskatoon, Environment Canada - Energy Mine and Resources, 52 plates.

Ommanney, C.S.L., J. Clarkson and M.M. Strome. 1973. Information booklet for the inventory of Canadian glaciers. Glacier Inventory Note No.4, Glaciology Division, Inland Waters Directorate, Department of the Environment, revised edition, January, 76 pp.

Østrem, G. 2002. Historical background of Peyto Glacier studies. In - Peyto Glacier: One Century of Science, M.N. Demuth, D.S. Munro and G.J. Young (eds.). *National Hydrology Research Institute Science Report* **8**:1-23.

Petts, G.E., A.M. Gurnell and A.M. Milner. 2002. Eco-hydrology: New opportunities for research on glacier fed-rivers. In - Peyto Glacier: One Century of Science, M.N. Demuth, D.S. Munro and G.J. Young (eds.). *National Hydrology Research Institute Science Report* **8**:251-274.

Rabus, B.T. and K.A. Echelmeyer. 1998. The mass balance of McCall Glacier, Brooks Range, Alaska, U.S.A.; its regional relevance and implications for climate change in the Arctic. *J. Glaciol.* **44**(147):333-351.

Sapiano, J.J., Harrison, W.D. and K.A. Echelmeyer. 1998. Elevation, volume and terminus changes of nine glaciers in North America. *J. Glaciol.* **44**(146):119-135.

Schook, K.R., D.M. Gray and J.W. Pomeroy. 1993. Temporal variation in snowcover during melt in prairie and alpine environments. *Nordic Hydrology* **24**:183-198

Schuster, C.J. and G.J. Young. 2002. The derivation of runoff from the Peyto Glacier catchment. In - Peyto Glacier: One Century of Science, M.N. Demuth, D.S. Munro and G.J. Young (eds.). *National Hydrology Research Institute Science Report* **8**:223-248.

Tanimoto, Y.N., N. Iwasaka, K. Hanawa ans U. Toba. 1993. Characteristic variations of sea surface temperature with multiple time scales in the North Pacific. *J. Climate* **9**:1153-1160.

Trenberth, K.E. 1990. Recent observed interdecadal climate changes in the Northern Hemisphere. *Bulletin American Meteorological Society* **71**(7): 988-993.

Trenberth, K.E. and J.W. Hurrell. 1994. Decadal atmosphere-ocean variations in the North Pacific. *Climate Dynamics* **9**:303-319.

UNEP. 1994: *Environmental Data Report, 1993-1994*. Blackwell Oxford.

Wallace, A.L. 1995. The volumetric change of the Peyto Glacier, Alberta, Canada 1896-1966. Unpublished Masters Thesis, Wilfrid Laurier University, Canada.

Wang, B. 1995. Interdecadal changes in El Nino onset in the last four decades. *J. Climate* **8**: 267-285.

Yarnel, B. 1984a. Relationship between synoptic-scale atmospheric circulation and glacier mass balance in south-western Canada during the International Hydrological Decade, 1965-74. *J. Glaciol.* **30**(105):188-198.

Yarnel, B. 1984b. A procedure for the classification of synoptic weather maps from gridded atmospheric pressure surface data. *Computers and Geosciences* **10**(4):397-410.

Young, G.J. 1981. The mass balance of Peyto Glacier, Alberta, Canada, 1965 to 1978. *Arctic and Alpine Res.* **13**:307-318.

Young, G.J. 1985. Overview - Techniques for prediction of runoff from glacierized areas (G.J. Young, ed.). *International Association of Hydrological Sciences Publication* **149**.

Young, G.J. 1991. Hydrological interactions in the Mistaya basin, Alberta, Canada. Snow, Hydrology and Forests in High Alpine Areas (Proceedings of the Vienna Symposium, August 1991). *International Association of Hydrological Sciences Publication* **205**.

Annex A - Kendall Test for Stationarity – Hydro-meteorological data

H0 : No trend is apparent in the observations
H1 : There is a trend in the observations: (↑) *Upper trend*; (↓) *Downward trend*
Significance level : *5%*

H1* : *H1 would be rejected at a significance level of 1%*
H0† : *H0 would be rejected at a significance level of 10%*

A1 Hydrometric variables

Station ID# : 05DA007
Station Name: **Mistaya River Near Saskatchewan Crossing**

Period / Variable	June-July	August-November	Annual
Minimum flow	H0	H1(↓)	H1(↓)
Mean flow	H0	H1(↓)	H1(↓)
Maximum flow	H0	H0	H0

Station ID# : 05DA010
Station Name: **Silverhorn Creek Near the Mouth**

Period / Variable	June-July	August-November	Annual
Minimum flow	H1(↑)	H0	H1*(↑)
Mean flow	H0	H0	H0
Maximum flow	H0	H1* (↓)	H0

Station ID# : 05DA006
Station Name: **North Saskatchewan River at Saskatchewan Crossing**

Period / Variable	June-July	August-November	Annual
Minimum flow	H0	H0	H1(↓)
Mean flow	H0	H0	H1 (↓)
Maximum flow	H0	H0	H0

Station ID# : 05DA009
Station Name: **North Saskatchewan River at Whirl Pool Point**

Period / Variable	June-July	August-November	Annual
Minimum flow	H1* (↑)	H0	H1* (↓)
Mean flow	H0	H0	H0
Maximum flow	H0	H0	H0

Station ID# : 05DC010
Station Name: **North Saskatchewan River below Bighorn Plant**

Period / Variable	June-July	August-November	Annual
Minimum flow	H1* (↑)	H0	H0
Mean flow	H1* (↑)	H0	H1* (↑)
Maximum flow	H0	H0	H0

Station ID# : 05DA002
Station Name: **Siffleur River Near the Mouth**

Period / Variable	June-July	August-November	Annual
Minimum flow	H1 (↑)	H0	H0
Mean flow	H0	H0	H0
Maximum flow	H0	H0	H0

Station ID# : 05DC006
Station Name: **Ram River Near the Mouth**

Period / Variable	June-July	August-November	Annual
Minimum flow	H0	H0†	H0
Mean flow	H0	H0	H0
Maximum flow	H0	H0†	H0

Station ID# : 05DC011
Station Name: **North Ram River at Forestry Road**

Period / Variable	June-July	August-November	Annual
Minimum flow	H0	H0	H0
Mean flow	H0	H0	H0
Maximum flow	H0	H0	H0

A2 Meteorological variables

Station ID# : 3050520
Station Name: **Banff**

Period / Variable	June-July	August-November	Annual
Total precipitation	H0	H0	H0
Minimum temperature	H1 (↑)	H0†	H1 (↑)
Mean temperature	H1 (↑)	H0†	H1 (↑)
Maximum temperature	H0	H0	H1 (↑)

Station ID# : 3053760
Station Name: **Lake Louise**

Period	June-July	August-November	Annual

Variable			
Total precipitation	H0	H0	H0
Minimum temperature	H1 (↑)	H0	H1* (↑)
Mean temperature	H0	H0	H0
Maximum temperature	H1 (↓)	H0	H0

Station ID# : 3015520
Station Name: **Rocky Mountain House**

Period / Variable	June-July	August-November	Annual
Total precipitation	H0	H0	H0
Minimum temperature	H0	H0	H0
Mean temperature	H0	H0	H0
Maximum temperature	H0	H0	H0

Station ID# : 3053520
Station Name: **Jasper**

Period / Variable	June-July	August-November	Annual
Total precipitation	H0†	H0	H0
Minimum temperature	H1 (↑)	H0	H1 (↑)
Mean temperature	H0	H0	H0†
Maximum temperature	H0	H0	H0

Station ID# : 1172870
Station Name: **Field**

Period / Variable	June-July	August-November	Annual
Total precipitation	H0	H0	H0
Minimum temperature	H0†	H0	H0
Mean temperature	H0	H0	H0
Maximum temperature	H1* (↓)	H0	H0

Station ID# : 1173210
Station Name: **Golden**

Period / Variable	June-July	August-November	Annual
Total precipitation	H0†	H0	H0
Minimum temperature	H1 (↑)	H1 (↑)	H1 (↑)
Mean temperature	H0†	H1* (↑)	H1 (↑)
Maximum temperature	H0	H0	H0

Other non-Parametric statistical analyses were conducted on the hydro-meteorological time series. Details and tabular results are provided in Technical Appendix A. They include:

Wilcoxon test for detection of a shift in the mean
H0 : The mean is the same before and after the most probable date of change
H1 : There is a shift in the mean after the most probable date of change
(The most probable date of change being given by the results of the Bayesian procedure)
Significance level* : *5%
(↑) : ***Upper shift***
(↓) : ***Downward shift***
H1* : ***H1 would be rejected at a significance level of 1%***
H0† : ***H0 would be rejected at a significance level of 10%***

Levene test for detection of a shift in the variance
H0 : The variance is the same before and after the most probable date of change
H1 : There is a shift in the variance after the most probable date of change
(The most probable date of change being given by the results of the Bayesian procedure)
Significance level* : *5%
(↑) : ***Upper shift***
(↓) : ***Downward shift***
H1* : ***H1 would be rejected at a significance level of 1%***
H0† : ***H0 would be rejected at a significance level of 10%***

Bayesian (univariate) procedure for detection of a shift in the mean
Model (a single change in the mean):

$X(1), X(2), X(3), ..., X(\tau) \sim N(\mu_1, \sigma)$

$X(\tau+1), X(\tau+2), ..., X(n) \sim N(\mu_2, \sigma)$

$n \equiv$ sample size

$\tau \equiv$ date of change

$P[\tau = n] \equiv$ probability for no change

$\Delta \equiv \mu_2 - \mu_1$ (i.e. the amplitude of the shift)

$\boldsymbol{\tau_{opt}} \equiv$ posterior mode for τ

$$\left(\text{i.e. } \max_{i\in\{1,\ldots,n-1\}} \left(\text{Prob}[\tau = i \mid \text{there is a change}]\right)\right)$$

$\boldsymbol{\Delta_{opt}} \equiv$ posterior mode for Δ $\left(\text{ i.e. } \max_{\delta}\left(f_{\Delta}(\delta \mid \text{there is a change})\right)\right)$

Bayesian (bivariate) procedure for the detection of a change-point

Model description:

$$Y_i = \begin{cases} \beta_1' \mathbf{X}_i + \varepsilon_i & \text{if } 1 \le i \le \tau \\ \beta_2' \mathbf{X}_i + \varepsilon_i & \text{if } \tau < i \le n \end{cases}$$

where Y_i, i = 1, 2, ..., n, is a sequence of (univariate) random variables ; $\mathbf{X}_i$, i = 1, 2, ..., n, is a sequence of m × 1 random vectors ; $\beta_1, \beta_2 \in \mathbb{R}^m$; the ε_i's are real-valued error variables and the changepoint $\tau \in \{1, 2, ..., n\}$. The model can be rewritten in matrix form such as:

$$\mathbf{Y} = \boldsymbol{\chi}_\tau \boldsymbol{\theta} + \boldsymbol{\varepsilon}$$

where

$$\mathbf{Y}' = [Y_1 \ldots Y_n] \ ; \ \boldsymbol{\chi}_\tau = \begin{bmatrix} \mathbf{X}_{1,1} & \cdots & \mathbf{X}_{1,m} & & & \\ \vdots & & \vdots & & \mathbf{0} & \\ \mathbf{X}_{\tau,1} & \cdots & \mathbf{X}_{\tau,m} & & & \\ & & & \mathbf{X}_{\tau+1,1} & \cdots & \mathbf{X}_{\tau+1,m} \\ & \mathbf{0} & & \vdots & & \vdots \\ & & & \mathbf{X}_{n,1} & \cdots & \mathbf{X}_{n,m} \end{bmatrix} \text{ (en posant } \mathbf{X}' = [\mathbf{X}_1 \ldots \mathbf{X}_n]) \ ;$$

$$\boldsymbol{\theta}' = [\beta_{1,1} \ldots \beta_{1,m} \ \beta_{2,1} \ldots \beta_{2,m}] \ \text{ (en posant } \beta' = [\beta_1 \ \beta_2]) \ ; \ \boldsymbol{\varepsilon}' = [\varepsilon_1 \ldots \varepsilon_n]$$

Hence, this model describes the response variable Y_i as a linear combination of the explanatory variables $\mathbf{X}_i$ and an error term ε_i. Plus, the relation between the Y_i's and the $\mathbf{X}_i$'s is redefined at time τ as the regression parameters change their values from β_1 to β_2. It is implied here that the first column of $\mathbf{X}$ contains only ones (i.e. $\mathbf{X}_{i,1} = 1$; i = 1, 2, ..., n), which means that $\beta_{1,1}$ and $\beta_{2,1}$ are the constant parts of the regression equation before and after τ respectively.

Annex B - The WATFLOOD Hydrological Model for the North Saskatchewan River Basin

B1 Background

The WATFLOOD distributed hydrological model uses earth observation data (land cover and Digital Elevation Model), a Grouped Response Unit (GRU) pixel grouping method (to deal with basin heterogeneity) and a physically based streamflow routing scheme. For more information see www.civil.uwaterloo.ca/watflood/

B2 Generating a Digital Elevation Model (DEM)

The contour and hydrography layers from four digital 1:250 000 NTS map sheets (83C, 83B, 82N and 82O) were utilised to create a Digital Elevation Model (DEM) of the North Saskatchewan River Basin (see Figure B 1). The contour lines were needed as elevation input and the hydrography layer was used to define the valley bottoms.

The contour layer displayed breaks in the isolines along the boundaries of map sheet 82N (see Figure B 2). The elevations of the disjointed lines did not correspond so no changes were made to this data. River polylines were extended through lakes and river sections represented by polygons to ensure connectivity. Additionally, braided river features were simplified for use in the DEM creation.

A North Saskatchewan River basin outline was created by merging existing watershed outline data from the Canada Land Inventory (Level-I) digital database and watershed boundaries that were digitized from a manually delineated basin based on the hard copy 1:250 000 map sheets. The basin outline was used to delineate ridges for the DEM interpolation algorithm.

A new database (N_Sask_RB.pix) was created in PCI to hold the North Saskatchewan River DEM. The vector layers (contours, rivers, and boundary) were imported into PCI format and transferred into the new database.

A 30m DEM was generated in PCI using an interpolation method that is based on the Distance Transform algorithm. The program uses 2D break lines (valleys, ridges, cliffs) as constraints for the interpolation and it smoothes out the interpolated elevation values based on the

neighbourhood values. The vector input types were the contour vectors (contours file), vectors specifying ridges (boundary file), and vectors specifying valleys/rivers (rivers file).

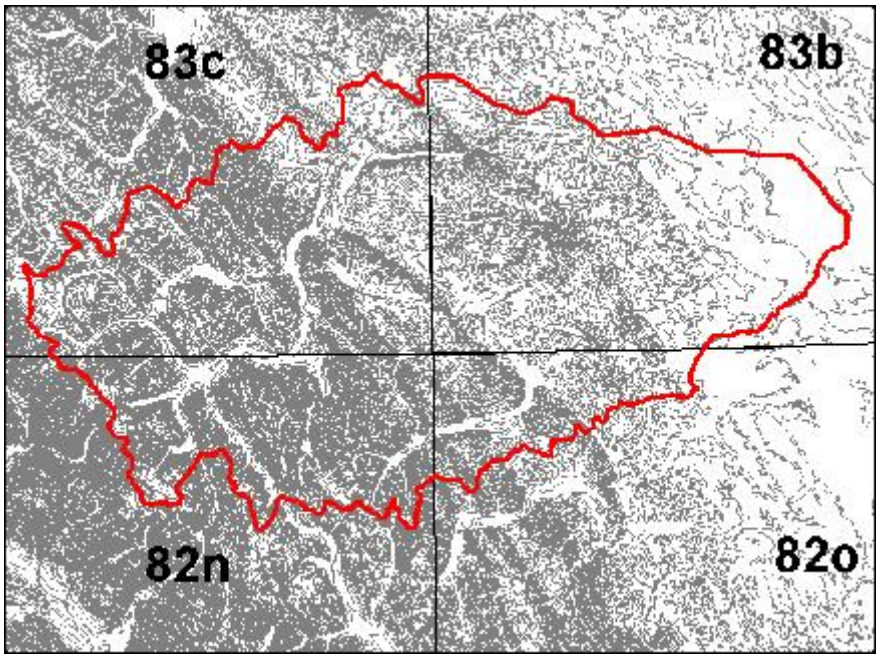

Figure B 1 - Study area showing contours and map sheet coverage.

a) b)

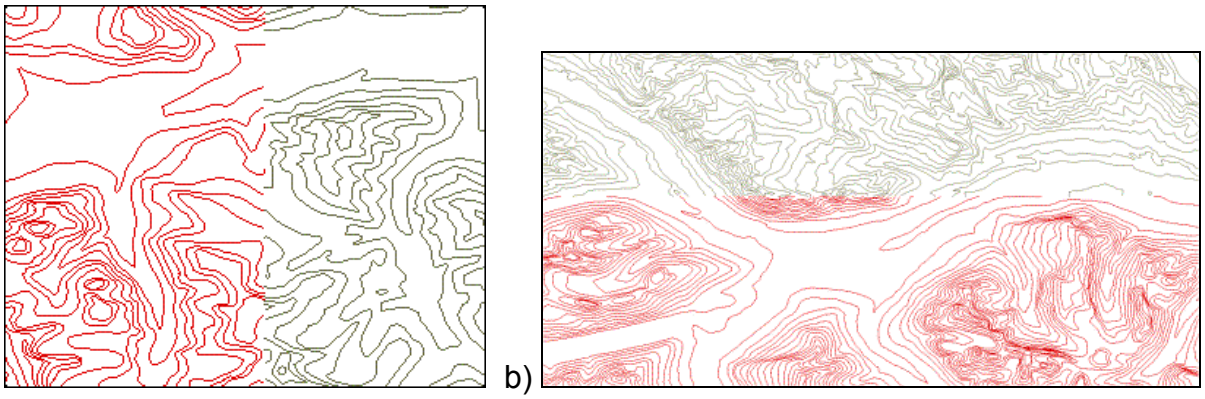

Figure B 2 - Mismatched contours along a) the boundary between map sheets 82N and 82O, and b) the boundary between map sheets 82N and 83C.

B2.1 DEM Validation

Once the DEM was created, a drainage watershed-conditioning program was run to derive the water flow direction and flow accumulation raster channels. These parameters were analysed to check the validity of the generated DEM. Problem areas were identified in the flow direction and flow accumulation channels. Figure B 3 shows black areas in the flow direction indicating

that the program could not identify a flow direction from the topography described by the DEM. In several areas these problems were linked to the discrepancies at the map sheet edges, or to flat areas, particularly on the eastern edge, that were incorrectly interpolated. The flow accumulation was also used as an indicator of potential problem areas as flow should be expected to follow the river course. Unexpected breaks in the flow accumulation also drew attention to potential problems in the DEM. Where the flow direction and flow accumulation layers indicated problems, the DEM was edited manually.

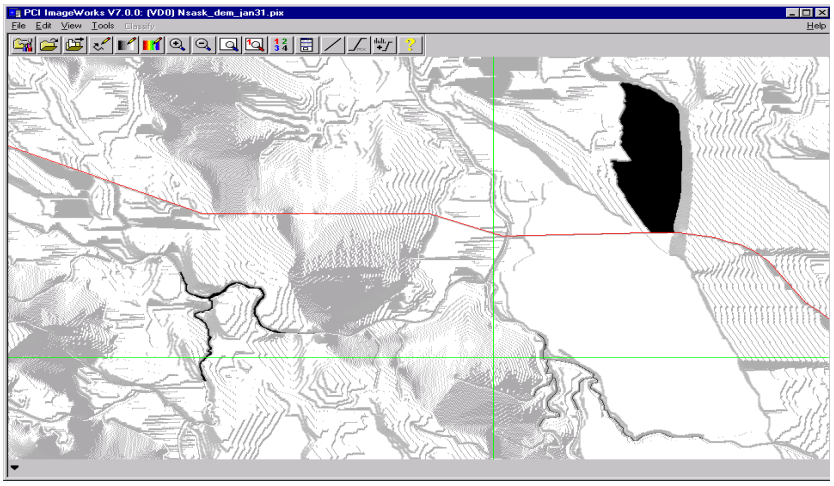

Figure B 3 - Flow direction problems indicated by black areas.

B3 Generating Land Cover Data

Two LandSat 5 images (pixel size 30m) were used to complete the land classification for the North Saskatchewan River Basin. The two images, one from August 29, 1998 and one from September 7th, 1998, are identified as NorthSask1 and NorthSask2 pix files covering the western and eastern portions of the basin, respectively.

B3.1 Orthorectification

The raw images were ortho-rectified based on Ground Control Points (GCP's), satellite ephemeris data and a DEM. The digital river vectors and the boundary vector were used as input for GCPs within the basin boundary, while the GCPs outside the boundary were collected from 1:50 000 NTS map sheets.

Once the images were ortho-rectified, an area in the north central portion of the basin was no longer covered by the two images. Coverage of this area would require a third image to be acquired and the area was deemed too small to warrant this expense.

B3.2 Land Cover Classification

Land cover classes were identified on the ortho-rectified images. In specifying the land classes, an attempt was made to adhere to the classes as defined by the WATFLOOD Modeling application. These classes were urban, needle, broadleaf, mixed forest, barren, wetland, crops, glaciers and water. Despite attempts to classify within the WATFLOOD structure, some additional classes were introduced to accommodate features of the imagery, such as shadow in forested areas (caused by the mountains), cloud and cloud shadow. The LandSat images were classified into the land cover classes listed in Table B 1 - Land cover classes used in the classification of the North Saskatchewan River Basin LandSat images. based on the maximum likelihood classification algorithm.

The two classified Landsat images were merged into one large database (NorthSaskc.pix). A vector of the basin is displayed on the merged classified image in Figure B 1. The land cover classes were aggregated to fit the WATFLOOD structure (see Table B 1 and Table B 2). The merged and aggregated land cover channel was transferred into the N_Sask_RB.pix database, which already contained the DEM channel.

Table B 1 - Land cover classes used in the classification of the North Saskatchewan River Basin LandSat images.

Land Cover Type	Class	Aggregated to Class…
Null	0	0
Water	1	2
Glaciers	2	3
Barren (clearcuts)	3	4
Needle forests	4	5
Mixed	5	6
Grass/shrubs	6	7
Bedrock	7	1
Forest Shadow	8	5
Clouds	9	0
Cloud Shadow	10	0
Crops	11	8

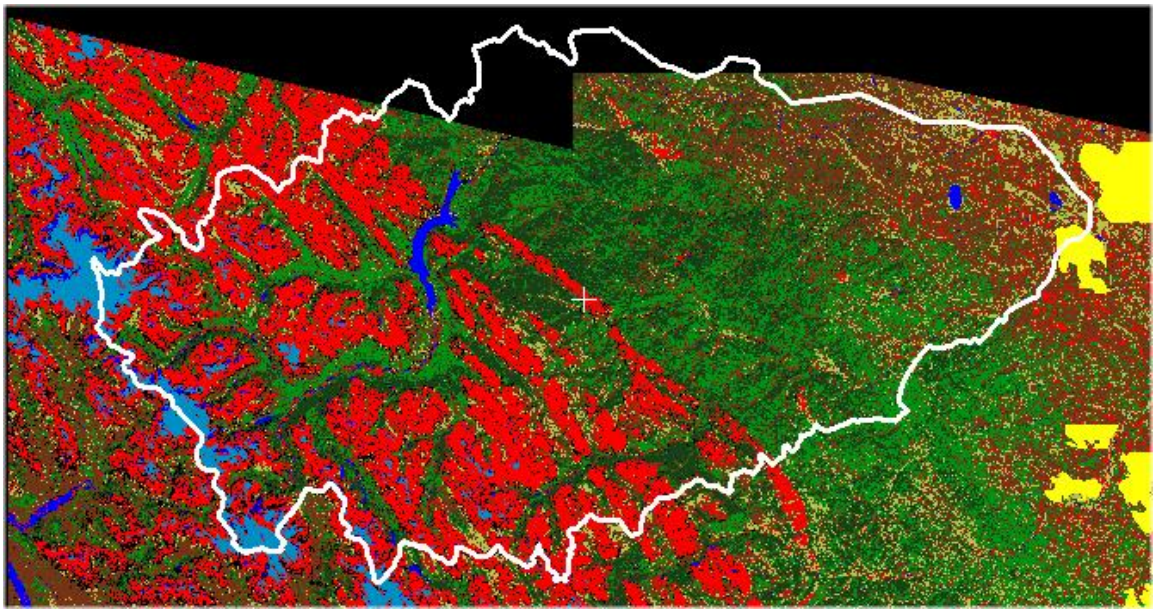

Figure B 4 - The merged, classified LandSat images. Note areas in the north that are not covered.

Table B 2 - The aggregated land cover classes for the North Saskatchewan River Basin

Land Cover Type	Class
Null	0
Bedrock	1
Water	2
Glaciers	3
Barren (clearcuts)	4
Needle Forests	5
Mixed	6
Grass/shrubs	7
Crops	8

B4 Using PCI and MAPMAKER to Generate a WATFLOOD Mapfile

B4.1 Extracting Watershed Information from the DEM

PCI was used to extract the watershed information and the physiographic parameters from the DEM in the N_Sask_RB.pix database. The drainage watershed conditioning program was first run to generate new flow accumulation and flow direction raster channels based on the DEM. A watershed seed point was specified at the outflow point where the basin boundary, the river channel and a high flow accumulation channel were coincident. The watershed generation

program uses the seed point and the flow direction channel produced by the drainage watershed conditioning program in its determination of the watershed boundary.

The resultant watershed was compared to the expected boundary. In Figure B 5, the white area depicts the watershed generated by the program. It extends beyond the expected watershed (the dark outline), particularly in the southeast section. The grey shading illustrates areas belonging to other watersheds, while the black zones represent sections excluded from all watersheds. The extension of the watershed beyond its bounds and the exclusions within the subject watershed indicate problems in the DEM. These issues were addressed by again editing the DEM. The black inclusion on the east side of the watershed in Figure B 6 was indicative of a flow problem. The extended white area draws attention to problems with the ridge of the watershed boundary. These issues were remedied by raising the boundary to force containment of the watershed and by lowering the rivers to force flow. In addition to manual editing, the elevation along the basin boundary was raised 14 metres to force the containment of the watershed and the elevation along the river outlines were lowered by four metres.

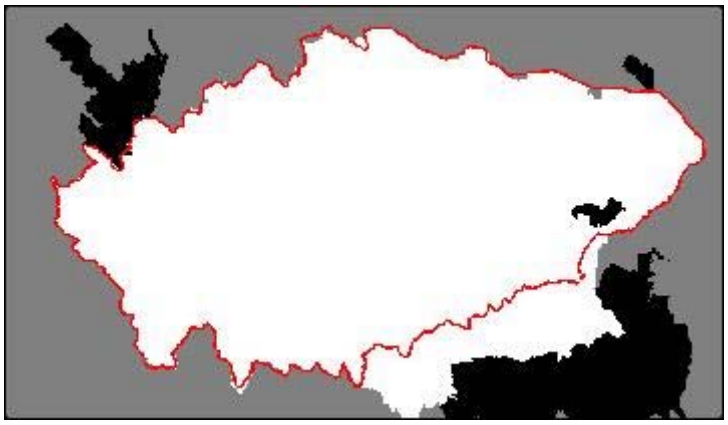

Figure B 5 - The generated watershed versus the expected watershed boundary (in red). White represents the subject watershed, grey represents other watersheds and black represents areas that are not included in any watershed (sink holes).

The output point on the boundary was lowered to allow for flow out of the watershed. The drainage watershed conditioning program and the watershed generation program were run again based on the modified DEM. Once the watershed boundary closely approximated the expected boundary, a watershed mask was created.

Watershed seed points for creation of the sub-basins were generated using an automated program that creates a seed point where the flow accumulation reaches a set threshold. In this case a threshold value of 20000 was used. An additional seed point was manually added to the outflow point. Once the sub-basins were created, the area outside of the watershed was assigned a value of –1 using an inverse of the watershed mask.

B4.2 Generating a WATFLOOD Mapfile Using MapMaker

The flow accumulation, flow direction, watershed, seed, DEM and land cover image channels were exported from the N_Sask_RB.pix database to ascii format (starting at the upper left corner of each image channel and moving down row by row). The ascii files contain one value per row. The six generated ascii files, named flowac.txt, direct.txt, seed.txt, wtrshed.txt, elev.txt and landcov.txt, were used as inputs for the MapMaker program. The MapMaker program two was selected and the parameters listed in Table B 3 were specified. The program generated the WATFLOOD map file based on 9x9km grids.

Table B 3 - MapMaker parameters

Number of Pixels in Line:	6900
Number of Lines in Image:	3900
Coordinate System (UTM-1):	1
UL Northing (North) km:	5830
UL Easting (West) km:	463
LR Northing:	5713
LR Easting:	670
Grid size in pixels:	300
Number of classes in image:	9
Greyscale 1:	1
Greyscale 2:	2
Greyscale 3:	3
Greyscale 4:	4
Greyscale 5:	5
Greyscale 6:	6
Greyscale 7:	7
Greyscale 8:	8
Greyscale 9:	0
Contour factor:	300
Main channel threshold:	10000
Type of input (0 - ascii, 1-binary):	0

B5 Using EnSim Hydrologic to Generate a WATFLOOD Mapfile

B5.1 EnSim Hydrologic

Developed by CHC, EnSim was created to meet the needs of a wide range of environmental prediction and decision support applications such as flood management and coastal management. EnSim is designed as an advanced numerical modelling framework, as well as a general-purpose data handling and visualisation system that can be readily adapted for any class of environmental data.

EnSim creates a virtual environment where simulation results can be viewed, animated and analysed in one, two and three dimensions. This allows the user to observe complex interactions of various phenomena in an intuitive manner, providing a realistic view of simulation results. Presentation of simulation results to non-technical audiences is greatly improved by providing seamless integration with other Windows applications such as word-processors, spreadsheets and multimedia tools.

EnSim Hydrologic is specific application software of the EnSim core. It is a generic hydrologic modelling environment and is designed to aid in the creation of distributed and physically based hydrologic models. It is currently integrated with WATFLOOD, and provides a variety of tools for data preparation, analysis and visualisation. EnSim Hydrologic allows the user to develop an accurate physical model of a watershed including the basin outline, topography and locations of channels, which can be displayed in either two or three dimensions. It provides the framework for integrating environmental data and GIS information to display or create digital elevation maps, to map land-use and to determine channel locations. EnSim Hydrologic can easily create the watershed map of square cells required when using WATFLOOD. The map can be displayed in two dimensions and full colour to help with editing the parameters of the cells. The simulation results from WATFLOOD can be viewed using EnSim Hydrologic in one, two or three dimensions and data associated with a time-series, like outflow, can be animated. EnSim Hydrologic allows the user to observe and interpret the results from WATFLOOD more easily and also aids in the explanation of the model and results to non-technical audiences.

B5.2 Generating the Watershed Object from the DEM

The first step in generating the WATFLOOD map was creating a watershed object using EnSim Hydrologic. A watershed object is a coherent collection of data concerning the physiographic features of the entire watershed being studied. It includes information about the topography, the channels and the extent of the watershed(s) within the study area. All of this information is based on the data contained within a digital elevation map (DEM).

A DEM, in the context of EnSim Hydrologic, is a georeferenced regular grid that carries a value for elevation at each vertex. When creating a watershed object, EnSim Hydrologic first fills any depressions in the original DEM and then uses this modified elevation data to determine the path of the flow of water from higher to lower elevations, creating an outline of the channels. The watershed boundary is also based on the elevation data contained in the DEM.

B5.2.1 Discussion of DEM Data

The DEM was obtained from the N_Sask_RB.pix database. The source data for the DEM was in raster format with each pixel covering an area 150 by 150m. The coordinates of the centre of each pixel corresponded to a vertex on the EnSim grid, creating a DEM with 150m resolution.

B5.2.2 Editing the DEM

The initial watershed object created from the DEM contained a few errors with respect to the calculated path of the channels and the outline of the watersheds. Errors were noted by laying a digital map of the channels over the paths of flow calculated by EnSim. These errors were corrected by editing the DEM and recalculating the path of flow and the watershed outlines with EnSim Hydrologic. The DEM was edited by lowering the elevation of the grid vertices that lay in the correct path of flow. This ensured that the flow was directed in the correct path. When the channels and watershed outlines were satisfactory, the WATFLOOD map was generated with EnSim. The final watershed object, showing the topography, channels and watershed outlines is shown in Figure B 6 and Figure B 7.

B5.3 Generating the WATFLOOD Map from the Watershed Object

From the information contained within the watershed object, EnSim Hydrologic calculates automatically nearly all of the physiographic features required to create a WATFLOOD map. The only feature that must be added by the user is land use data.

The WATFLOOD map cells were 9km by 9km square. There were 23 cells running west-east and 15 cells running north-south. The UTM projection coordinates of the bottom left corner of the grid were 463000 East and 5704000 North. The study area was in UTM zone 11 and the datum was NAD 1983.

B5.3.1 Adding Land Use Data

Nine classes were used to describe the land use: urban and rock, coniferous forest, deciduous forest, mixed forest, barren (short, sparse vegetation), wetland, crop, glacier, and water. The land use was classified by CCRS and the imagery was from NOAA, having a resolution of 1 km. The land use data was obtained from NHRC after it had been formatted for use in WATFLOOD and was simply added to the map file. Zeros were added at the top and at the bottom of the formatted data of each of the land use classes to account for the border of blank cells that must surround the modelled watershed. The area in percent of each cell of the map is described in terms of the nine land use classes. For example, the land use in one cell of the map could consist of 73% coniferous forest, 11% mixed forest and 16% barren. The remaining land use classes would be assigned values of 0% for that cell.

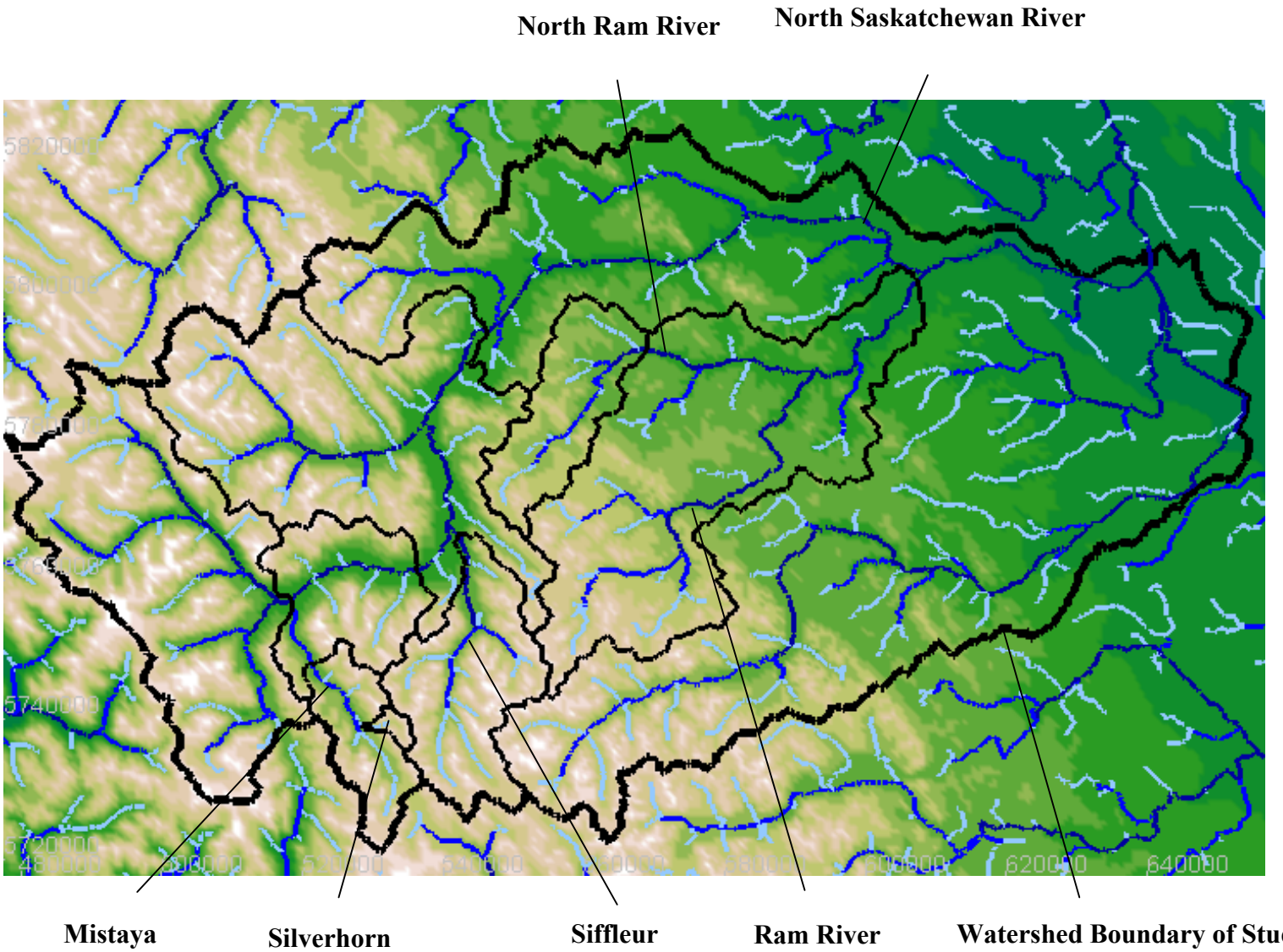

Figure B 6 - Completed EnSim watershed object in 2D. Channels of interest are noted.

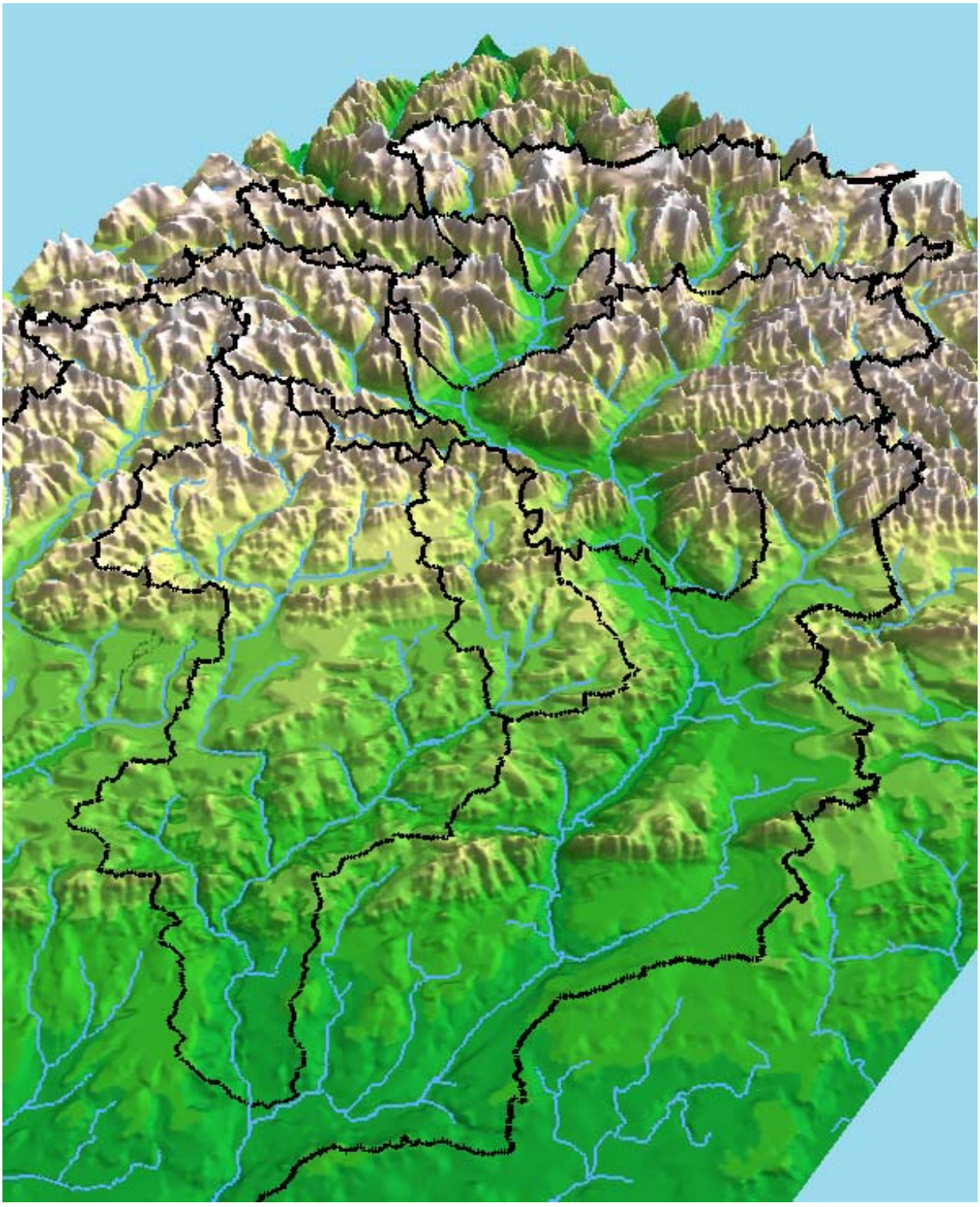

Figure B 7 - Partial view of EnSim Hydrologic watershed object showing the depressionless DEM, the outline of the watersheds and the paths of water flow in 3D. The image has been rotated so that the observer is looking approximately southwest.

B5.3.2 Editing the WATFLOOD Map

The contour interval was changed to 50m, since WATFLOOD cannot accept a contour density greater than 99.

Both the drainage direction and the drainage area of the cells were edited to better represent the hydrology of the study area. This was necessary due to the numerous small watersheds at the western end of the study area. Each cell can have only one value for both drainage area and drainage direction. When a cell contains a watershed boundary, the two (or more) areas divided by the boundary flow in different directions. The cell can only represent one of these areas. The other area must be added to the adjacent cell that receives the flow from this area (see Figure B 8).

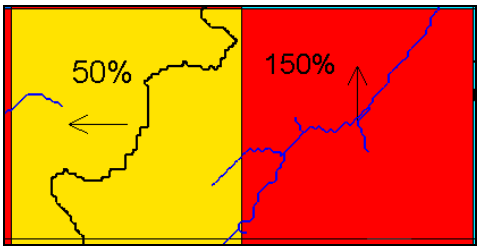

Figure B 8 - Drainage directions in cells.

The yellow cell is divided approximately in half by a watershed boundary (the thick black line). From the channels, shown in blue, the left half flows into the cell to the west and the right half flows into the cell to the east. The yellow cell is given the drainage direction of west and a drainage area of 50%, representing the left half of the yellow cell. The area of the right half of the yellow cell is added to the red cell, giving the red cell a total of 150%. The final WATFLOOD map is shown in Figure B 9.

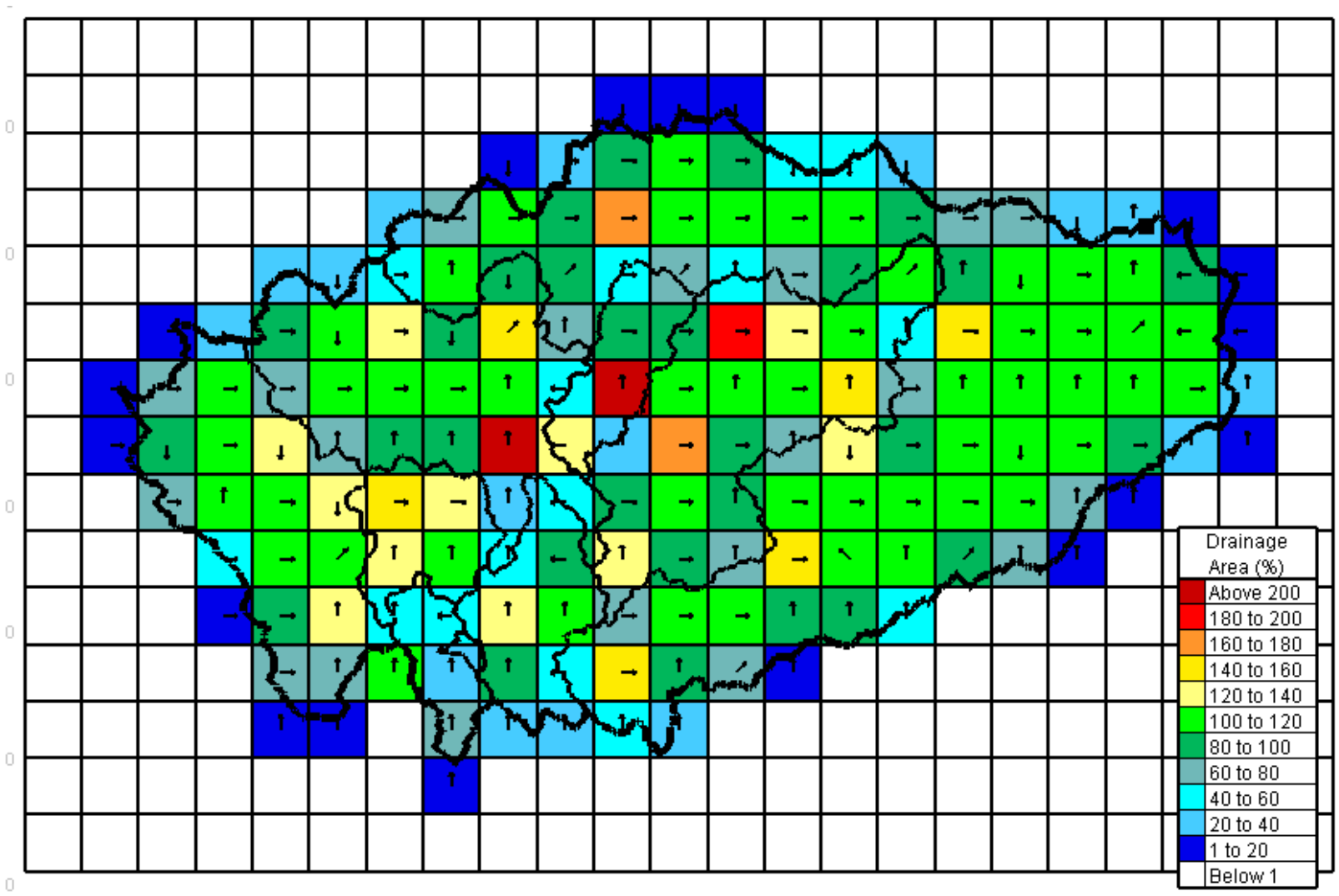

Figure B 9 - Map of the WATFLOOD model domain as displayed with EnSim Hydrologic. Drainage direction and drainage area are shown for each cell.

B6 Generating data files for WATFLOOD

In general, the following procedures are completed to set up the WATFLOOD model files.

- Run the BSN program to create a basin (*.shd) file from the WATFLOOD map file that was generated with EnSim Hydrologic.
- Alter the parameter file (*.par) to include the land use classes and the corresponding parameter values for each class.
- Create rain gauge and streamflow header files (*.rag and *.str) that identify the quantity and location of the meteorological and hydrometric stations.
- Create the following data files for each month of simulation:
  - Point gauge rain data file (*.rag)
  - Distributed rain gauge data file (*.met) -- created with WATFLOOD RAGMET
  - Reservoir release files (*.rel) -- for the 1970s and 1990s only
  - Streamflow data files (*.str)
  - Point gauge temperature data file (*.tag)
  - Gridded temperature file (*.tem) -- created with WATFLOOD TMP

**It should be noted that files for modelling snow and glacier melt were *not* generated at this stage.

B6.1 Simulation Periods

The model was intended to simulate a period of 5 years in each of three decades, the 1950s, '70s and '90s. The availability of data for each of these periods varied. Also, the Bighorn Dam on the North Saskatchewan River was not in operation until the late 1970s, so the Abraham Lake reservoir could not be included in the model of the 1950s. Therefore, each decade was organised as a separate watershed within WATFLOOD, and named NSASK50, NSASK70 and NSASK90 respectively.

WATFLOOD can run up to 744 hours (equivalent to 31 days) for one event. Consecutive months can be chained to produce one continuous set of results. Only 3 months, August, September, and

October, were being modelled in each year. These three months were chained, but each year had to be run independently of the others.

The years chosen for the simulations were based upon the availability of data. For each of the decades (1950s, 1970s, 1990s), the five-year period chosen represented the five consecutive years with the most available data. For the 1950s, the same amount of data was available for all years, so the five-year period was chosen as the middle five years in the decade. The simulation periods are indicated by plum-coloured rectangles in Figure B 10.

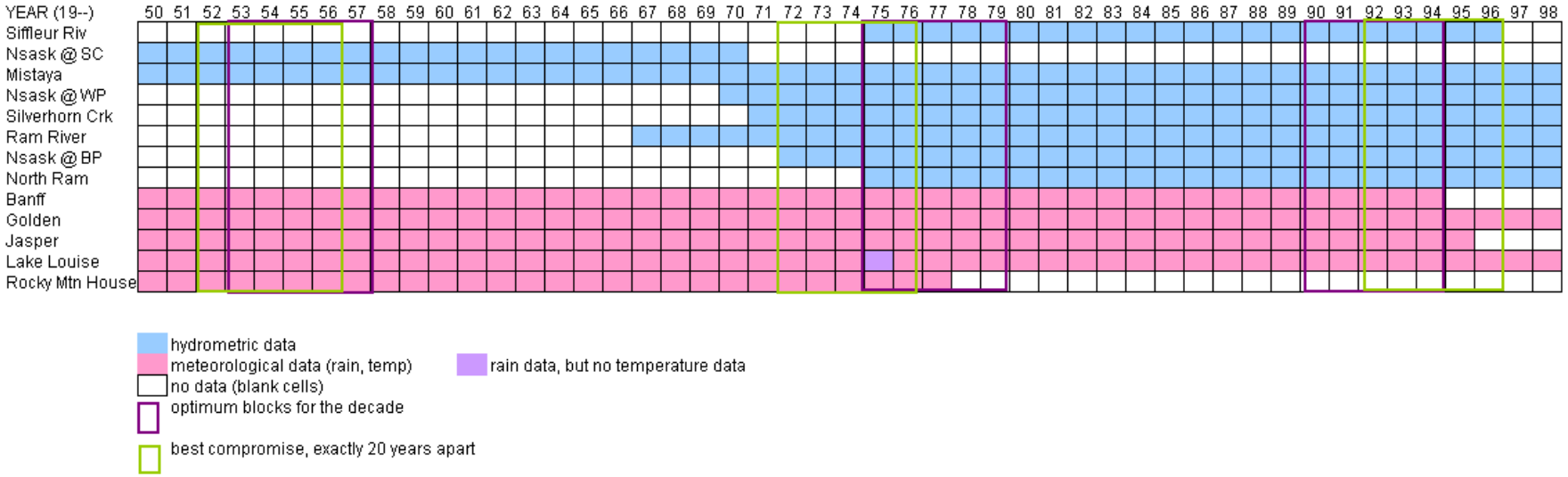

Siffleur Riv:	**Siffleur River near the mouth**
Nsask @ SC:	**North Saskatchewan River at Saskatchewan Crossing**
Mistaya:	**Mistaya River near Saskatchewan Crossing**
Nsask @ WP:	**North Saskatchewan River at Whirlpool Point**
Silverhorn Crk:	**Silverhorn Creek near the mouth**
Ram River:	**Ram River near the mouth**
Nsask @ BP:	**North Saskatchewan River below Bighorn Plant**
North Ram:	**North Ram River at Forestry Road**

Figure B 10 - Availability of hydrometric and meteorological data between 1950 and 1998.

B6.2 Source Data

B6.2.1 Hydrometric Data

Hydrometric data were obtained from NHRC. They had been extracted from the HYDAT database, with data ending in 1998, for the stations listed in Table B 4.

Table B 4 - Hydrometric stations in the upper North Saskatchewan River Basin

Station ID	Station Name
05DA002	Siffleur River near the mouth
05DA006	North Saskatchewan River at Saskatchewan Crossing
05DA007	Mistaya River near Saskatchewan Crossing
05DA009	North Saskatchewan River at Whirlpool Point
05DA010	Silverhorn Creek near the mouth
05DC006	Ram River near the mouth
05DC010	North Saskatchewan River below Bighorn Plant
05DC011	North Ram River at Forestry Road

Data were daily and in units of $m^3 s^{-1}$. Missing data had been filled in using interpolation. Gaps of less than 10 days had been filled in using linear interpolation. Larger gaps in data had been filled using interpolation and normalised data.

Availability of data at each station for the period of 1950 to 1998 is shown in blue in Figure B10. The locations of the stations are shown in Figure B 11.

B6.2.2 Meteorological Data

Meteorological data were obtained from NHRC. They had been extracted from the national climate data archive and consisted of daily values for temperature (minimum, maximum, and mean) and precipitation (rain, snowfall, and total). Temperature was given in units of degrees Celsius. Precipitation was in millimetres for rain and total precipitation, while snowfall was given in centimetres. Stations containing data for the period of study were Banff, Golden, Jasper, Lake Louise and Rocky Mountain House.

Availability of data at each station for the period of 1950 to 1998 is shown in pink in Figure B10. The locations of the stations are shown in Figure B 12.

B6.2.3 Land Use Parameters

The parameter values (in the WATFLOOD *.par files) for eight of the nine land use classes were from NHRC. The values were the same as those used for a previous model of a system in Northern Alberta, which had similar land-use classes. The values used for the parameters of the ninth land use class, urban and rock, were those in the standard WATFLOOD parameter file for the 'urban' class.

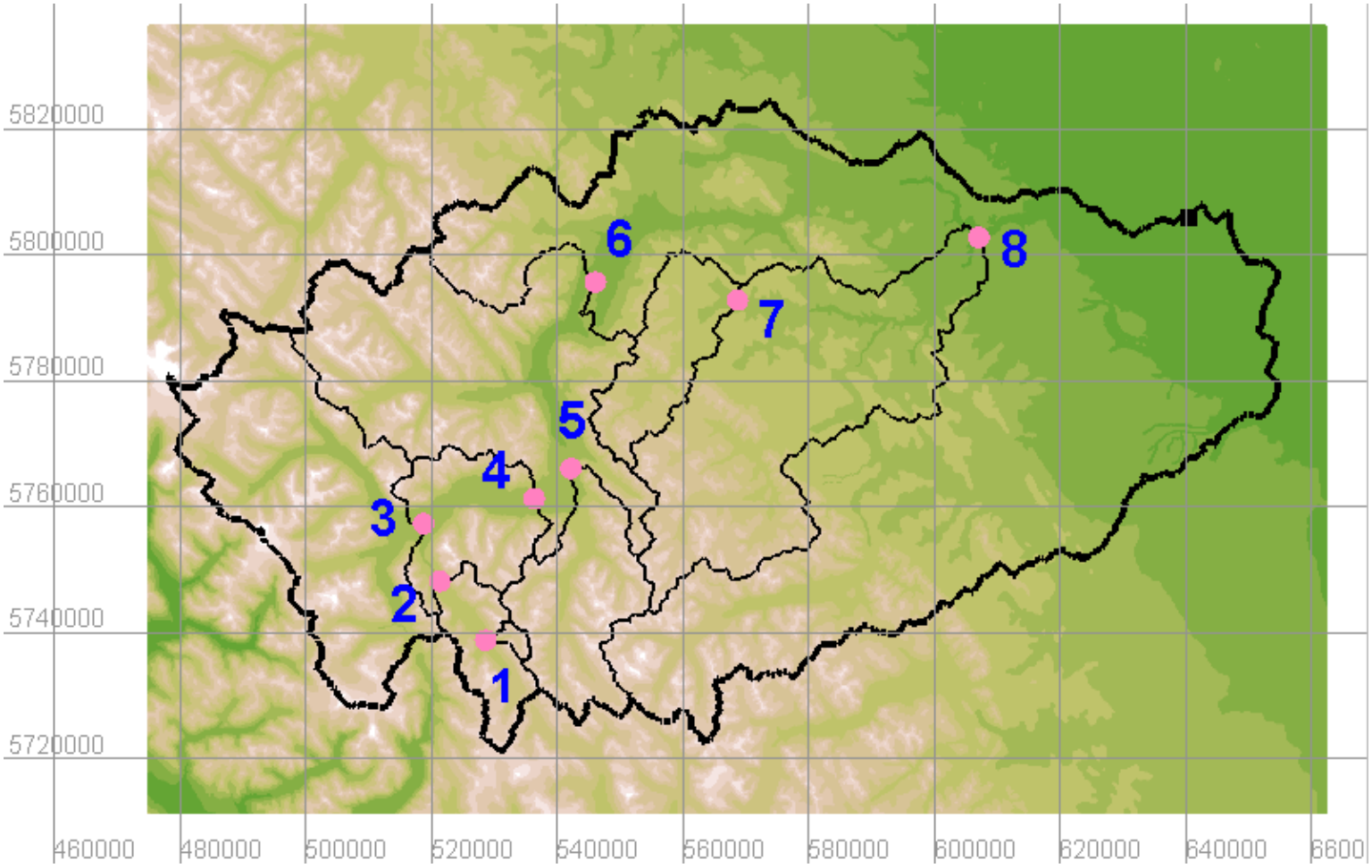

Figure B 11 - Locations of hydrometric stations.

1. Silverhorn Creek near the mouth, 2. Mistaya River near Saskatchewan Crossing, 3. North Saskatchewan River at Saskatchewan Crossing, 4. North Saskatchewan River at Whirlpool Point, 5. Siffleur River near the mouth, 6. North Saskatchewan River below Bighorn Plant, 7. North Ram River at Forestry Road, 8. Ram River near the mouth. The grid superimposed on the image is for georeferencing. Units are in metres. Projection is UTM, Zone 11, NAD 1983.

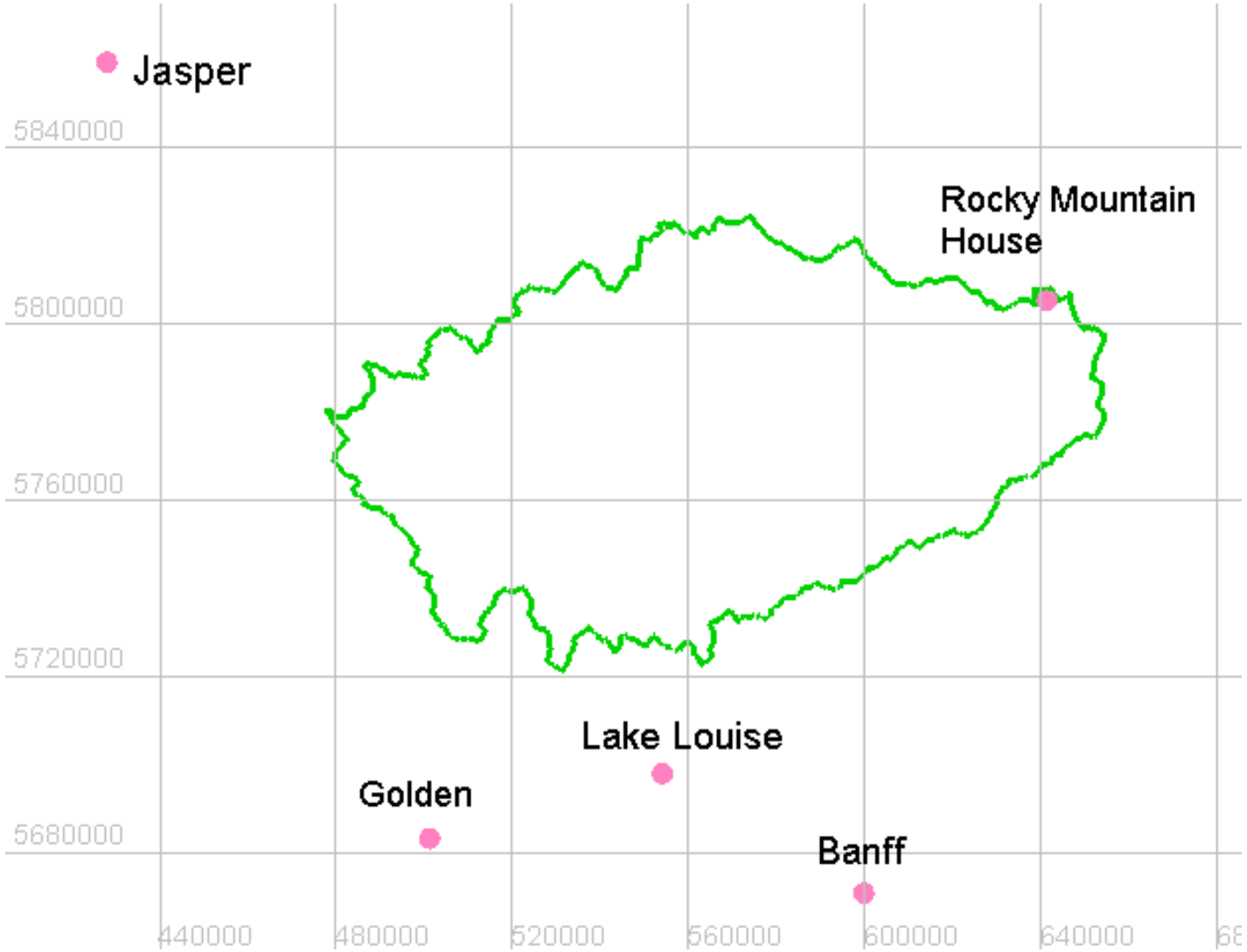

Figure B 12 - Locations of the meteorological stations in the vicinity of the North Saskatchewan River Basin. Grid coordinates are in metres. Projection is UTM, Zone 11, NAD 83.

B6.3 Hydrodynamic Data Files (.str and *.rel files)*

The data were entered in 24-hour intervals for both streamflow and reservoir release files. For the 1950s, data were only available from 2 stations (see Figure B 11). Since the Bighorn Dam was not yet constructed, there was no reservoir to model for this period. For the 1970s and 1990s, there were data available from 6 stations (see Figure B 11). The data from the North Saskatchewan below Bighorn Plant were modelled as reservoir releases.

B6.4 Meteorological Data Files (.rag and *.tag files)*

B6.4.1 Rain Gauge Files

From the available precipitation data, total precipitation was used in setting up the model. Measurements of rain alone could not be used, as there were small quantities of snowfall during October for many of the simulation years.

Data in the rain gauge (*.rag) files must be given hourly, however only daily data were available. The other 23 hours were entered as -1.00 and treated as missing data. Negative values are ignored, however zero values are considered as actual data and treated as such. Data were not 'smeared'. Therefore, daily values were taken as an hourly amount instead of being divided evenly among the 24 hours in the day.

For the 1950s, and from 1975-1977, data were available from all five meteorological stations. For 1978, 1979, and the 1990s data were no longer available from the Rocky Mountain House station (Figure B 11).

B6.4.2 Temperature Gauge Files

For temperature data, the daily maximum and minimum values were used instead of the daily mean. As a result, data were given in 12 hour intervals in the temperature (*.tag) files. The maximum temperature was defined as the noon temperature and the minimum was defined as that at midnight.

For the 1950s, 1976 and 1977, data were available from all meteorological stations. For 1975, data were not available from the Lake Louise station. For 1978, 1979 and the 1990s, data were not available from the Rocky Mountain House station (Figure B 11).

B7 Preliminary Simulation Results

Simulated versus actual flow test runs, for the 1950s, 1970s and 1990s for the Mistaya (glacierised) and the Ram River (unglacierised) catchments show encouraging results despite the lack of site-specific calibration. Such calibration is currently underway.

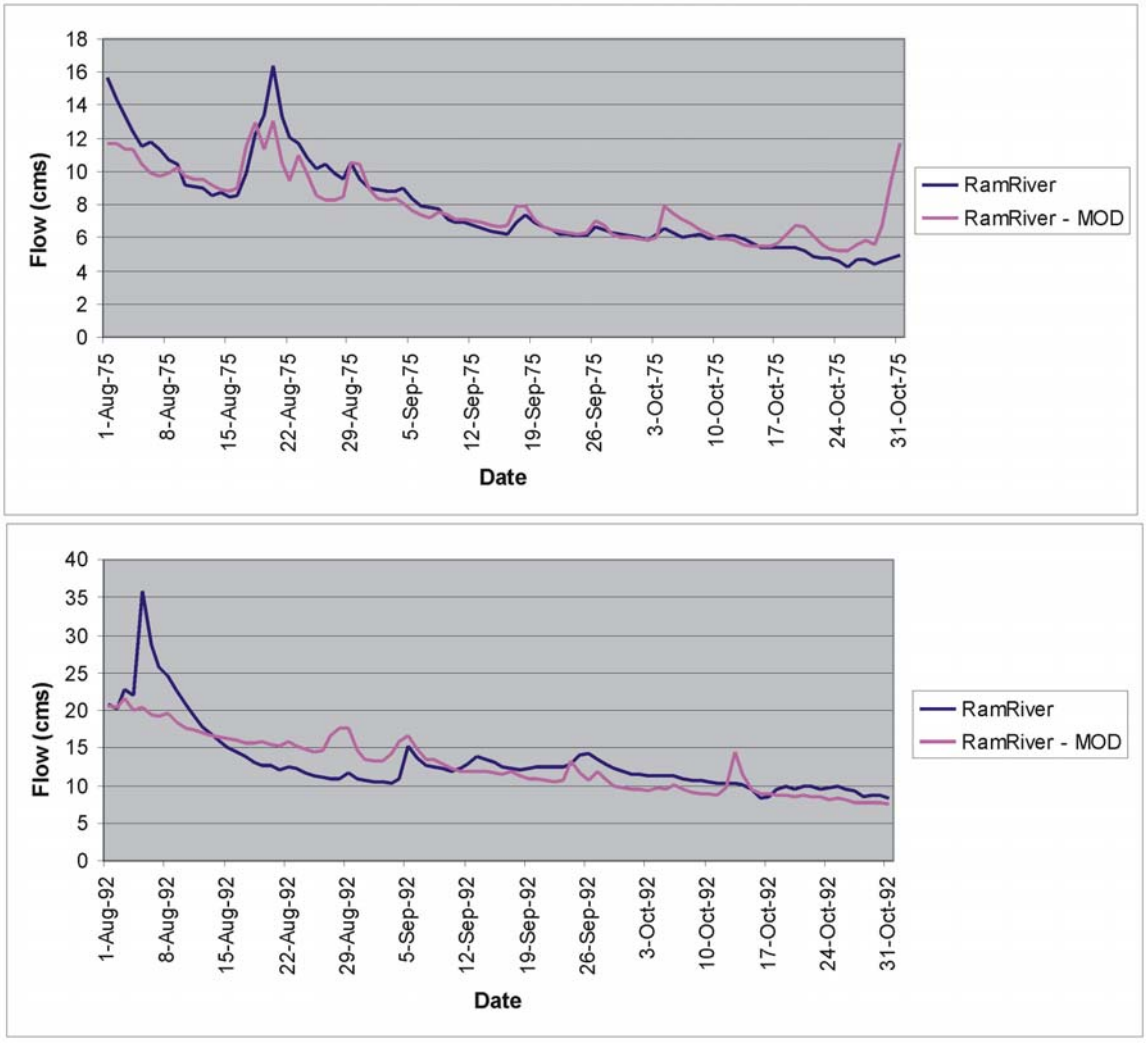

Figure 23 - Simulation of the Transition to Base Flow period for the North Ram River for 1975 and 1992.

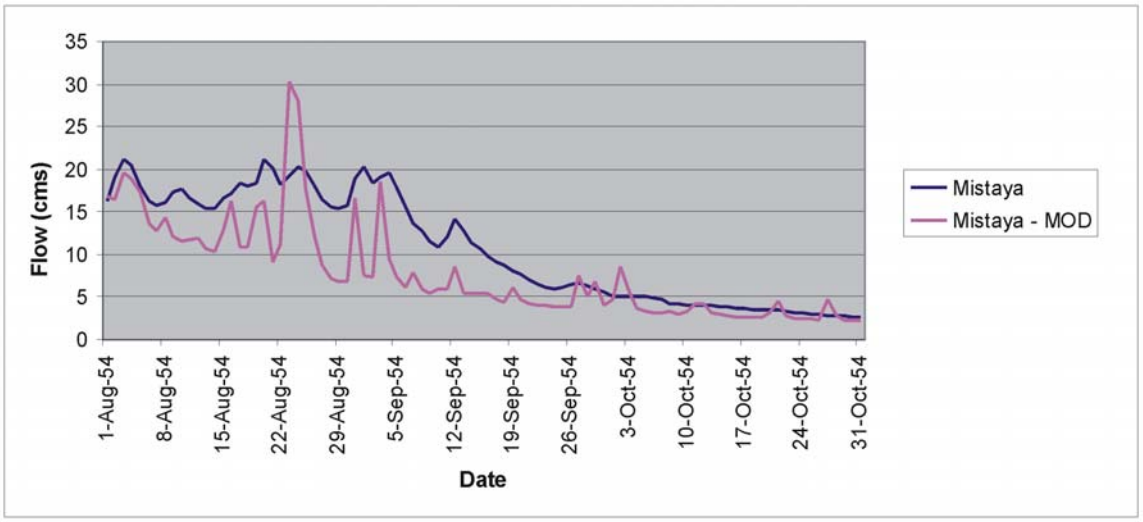

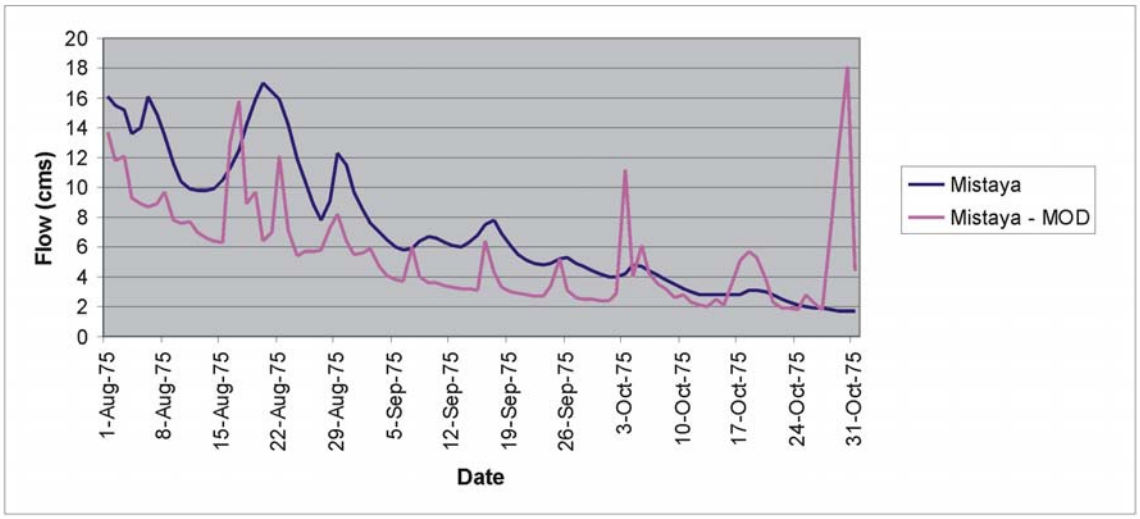

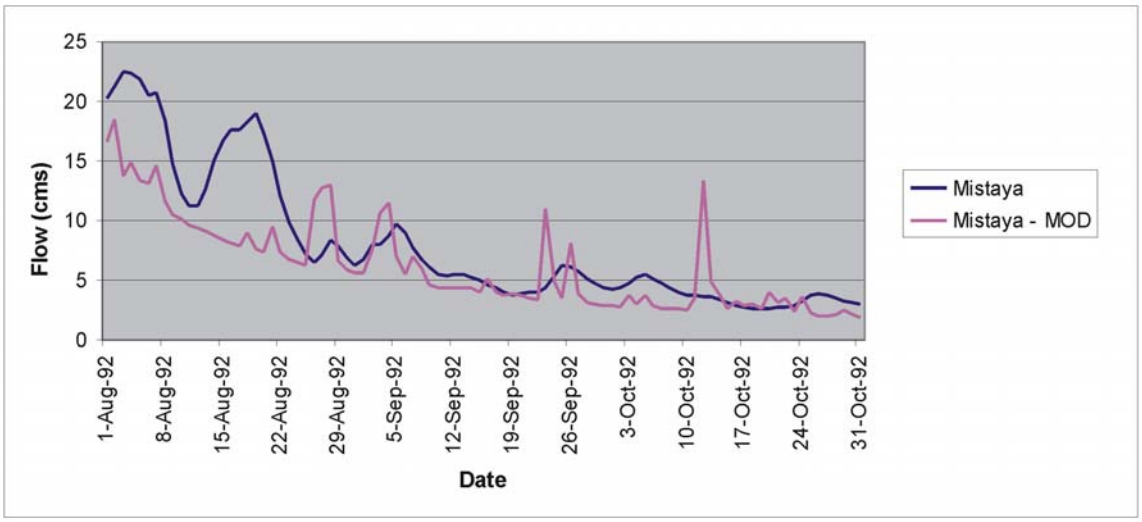

Figure 24 - Simulation of the Transition to Base Flow period for the Mistaya River for 1954, 1975 and 1992.

Annex C - Baseline Climatology and General Circulation Model Evaluation for the North Saskatchewan River Basin

C1 Background

To understand the implication of a future climate on the North Saskatchewan River Basin, it is important to compare the GCM model results for the 1961-90 climatology, to obserbed data for the basin. This was achieved by comparing a Canada-wide derived interpolated climatology to the IPCC data. The methodology developed for performing this comparison, along with the result are presented below.

C2 Observed Baseline Climatology

The observed data set is based on an interpolated 50 km grids derived by the University of Waterloo. This interpolated climatology is yet unpublished, but was derived from historic climatological records available from Environment Canada. This gridded dataset represents the monthly mean average monthly climatology and matches the period of record for the IPCC comparison.

C2.1 GCM Grids and Climate Data

The monthly 1961-1990 precipitation and temperature data, the monthly 2040-2069 precipitation and temperature data, the grid centre information, and the land/sea mask for each GCM were downloaded from the IPCC web-site. The grid centre information consists of the Longitude and Latitude of each grid cell centre. Table C 1 lists the reported approximate grid centre spacing for the different models. According to the Longitude and Latitude co-ordinates, the actual grid centre spacing varied in north-south direction for some of the models. The average grid centre spacing was calculated for Canada (see Table C 1) and used to create the GCM grids. The grid cell centre closest to Winnipeg was used as the starting point for the grid. A line graticule, representing the edges of the grid cells, was created for each model and, thereafter, used to generate grid cell polygons with true topology. Figure C 1 illustrates the generated grid centres, graticule lines and grid cell polygons for one of the GCMs.

Table C 1 - The reported and calculated average grid centre spacings for Canada in Decimal Degrees (DD). The start cell was used as starting point when generating a grid for Canada based on the average grid cell spacing.

GCM	Reported Approximate Grid Centre Spacing (DD)		Average Grid Cell Spacing for Canada (DD)		Start Cell (DD)	
	X (E-W)	Y (N-S)	X (E-W)	Y (N-S)	X (E)	Y (N)
CCSR/NIES	5.625	5.625	5.625	5.535	264.3750	52.6065
CGCM1	3.75	3.75	3.750	3.710	262.5000	50.0995
CSIRO-MK2b	5.625	3.214	5.625	3.185	264.3750	49.3779
ECHAM4	2.8125	2.8125	2.812	2.790	267.1875	48.8352
GFDL-R15	7.5	4.5	7.500	4.443	262.5000	51.1057
HADCM2	3.75	2.5	3.750	2.500	266.2500	50.0000
NCAR-DOE	7.5	4.5	7.500	4.443	262.5000	51.1057

The land/sea mask attributes were associated with the grid centre co-ordinates and joined spatially to the grid cells. Based on the land/sea mask, all sea grid cells were deleted, leaving only grid cells that cover land. Each GCM polygon grid were superimposed on the Waterloo raster data and all grid cells that included less than 40% of Waterloo data were removed. Grid cells that covered USA and did not include Canadian land were also deleted from the data set. Figure C 2 shows the resulting GCM grids.

The monthly 1961-1990 and 2040-2069 precipitation and temperature data were originally expressed in mm per day and degrees Celsius, respectively. The precipitation data were converted to mm per month to be consistent with the Waterloo data. The 2040-2069 climate data are expressed as the change in temperature and precipitation from to the 1961-1990 climate scenario. The monthly climate data were associated with the grid centre co-ordinates and joined spatially to the grid cells so that each grid cell obtained a precipitation and a temperature value for each month and for each climate scenario.

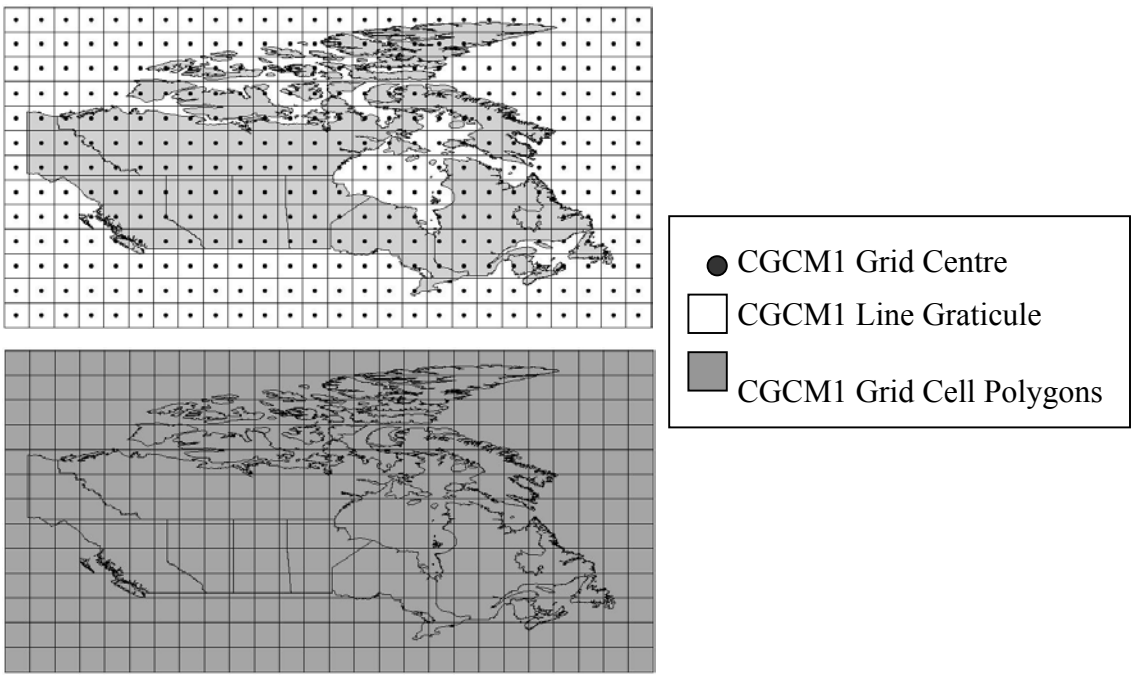

Figure C 1 - Generated CGCM1 grid centres and grid cell polygons.

C3 Comparison of GCM Data to Observed Data

The GCM grids were in vector polygon format with the climate data contained in attribute tables, whereas the gridded observed data from the University of Waterloo were in raster format with the climate data represented as the digital number of the pixels. To evaluate the GCM data, each of the seven GCM grids were superimposed on the Waterloo raster data layers. Average Waterloo values were extracted within each grid cell and added as attribute data to the GCM vector grid files.

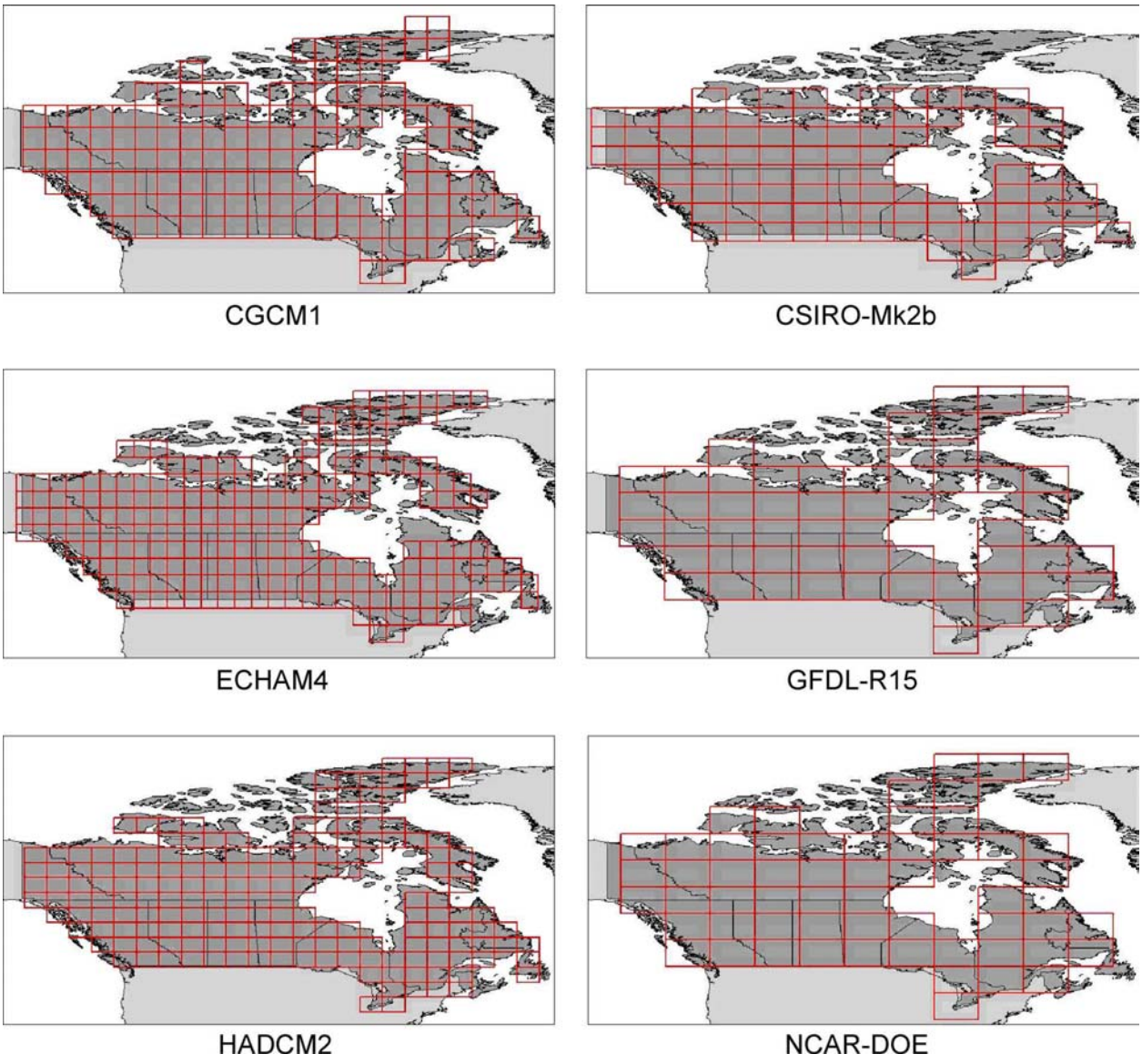

Figure C 2 - Edited GCM polygon grids. All polygons with less than 40% of Waterloo data were deleted from the dataset. In addition, all polygons that covered US land were removed.

C3.1 Preliminary Results

The database described above was used to derive the comparison of observed and GCM derived monthly climatology for the North Saskatchewan River Basin. The vector outline of the entire region was overlaid on the raster grid and an average value for each of the GCM's and the observed climatology was estimated. Figure C 3 and Figure C 4

show the estimated monthly total precipitation (mm/month) and temperature (º C) for the North Saskatchewan River Basin derived from the observed climatology (WAT) and the GCM's for every month of the year during the 1961-90 period.

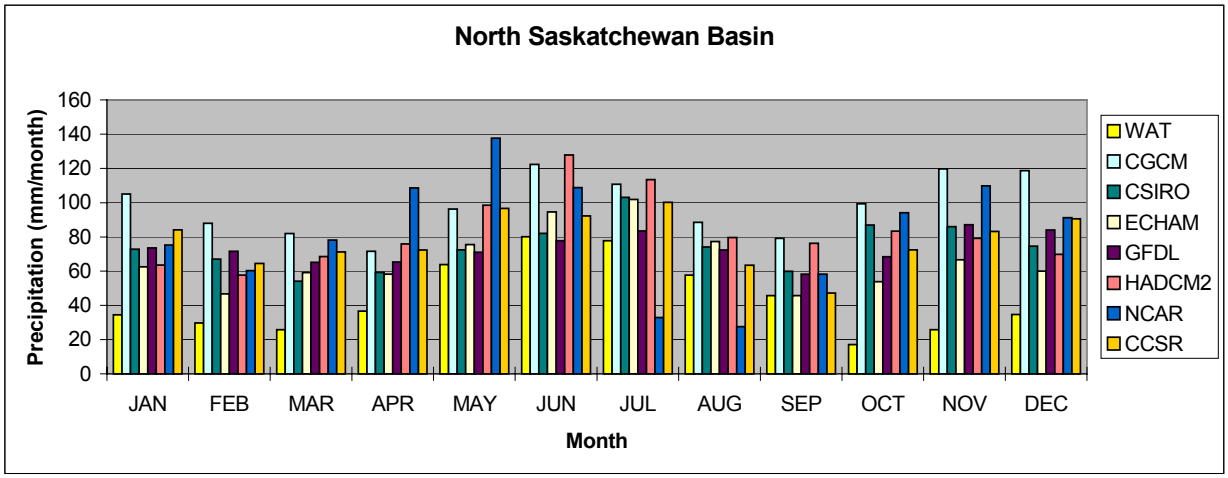

Figure C 3 - Precipitation for the North Saskatchewan River Basin derived from observed climatology (WAT) and each of the GCMs.

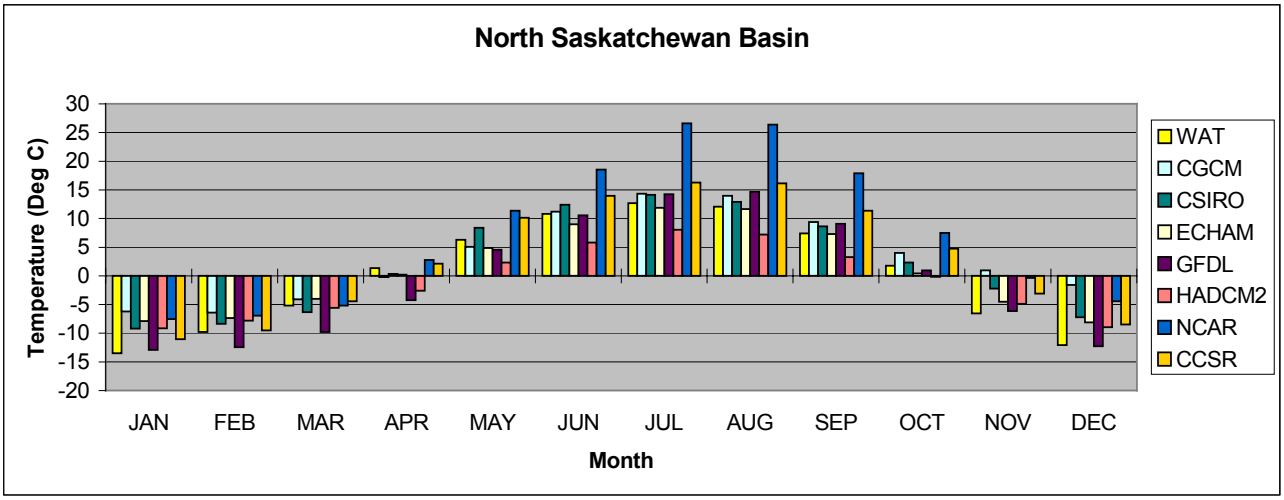

Figure C 4 - Temperature for the North Saskatchewan River Basin derived from observed climatology (WAT) and each of the GCMs.

Table C 2 and Table C 3 highlight the average absolute difference between each of the respective GCMs and the observed estimate for the basin, averaged for each month. Clearly these tables indicate that the ECHAM and GFDL and CSIRO models appear to simulate the 1960-91 climatology reasonably well for both the precipitation and

temperature. Monthly differences are plotted in Figure C 5 and Figure C 6. Of particular interest is Figure C 6, which shows a clear bias in all the models in terms of precipitation.

Table C 2 - Precipitation comparison and rank for all months for each of the GCM models (differences are expressed in mm/month)

GCM	**Average Abs Diff.**	**Rank**
CGCM	54.32	7
CSIRO	30.27	3
ECHAM	22.76	1
GFDL	29.46	2
HADCM2	38.69	5
NCAR	50.25	6
CCSR	34.06	4

Table C 3 - Temperature comparison and rank for all months for each of the GCM models (differences are expressed in degrees celcius)

GCM	**Average Abs Diff.**	Rank
CGCM	3.38	6
CSIRO	2.07	3
ECHAM	1.86	1
GFDL	1.89	2
HADCM2	3.33	5
NCAR	6.77	7
CCSR	2.74	4

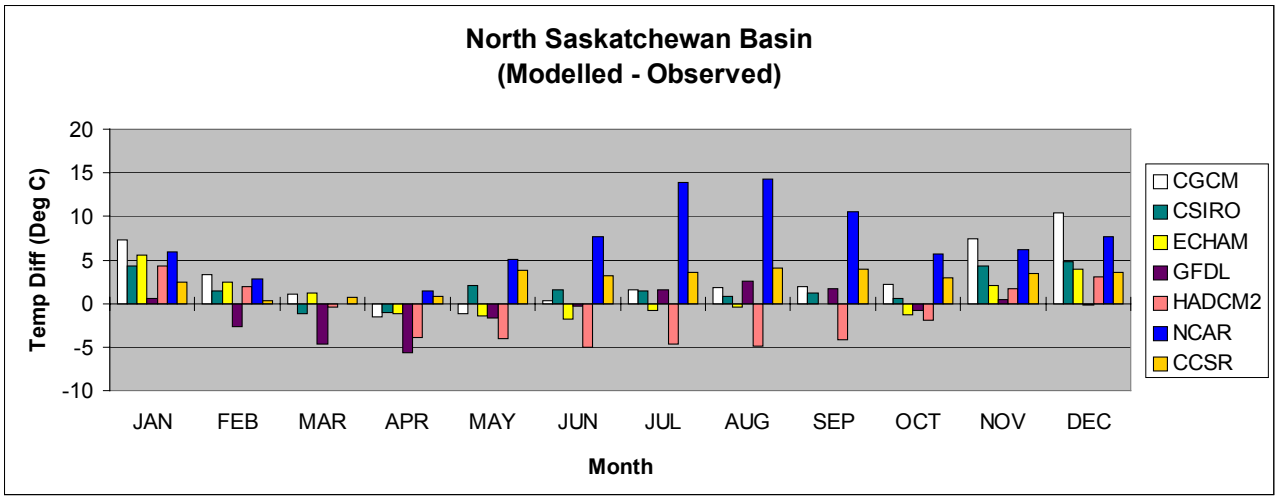

Figure C 5 - Temperature differences (Observed-GCM) for each of the GCM models for the North Saskatchewan River Basin.

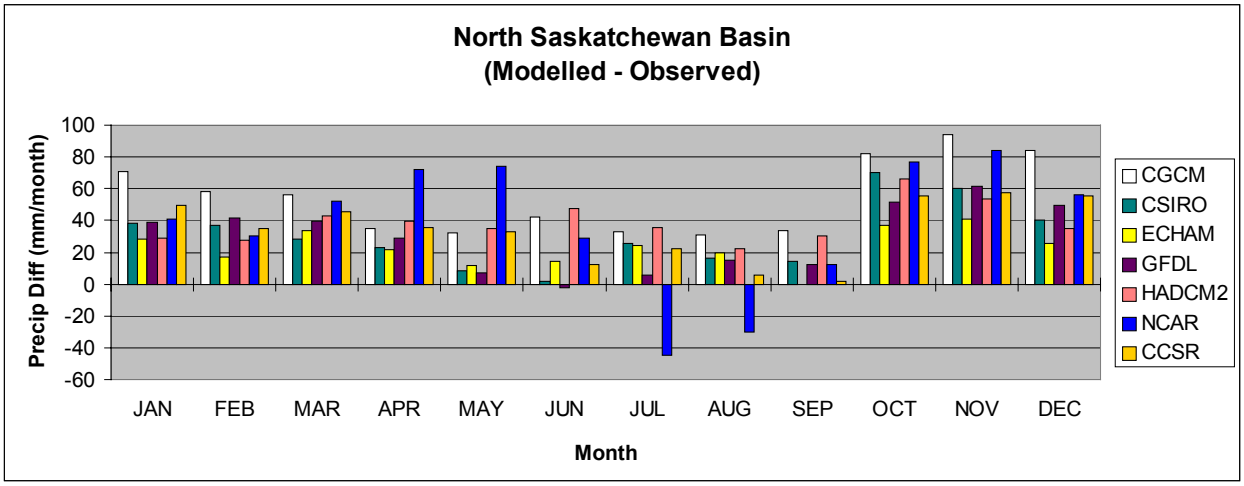

Figure C 6 - Precipitation differences (Observed-GCM) for each of the GCM models for the North Saskatchewan River Basin.

C4 Future Climate Predictions

Using the same methodology for current climate comparisons, it was also possible to derive basin-wide estimates of potential climate change to the basin, as predicted by the GCMs analysed.

C5.1 2040-2069 Climate Scenario for the North Saskatchewan River Basin

The 2040-2069 precipitation and temperature data from each GCM vector polygon grid were rasterised to the same pixel resolution as the Waterloo precipitation and temperature data, respectively. All pixels that were covered by a cell obtained the value of that grid cell. One raster layer was created for each month of precipitation and temperature data. A vector polygon of the North Saskatchewan River watershed was superimposed on the raster layers and average precipitation and temperature change values within the outline were extracted for each month. The extracted data were added to the attribute table of the basin polygon. The average 2040-2069 climate values for the North Saskatchewan River Basin, representing the change in temperature and precipitation compared to 1961-1990, could then be applied to the observed data from Waterloo. The plots for predicted change in are shown in Figure C 7.

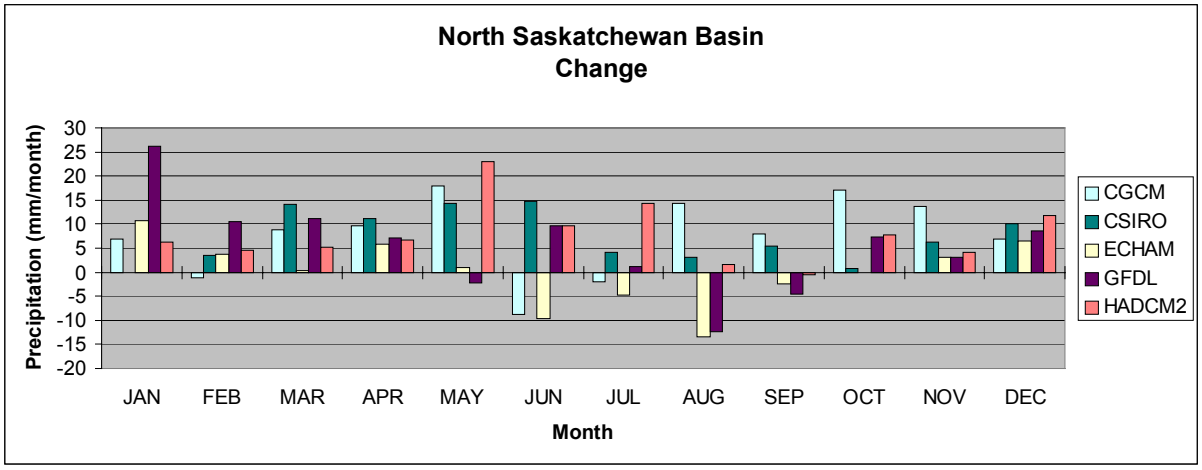

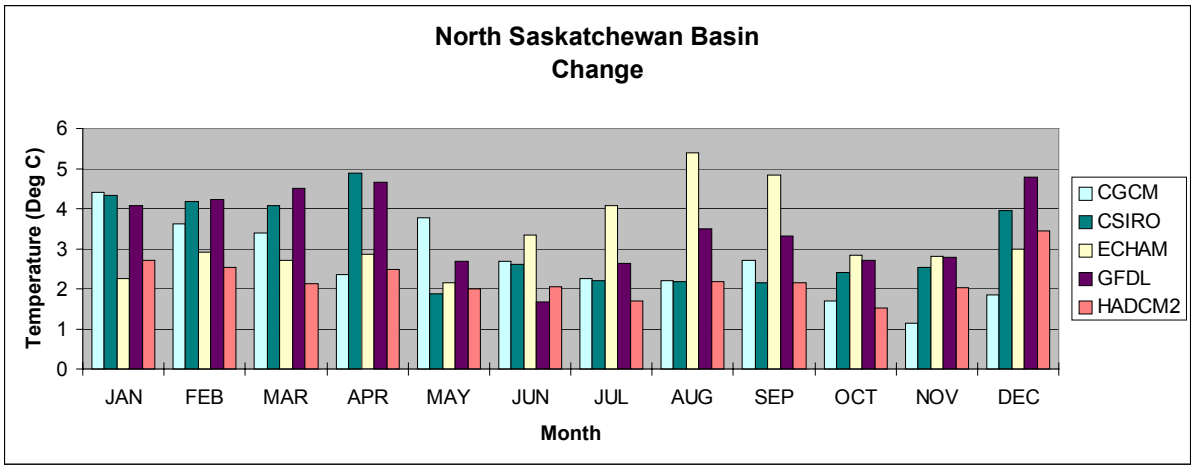

Figure C 7 - Preciptation and temperature change between 1961-1990 and 2040-2069 for the North Saskatchewan River Basin.